Synthesis, Characterization and Application of Calcium Phosphate Nanoparticles for the Transfection of Cells

Dissertation

zur Erlangung des Grades
eines Doktors der Naturwissenschaften
vorgelegt von

Viktoriya Sokolova

aus Kharkiv / Ukraine

Fachbereich Chemie

der

Universität Duisburg-Essen

Essen 2006

Dedicated to my husband and my parents

Die vorliegende Arbeit wurde in der Zeit von September 2003 bis Oktober 2003 am Lehrstuhl für Anorganische Chemie I, Arbeitskreis Prof. Dr. Matthias Epple (Festkörperchemie), an der Ruhr-Universität Bochum und in der Zeit von Oktober 2003 bis Mai 2006 am Institut für Anorganische Chemie, Arbeitskreis Prof. Dr. Matthias Epple, an der Universität Duisburg-Essen angefertigt.

1. Gutachter:	Prof. Dr. M. Epple
2. Gutachter:	Prof. Dr. W. Streit

Tag der mündlichen Prüfung: 17.10.2006

List of contents

1 Introduction

The main subject of this work was the synthesis of stable calcium phosphate colloids, their characterization and examination on cells.

The non-viral transfer of DNA into cells is called transfection. The main problem of non-viral transfection methods is their low efficiency, e.g. a low uptake of DNA by the cells and low gene expression. Because of that it is necessary to develop an appropriate drug delivery system which can protect DNA and RNA from the degradation by nucleases and successfully deliver it into the nucleus.

To study the interaction between organic and inorganic molecules in order to understand the mechanism of uptake and pathway of nanoparticles inside the cells is a great challenge in gene therapy, therefore, the cooperation with other fields of science such as colloid and physical chemistry or biochemistry was necessary. In the cooperation with Max-Planck-Institute of Colloids and Interfaces and with the University of Dortmund, department of physical chemistry, the main characteristics of calcium phosphate colloids and the developing of monodisperse ones for the biological application were accomplished. In the cooperation with the University of Bochum, chair of biochemistry, and with the institute of physico-chemical biology in Moscow the influence of physical parameters of the colloids, such as particle size, charge and stability, on the transfection efficiency and gene silencing were shown.

The aim of the work was to create a delivery system not only for DNA and RNA, but also for oligonucleotides which are used for down-regulation of gene expression by targeting the mRNA, resulting in effective gene silencing.

The open question in non-viral gene therapy is the understanding of all extracellular and intracellular physico-chemical barriers which DNA has to overcome for a successful incorporation into the nucleus. For this purpose it was

necessary to follow the pathway of nanoparticles into the cell by laser confocal microscopy.

The last topic was to develop a method for the preparation of ubiquitin-loaded calcium phosphate materials. Ubiquitin has very similar adsorption properties like rhBMP-2, which leads to enhanced bone growth and can be used as a model protein for the experiments. Understanding the interaction between calcium phosphate and ubiquitin can help to develop long-term implants for successful osseointegration.

2 Theoretical background

2.1 Nanoparticles and Nanotechnology

Nanotechnology comprises technological developments at scales less than 100 nm. The technology stretches across the whole spectrum of science, touching medicine, physics, engineering, and chemistry.

Nanoparticles are distinguished from the bulk phase by their high surface-to-volume ratio which causes their specific optic, electronic and catalytic properties.

Semiconducting nanoparticles, e.g. CdS or CdSe, are used for light-emitting applications in telecommunication systems. TiO_2 , ZnO and Ta_2O_5 nanoparticles are used in solar cells[1, 2], TiO_2 and ZnO nanoparticles find in addition a comparatively "trivial" application as pigments in dye and lacquers. Nanoparticles of TiO_2 are also used in sun screen lotions, because they absorb UV light[3].

Great attention is paid to ferromagnetic nanoparticles[4] due to their potential application in computer technologies and medicine, where they are used for magnetic hyperthermia to destroy cancerous tissue with heating.

Bio-oriented nanotechnology research is focused on main directions like developing fluorescent markers using semiconducting nanoparticles, biomolecule detection and drug delivery[5].

2.1.1 Colloids

A colloid is a system which consists of a dispersed phase finely divided and distributed throughout dispersion medium. The dimensions of the disperse phase lie in the range of 1 nm to 1 μm. Colloidal systems have large ratio of surface area to volume of the dispersed particles.

Colloidal system have been known and exploited by mankind for centuries in areas ranging from pigments and paints to medicines, photography, agriculture and others[6].

There are various combinations of gas, liquid, and solid as dispersed phase or as continuous medium in disperse systems. Familiar colloidal systems are the following: fog, smoke, milk and glass (Table 2.1.1.1).

Table 2.1.1.1: Examples of two-phase colloidal systems

Dispersed phase	**Dispersion medium**	**Name**	**Examples**
liquid	gas	liquid aerosol	fog, liquid spray, mist
solid	gas	solid aerosol	smoke, dust
gas	liquid	foam	soap foam
liquid	liquid	emulsion	milk, mayonnaise
solid	liquid	sol, suspension	gold sol, paste, gel
gas	solid	solid foam	expanded polystyrene
solid	solid	solid suspension	alloy, pigmented plastics

Many biological systems, including cell membrane formation, certain digestive processes and blood transport phenomena, involve various forms of associated colloidal structures[7].

2.1.2 The electrical double layer

At any surface there is always an uneven distribution of electrical charges between the two phases. The particles in a colloid are almost always electrically charged. This charge on the particle is balanced by an opposite charge in the surrounding fluid. The charge in the fluid is in the form of ions. Ions in immediate contact with the surface are located in the Stern layer. Ions farther away from the surface form a diffuse layer (Figure 2.1.2.1). The electrical double layer exists at the solid-liquid interface.

The zeta potential is the difference in electrical potential between the dense layer of ions surrounding the particle and the bulk of the suspended fluid.

When ions or polymers are adsorbed on a particle in a colloidal system, or by the dispersed liquid in an emulsion, the charge of the layer surrounding the particle is changed. This results in a change in the potential difference between the surrounding layer of ions and the bulk of the suspending fluid. This is a change in the zeta potential. The stability of a colloidal system is dependent on the degree of ion adsorption, and, therefore, on the zeta potential. Zeta potential measurements make it possible to control the process of dispersion or agglomeration.

All aqueous colloids have a negative or positive charge. The stability of the system is increased when the zeta potential exceeds ± 30 mV generally represent sufficient mutual repulsion to result in stability. This can be accomplished by the addition of an anionic electrolyte or polyelectrolyte. Stability is assured within a zeta potential range of ± 45 to ± 70 mV.

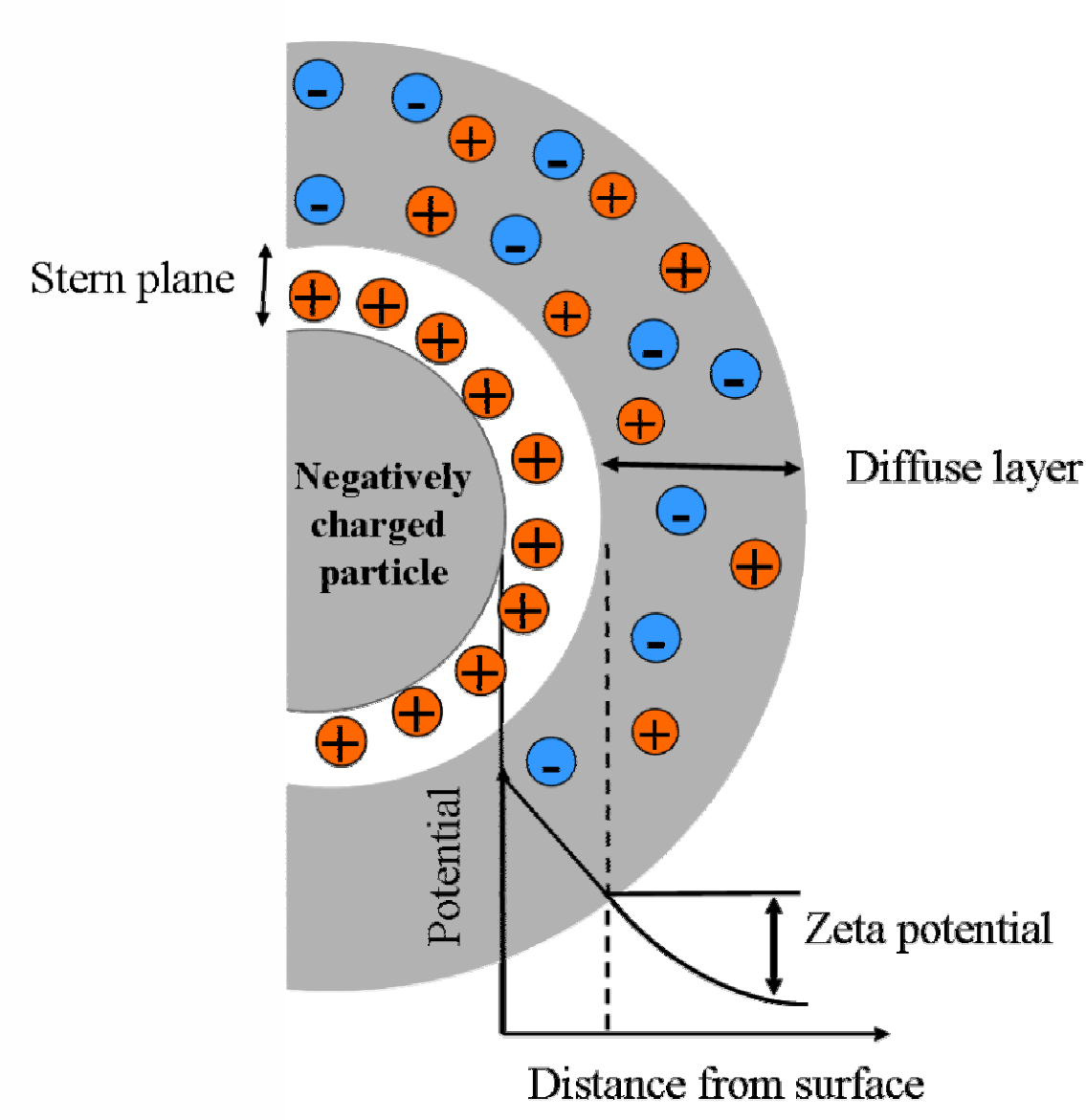

Figure 2.1.2.1: Schematic representation of the electrical double layer.

When agglomeration is desired, it is necessary to bring the zeta potential closer to zero. This can be achieved by the addition of polyelectrolytes.

2.1.3 Colloid stability and DLVO theory

A colloidal dispersion may be stable or unstable towards aggregation. A stable colloidal system is one in which the particles resist flocculation or aggregation. This will depend upon the balance of the repulsive and attractive forces that exist between particles as they approach each other.

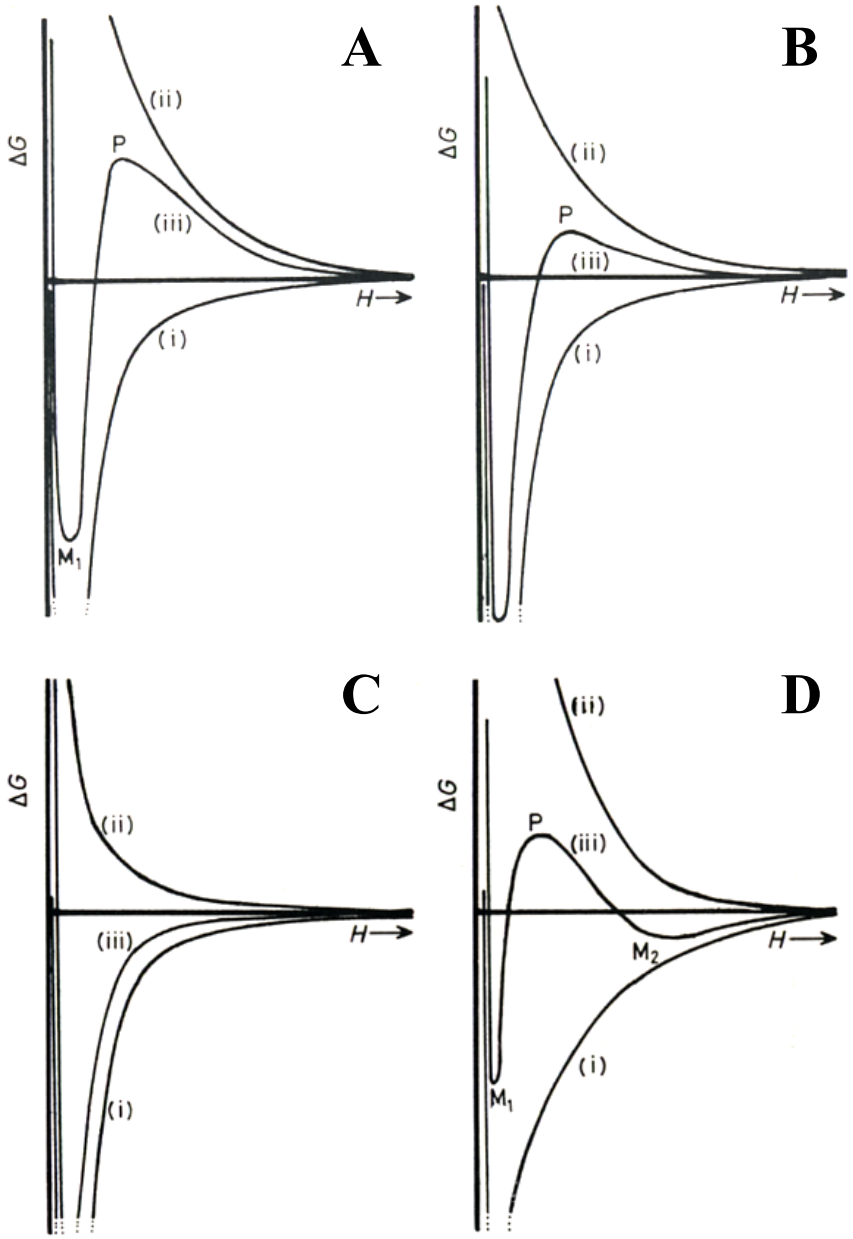

Figure 2.1.3.1: Illustration of four possible forms of the total free energy (iii), resulting from the combination of attractive (i) and repulsive (ii) combinations[8].

The DLVO theory (developed by Derjaguin, Landau, Verwey and Overbeek)[9, 10] proposes that the stability of a particle in solution depends on the total interaction energy, which is the sum of the attractive van der Waals force and the repulsive force that arise when the diffuse double layer round the two particles overlap[11] (Figure 2.1.3.1).

In Figure 2.1.3.1 is shown the interaction-free energy ΔG as a function of the distance (*H*) between the particles. The total free energy (iii) is the sum of the attractive (i) and repulsive (ii) energy. Diagram A on the Figure 2.1.3.1 shows states of separation and contact separated by a high energy barrier (primary maximum P) arising from strong repulsive interaction. This colloidal dispersion is stable. If conditions are adjusted so that the energy barrier becomes negligibly small by reduction of repulsive interactions or decrease in their range, the system will be able to pass over into the primary minimum M_1 and then the colloid becomes unstable (Figure 2.1.3.1 B). By elimination of the energy barrier, the system will be able to pass over into the primary minimum M_1 without any activation energy (Figure 2.1.3.1 C). On the Diagram C the existence of the secondary minimum M_2 is shown. In this situation flocculation may occur. An important feature of such a situation is that although the agglomerates are sufficiently stable to be not completely dissociated by Brownian motion, they may disintegrate under externally applied hydrodynamic forces.

2.1.4 Aging and coagulation of colloids

The aging process is the tendency of the dispersion to achieve a thermodynamically stable state. The solubility of each substance depends on the particle size. Small particles have a higher solubility than large particles.

The aging speed d*m*/d*t* is given by:

$$\frac{dm}{dt} = \frac{qDc_0}{\delta} \exp\left[\gamma / f(r_1) RT\right] - \exp\left[\gamma / f(r_2) RT\right]$$

The aging speed depends on the concentration of the macroscopic phase (c_o), the surface tension (γ), the particle radius (r_1; r_2), the diffusion coefficient (D), the temperature (T) and the viscosity (δ).

According to the equation, monodisperse colloidal systems should not age. However, it is difficult to prepare really monodisperse colloids. Monodisperse colloids age substantially more slowly. Aging can be accelerated by increasing the temperature because the solubility and the diffusion coefficient are increasing with increasing temperature. Aging is the natural, spontaneous and slowly occurring process of the destruction of a colloidal dispersion. At the end of this process, the separated solid phase and the dispersion medium are present. Increasing temperature promotes the coagulation, because it strengthens the Brownian motion of the particles. In consequence of the coagulation, colloidal particles assemble to larger aggregates.

Under these conditions the coagulation is also called agglomeration. The assembled particles in the agglomerates initially keep their original size and shape. Then, in a subsequent process, recrystallisation occurs. If such features arise, then the coagulation will be irreversible and can not go backwards to a redispersion.

The final state of the coagulation process is a coagulate, which usually possesses the structure of a gel, which is also called lyogel or xerogel. The gel structure depends on the structure of colloidal particles and the solvatation conditions. We differentiate between reversible and irreversible coagulations.

2.1.5 Stabilization of colloidal systems

In general, there are two mechanisms for stabilization of colloids: electrostatic repulsion between the electrical double layer and steric stabilization. The electrostatic stabilization was discussed above.

The steric stabilizing mechanism includes the adsorption of polymeric protective agents or steric stabilizers on the particle surface. Such molecules do not have to carry an electrical charge but must have a relatively low solubility in the dispersion medium and a high tendency to adsorb onto the particle surface, which results in the formation of an adsorbed layer and improves the stability of the colloid by the imposition of a barrier to close particle approach.

The calcium phosphate colloids in the presence of DNA or proteins involve a combination of both electrostatic and steric stabilization mechanisms. DNA and proteins in this case are excellent protective agents. DNA, for example, is a biopolymer and provides good steric stabilization and because of its negative charge, DNA provides electrostatic stabilization as well.

2.1.6 Calcium phosphate

Calcium phosphates are a very important inorganic component of biological hard tissues. They are present in bone, teeth, and tendons in form of carbonated hydroxyapatite (HA) to give stability, hardness, and function of these organs.

Calcium phosphate crystals are also found in the nature as mineral deposits of considerable size, having grown over many years under sometimes extreme conditions of pressure and temperature. Biologically formed calcium phosphates that are precipitated under mild conditions (ambient pressure, near room temperature) are often nanocrystals.

Calcium phosphates are of great interest in medicine, biology and materials sciences[12]. Due to their biocompatibility, they are used as bone substitution

materials. In addition, calcium phosphate nanoparticles are used as non-viral DNA delivery system in cell biology.

The existence of various calcium phosphate salts of ortho-phosphoric acid can be explained by the combination of calcium with three protolysis steps of phosphoric acid:

$H_3PO_4 + H_2O \rightarrow H_3O^+ + H_2PO_4^-$ $\quad pK_1 = 2.16$

$H_2PO_4^- + H_2O \rightarrow H_3O^+ + HPO_4^{2-}$ $\quad pK_2 = 7.21$

$HPO_4^{2-} + H_2O \rightarrow H_3O^+ + PO_4^{3-}$ $\quad pK_3 = 12.33$

All calcium phosphate in pure state are white solid bodies and the most of them are just a little soluble in water, but all calcium phosphate are soluble under acidic conditions. A variety of stoichiometric calcium phosphates is known, but we will discuss only those which are of interest here: ACP (amorphous calcium phosphate) and HA (hydroxyapatite).

ACP is often encountered as a transient phase during the formation of calcium phosphates in aqueous systems. ACP is the first phase that is precipitated from a supersaturated solution prepared by rapid mixing of solutions containing of calcium cations and phosphate anions[13-17]. The solution pH value and the concentrations of calcium and phosphate ions in the mother liquor have a strong influence on the chemical composition of ACP. Electron microscopy of ACP usually reveals spherical particles with typical diameters of 20-200 nm and X-ray diffraction experiments show the amorphous state. IR spectra of ACP show broad, featureless phosphate absorption bands. In medicine, ACP is sometimes used in calcium phosphate cements[18-20].

HA ($Ca_{10}(PO_4)_6(OH)_2$) is the most stable and least soluble of all calcium orthophosphates. HA can be prepared in aqueous solutions by mixing exactly stoichiometric quantities of calcium- and phosphate-containing solutions at pH>9, followed by boiling for several days under a CO_2-free atmosphere,

filtration, and drying. In HA calcium ions may be partially replaced by Sr, Ba, Mg, K, Na, Fe, phosphate ions may be replaced by AsO_4^{3-}, CO_3^{2-}, and VO_4^{3-} and hydroxide ions may be replaced by F^-, CO_3^{2-} and Cl^-.

Pure HA never occurs in biological systems. However, because of the chemical similarities to bone and teeth mineral, HA is widely used as a coating for orthopedic and dental implants, and a calcium phosphate cement with HA has also been developed[21]. Because of the great similarity to bone mineral, HA is also used as solid phase in liquid chromatography of proteins and other biological compounds[22-26].

2.2 Biopolymers applied for the stabilization of calcium phosphate colloids

2.2.1 Desoxyribonucleic acid (DNA)

Desoxyribonucleic acid (DNA) is the molecular carrier of the hereditary information. This term does not describe a certain molecule, but rather a molecule class, which occurs in different variants in the nucleus and in the organelles of the individual cells. DNA is a linear polymer composed of monomers, called desoxynucleotides. All nucleotides consist of three components: A purine (adenine or guanine) or a pyrimidine (cytosine or thymine), a desoxyribose and a phosphate moiety.

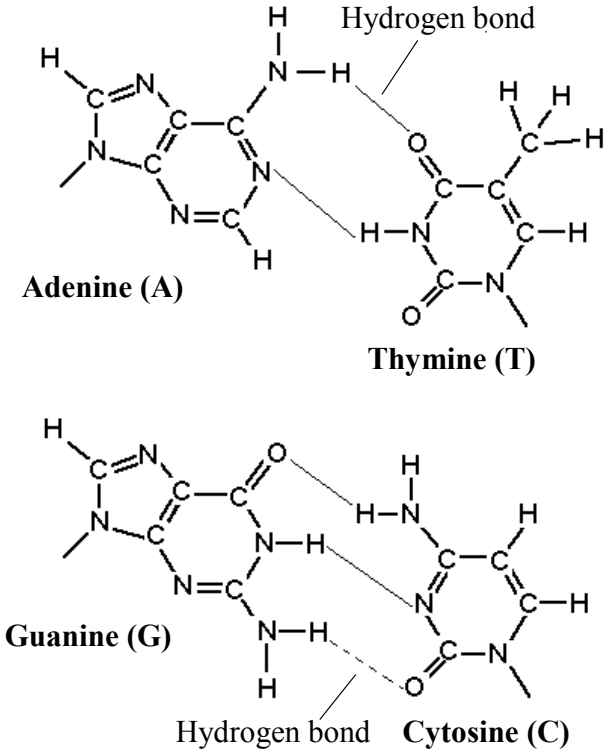

Figure 2.2.1.1: The chemical structures of purine (adenine and guanine) and pyrimidine (cytosine and thymine) bases in desoxyribonucleic acids.

A phosphate group is linked by a phosphoester bound to a desoxyribose which is linked to an organic base. The links between the nucleotides are called phosphodiester bonds. Therefore each chain has a 5' and 3' end, where the 5' end is shown as a start and the 3' end as an end.

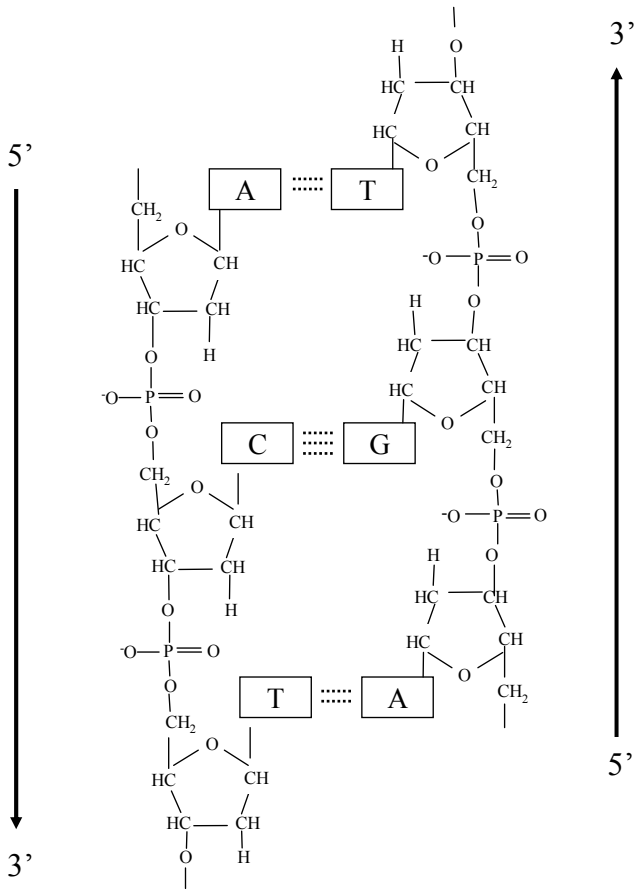

Figure 2.2.1.2: Representation of contacts within the DNA double helix.

Nucleotides are complementary to each other, i.e. purines (A, G) are paired with pyrimidines (C, T) (Figure 2.2.1.1). The complementary pairs of nucleotides adenine (A) and thymine (T) are stabilized by two hydrogen bonds. On the other hand the complementary pair of nucleotides guanine (G) and cytosine (C) has three hydrogen bonds, so that this structure is more stable than between A and T, and it can explain the higher melting temperature for G/C-rich DNA double helix at which the strands of DNA will separate.

Complementary nucleic acid strands are always antiparallel, that is their 5' → 3' directions are opposite (Figure 2.2.1.2)[27, 28].

2.2.2 Ribonucleic acid (RNA)

Beside the DNA there are also other nucleic acids: ribonucleic acid (RNA). In RNA, the pentose is ribose, and instead of thymine presented in DNA, uracil is present in RNA (Figure 2.2.2.1).

Fundamentally, RNA can be divided into three functional groups:

1. Ribosomal RNA (rRNA) is a component of the ribosomes, the protein synthetic factories in the cell.
2. Transfer RNA (tRNA) transfers a specific amino acid to a growing polypeptide chain at the ribosomal site of protein synthesis during translation.
3. Messenger RNA (mRNA) is RNA that encodes and carries information from DNA during transcription to sites of protein synthesis to undergo translation[27, 28].

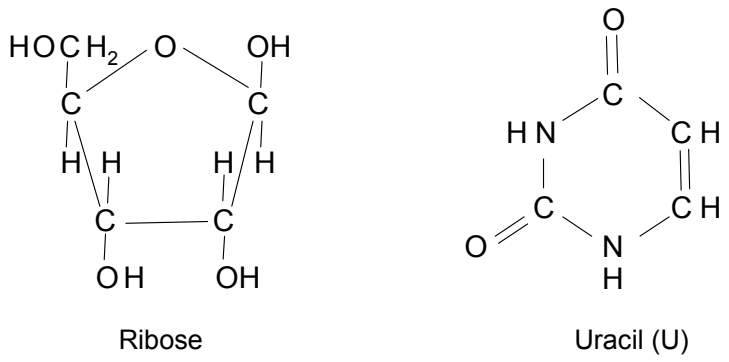

Figure 2.2.2.1: The chemical structures of ribose and uracil in ribonucleic acids.

2.2.3 Oligonucleotides

An oligonucleotide is a molecule which is formed by several nucleotides (DNA or RNA). Its sequence consists of approximately 10-30 nucleotides.

In 1978 Stephenson *et al.* published the specific inhibition of Rous sarcoma viral RNA translation by a specific oligonucleotides[29, 30]. This was the start of a large

amount of research work in the field of oligonucleotides, in order to make these accessible for a pharmacotherapy.

Oligonucleotides as potential pharmaceutics are short, single-stranded DNA and single-stranded or double-stranded RNA. Such oligonucleotides are usually obtained by solid phase syntheses[31].

2.2.4 Proteins

2.2.4.1 Protamine

Protamine is a highly cationic peptide (due to the presence of 21 arginine residues) with a molecular weight around 4000-10000 Da and an average number of approximately 30-35 amino acids per molecule[32].

During spermatogenesis, nuclear histones are gradually replaced by new synthesized sperm-specific protamine[33]. Histones are located in somatic cells[34], however protamine are found exclusively in sperm cells. Protamine binds to DNA and causes a compact packing of the hereditary information in the sperm cells, thereby protecting chromosomal DNA from degradation.

Protamine contains four nucleic localization sequences (NLS), which help DNA in the overcoming of the nuclear membrane barrier. This is an important factor for later developments of delivery systems for DNA and oligonucleotides[35-37].

Protamine sulfate can induce higher levels of gene expression than poly-L-lysine and other types of protamines when combined with DNA[38, 39].

2.2.4.2 Bovine serum albumin (BSA)

Bovine serum albumin (BSA) is one of the most widely studied proteins. It belongs to the class of serum proteins called albumins, which make up about half of the protein in plasma and are the most stable and soluble proteins in plasma (Figure 2.2.4.2). The molecular weight of BSA is 67000 Da[40]. It is a

popular delivery system for weakly antigenic compounds. BSA serves as delivery system for DNA and oligonucleotides into cells[37, 41].

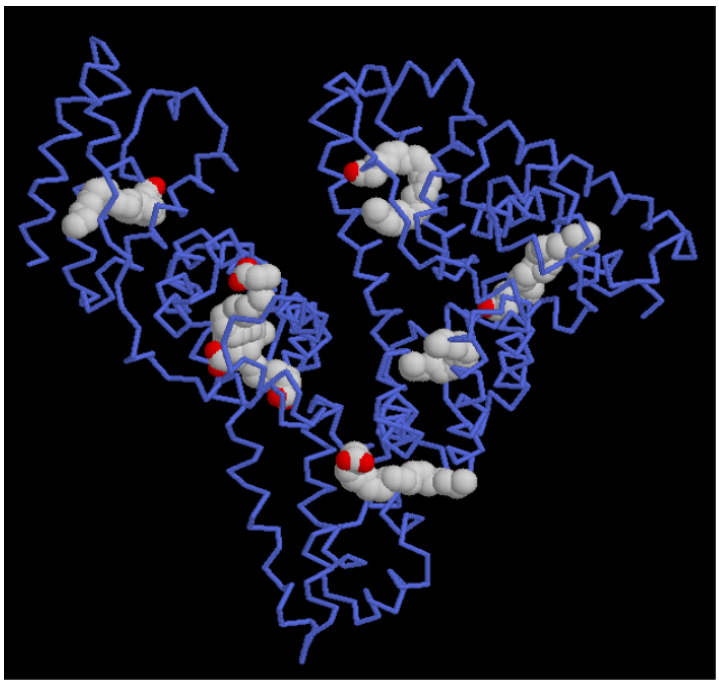

Figure 2.2.4.2: Structure of human serum albumine (from protein data base). The structure has seven molecules of arachidonic acid bound to it. The protein is shown with lines and the fatty acids are shown with spheres at each atom. Arachidonic acid is an unsaturated fatty acid with several double bonds that form rigid kinks in the carbon chain.

2.2.4.3 Ubiquitin

Ubiquitin contains 76 amino acids with a molecular weight of approximately 8500 Da. This protein is found both as free monomer in eukaryotic cells, and covalently attached to other proteins[42, 43].

Nuclear magnetic resonance (NMR) and chemical studies showed that ubiquitin is a compact, globular protein (Figure 2.2.4.3)[44].

Ubiquitin has different functions. On the one hand it serves as a marker to the marking of proteins which have to be destroyed. The protein which has to be removed is covalently bound under ATP consumption to several ubiquitin

molecules. This process is called ubiquitination. A further function is the marking of defective or denatured molecules or those, which were not correctly synthesized. These marked molecules will afterwards also be decomposed[45].
Ubiquitin and its conjugates also play a significant role with other proteins in various biological functions such as in the regulation of the cell cycle[46, 47], in cell division[48], in DNA repair[49, 50], in the morphogenesis of neurons[45] and some other processes[51].

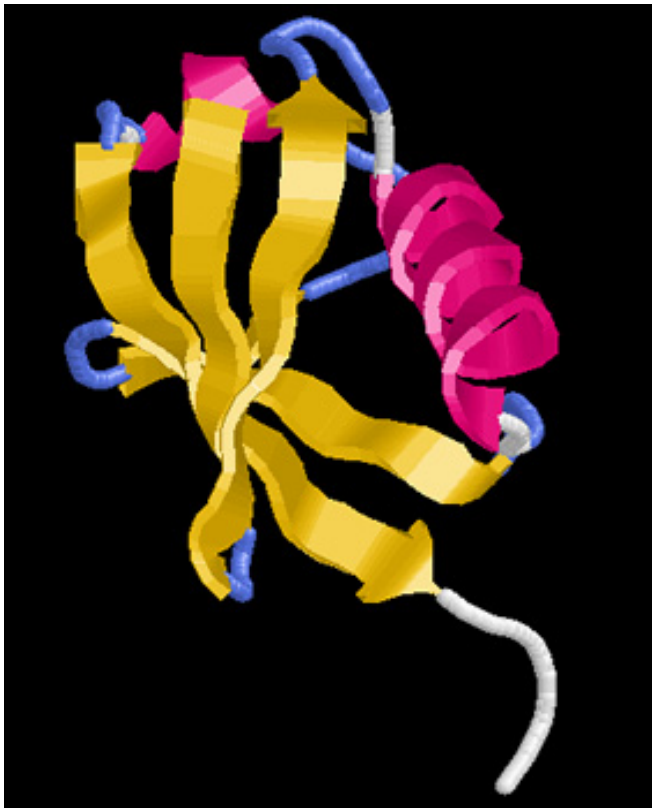

Figure 2.2.4.3: Ubiquitin consists of two α-helices and two β-sheet structures (from www.mdc-berlin.de/dittmar/ubiquitin.png).

2.3 Transfection methods

Introducing DNA into eukaryotic cells is called transfection. This process involves the entry of extracellular molecules, such as plasmid DNA, siRNA or oligonucleotides, through the plasma membrane all the way to the nucleus.

Such an introduction of desirable genetic sequences into mammalian cells is an essential tool for analyses of gene structure, function and regulation; it is also a medical technique that potentially allows the treatment of a wide variety of diseases of both genetic and acquired origin.

The development of an efficient method for the introduction of therapeutic gene into cells is a major challenge in gene therapy.

Gene delivery systems are generally divided into two categories, viral and non-viral systems.

2.3.1 Viral gene delivery systems

Viral gene delivery systems are base on the ability to infect the cells[52]. It is the oldest method for gene transfer, which was first demonstrated on *Salmonella* in 1952[53]. Later, for gene transfer into cells, different viral vectors based on retroviruses[54, 55], adenoviruses[56], adeno-assotiated viruses[57] and herpes simplex virus[58] and other viruses were used.

In viral carriers, a part of the original gene segment is eliminated to have a space for the reporter gene to be placed.

It is the most efficient method to transfer of DNA into cells, but it has serious drawbacks such as the risk of recombination, strong immunogenicity and carcinogenicity[56, 59, 60].

There are no methods available that would allow a safe and efficient viral-based gene delivery in the clinic[61]. Because of that, non-viral delivery systems have potential advantages for gene transfer even if they show a lower efficiency than virus-based systems.

2.3.2 Physical methods

Electroporation[62, 63], microinjection[64] and gene gun techniques[65] belong to the physical methods.

2.3.2.3 Electroporation

Electroporation is a popular technique for introducing plasmid DNA into many cell types. Since 1982, electroporation has been used as a method for transfection of mammalian cells[66].

The application of electric pulses opens up pores in the cell membrane through which DNA can pass and directly enter into the cytoplasm. After initial permeabilization, the pores close and DNA is trapped within the cell[62, 63, 67]. This technique has been applied to introduce plasmid DNA into tissues such as muscles[68], melanoma[69], and liver[70].

A number of parameters, including the voltage and the length of the pulse, are important for optimal gene expression. However, there is a great variation in the efficiency with different cell types[68, 71].

2.3.2.1 Microinjection

The microinjection of naked plasmid DNA is the simplest method for DNA delivery. The drawback of the approach is that microinjection can reach only one cell at a time, i.e. it is not applicable for research with large numbers of cells and for DNA delivery in vivo[72].

It was shown that naked DNA cannot successfully enter cells unless it is assisted by a vector[73]. There are many reports about direct injection of naked DNA into the interstitial space of the corresponding tissue: skeletal muscle [74], liver [75], thyroid [76], heart muscle [77], brain [78], and urological organs [79].

The uptake of plasmid DNA by injection is relatively inefficient (in muscle cells less than 1% of the injected dose)[74]. A tail vein injection of naked DNA into

mice did not result in gene expression in major organs[80], because of its rapid in vivo degradation by nucleases [81].
Therefore, the plasmid DNA needs to be protected from degradation before reaching the target cells.

2.3.2.2 Gene gun

Gene gun is the most recent physical transfection technology[82]. The full name of the gene gun is the "biolistic particle delivery system". This technique is based on gold particles which are coated with DNA and shot into target tissues or cells[65]. There are a variety of different engineering strategies, but one way is to accelerate the particles using a pulse of helium. This approach allows DNA to penetrate directly through cell membranes into the cytoplasm or even the nucleus, and to bypass the endosomes, thus avoiding enzymatic degradation. The major limitation concerns the shallow penetration of particles into the tissue. The depth of the particle penetration in skeletal muscle of mouse did not exceed 0.5 mm[83].
Skin, liver, and muscle were transfected by the gene gun technique. The efficiency of transfection varied among tissues, from 10 to 20 % for skin epidermal cells and from 1 to 5 % for muscle cells[65, 83, 84].
However, in vivo gene gun application typically results in short-term and low-level gene expression. Nevertheless, it might be suitable for genetic vaccination[85].

2.3.3 Chemical methods

The chemical methods are generally based on nanoparticles which form a complex with DNA and serve as carriers. These methods can be divided into three big groups: Cationic compounds, recombinant proteins and inorganic nanoparticles.

2.3.3.1 Cationic compounds

Felgner and co-workers[86] were the first to use the cationic lipid dioleoyltrimethylammonium chloride (DOTMA) in a 1:1 molar ratio with the neutral lipid dioleoylphosphatidylethanolamine (DOPE) to condense and transfect DNA. Since then, a variety of cationic lipids was developed for gene transfection. Lipids forms in water vesicular structure are termed liposomes, which can efficiently interact with DNA[87, 88].

The addition of cationic lipids to plasmid DNA decreases its negative charge, thus facilitates its interaction with cell membranes[89, 90]. Neutral lipids such as DOPE or cholesterol are generally added in cationic lipid-DNA complex to facilitate the release of plasmid DNA from the endosome in the cytoplasm[91].

Some cationic lipid-DNA complexes were used in clinical trials[92, 93]. They could be successfully applied to deliver plasmid DNA to lung[94], brain[95], tumors[96, 97], and the skin[98].

One of the first polymers to be used in non-viral gene delivery was poly-L-lysine (PLL)[99, 100]. PLL complexes with a size around 100 nm can be easily taken up by cells, although the transfection efficiency remained low[99]. The reporter gene expression could be improved by inclusion of targeting moieties such as chloroquine[101] or fusogenic peptides.

Another polymer which is widely used for transfection is polyethylenimine (PEI). The major drawback of this polymer is its toxicity[102, 103]. Modified PEI particles were delivered to the liver[104] and to the lungs[105].

The formulations of nanoparticles from biodegradable polymers aimed at gene delivery were also investigated. Poly(D,L-lactide-*co*-glycolide) (PLGA) and polylactic acid (PLA) were most extensively studied[106, 107].

2.3.3.2 Recombinant proteins

Recombinant proteins are a special type of DNA vectors. These proteins have similar properties like viral vectors which are necessary for efficient gene delivery.

Recombinant proteins may include polylysine segments, protamine, or histones to bind DNA to form stable complexes. Polylysine[108] and protamine[109, 110] have properties of DNA condensation which helps to protect DNA from nuclease degradation[110].

They may also contain antibodies, antibody segments for targeting cell delivery and some short peptide sequences acting as nuclear localisation signals.

2.3.3.3 Inorganic nanopartcles

Inorganic materials for DNA delivery such as calcium phosphate[111], carbon materials[112], silica[113], gold[114, 115], magnetite[116], strontium phosphate[117], magnesium phosphate and manganese phosphate[118], and double hydroxides[119, 120] are widely used.

Salem *et al.* reported about bi-metallic nanorods consisting of gold and nickel as a non-viral gene delivery system[121]. The gold and nickel segments in these nanorods can selectively bind plasmid DNA and target ligands. Small biomolecules can be loaded into carbon nanotubes[112]. Choy *et al.* reported about a biomolecular-inorganic hybrid, a class of anionic exchanging clays[119]. Because of its negative charge, DNA can be strongly incorporated into a layered double hydroxide. Gould *et al.* reported about iron oxide particles with diameters ranging from 300 nm to less than 10 nm, which serve as a carrier for DNA[122]. Bhakta *et al.* prepared magnesium and manganous phosphate nanoparticles with a particle size of 100-130 nm functionalized with DNA[118].

The standard calcium phosphate transfection method, originally discovered by Graham in 1977, is the cheapest one[111]. The preparation of the calcium phosphate carrier for transfection consists of a few steps: Mixing of calcium

chloride solution with DNA and addition of HEPES-buffered saline solution containing phosphate ions which results in the formation of fine precipitates of calcium phosphate with DNA. Calcium phosphate nanoparticles have a high biocompatibility and a good biodegradability compared to other types of nanoparticles used for cell transfection.

In Table 2.3.3.1, different transfection methods are summarized and their advantages and disadvantages are shown. Viral carriers are most effective, but a rather dangerous method because of a risk of recombination. Electroporation is a safe, easy and rather efficient method, but it needs a large amount of DNA and has to be optimized for every cell type. Only one cell at a time can be transfected by microinjection which is not suitable for the whole organism. By gene gun technique a shallow penetration of DNA into the tissue is obtained. Cationic compounds and recombinant proteins can be used in clinical trials, but cationic compounds are rather toxic and recombinant proteins are expensive in preparation.

Although inorganic nanoparticles show low transfection efficiencies, the advantages of inorganic nanoparticles over organic ones are that they are not subject to microbial attack, can be easily prepared, have low toxicity and exhibit good storage stability. Therefore, the development of inorganic nanoparticles with all required properties for the efficient and safe gene delivery is the main point of investigations.

Table 2.3.3.1: Comparison of different gene delivery systems

Transfection method	**Advantages**	**Disadvantages**
viral	highly efficient	immunogenicity, carcinogenicity
electroporation	easy to perform; efficient	optimization for every cell line required; expensive; a lot of DNA is necessary
microinjection	exact direction of nucleic acid into a certain cell	one cell at a time
gene gun	use for genetic vaccination	shallow penetration of DNA into the tissue
cationic compounds	easily prepared	high toxicity
recombinant proteins	high biocompatibility	expensive
inorganic nanoparticles	easily prepared; size-controllable; low toxicity	low efficiency

2.4 RNA interference

RNA interference (RNAi) is a process of sequence-specific post transcriptional gene silencing initiated by double-stranded siRNA (small interfering RNA). This phenomenon was discovered in the nematode *Caenorhabditis elegans*[123]. Later this process was extensively studied in other organisms including plants (*Arabadopsis*)[124], flies (*Drosophila*)[125], and humans[126, 127].

When long siRNA is delivered into the cell, it is processed by the RNase III-type endonuclease Dicer into 21-25 bp functional small interfering RNA[128](Figure 2.4.1).

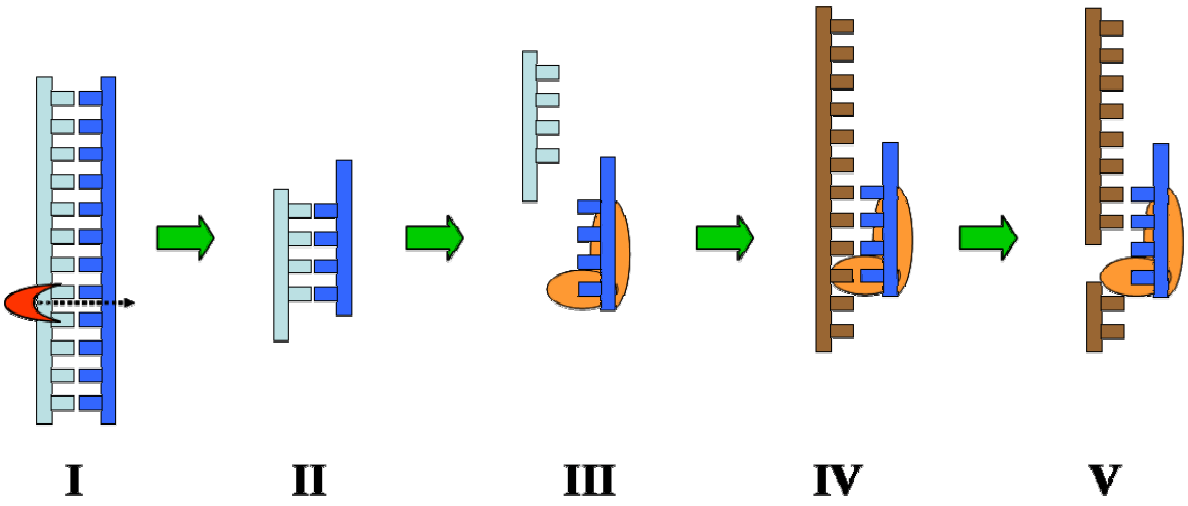

Figure 2.4.1: Schematic representation of gene supression by RNA interference. I: Double stranded RNA, consisting of sense and anti-sense strands, is cleaved by Dicer to produce siRNAs. II: siRNA duplex. III: Incorporation of siRNA into a RISC complex and its unwinding by helicase activity. IV: Hybridization of an anti-sense agent to mRNA. V: Cleavage of target mRNA.

The siRNAs subsequently assemble with protein components into an RNA-induced silencing complex (RISC). The siRNA strands are then unwound to form activated RISCs. These activated RISCs then bind to complementary RNA molecules by base pairing interactions between the siRNA antisense strand and

the mRNA. The bound mRNA is cleaved and sequence specific degradation of mRNA results in gene silencing.

In plants, worms and flies, the introduction of large siRNAs can efficiently induce gene silencing. This process has been also extended to mammalian cells with a few modifications. In mammalian system only short RNA duplexes of length approximately 21 bases can be used because longer siRNA evokes a nonspecific interferon response, which usually leads to nonspecific shutdown of protein synthesis and global RNA degradation[129]. Mammalian cells, in contrast to worms and flies, require a delivery system for RNA, such as a cationic lipid or calcium phosphate.

RNAi technology has been successfully applied to identify genes with essential roles in biochemical signalling cascades, embryonic development, and other basic cellular process[130]. This technology is also widely applied for analyzing gene functions and for identifying and testing the new targets for diseases including cancer[131, 132].

3 Results and Discussion

3.1 Synthesis and characterization of DNA-functionalized calcium phosphate nanoparticles and their role as carriers for transfection

Calcium phosphate is the inorganic component of many biological hard tissues, e.g. teeth and bone[133-135]. Therefore, it generally has a high biocompatibility which makes it suitable for the preparation of biomaterials[12]. In biochemistry, *in situ* precipitated dispersions of calcium phosphate are used for cell transfection[136, 137], i.e. for the non-viral introduction of DNA into living cells, first introduced by Graham *et. al.* in 1973[111].

Calcium phosphate nanoparticles are very well suited for cell transfection, because an *in-situ* precipitation of the inorganic salt in the presence of DNA gives nanoparticles which cells can immediately take up. This has been the subject of extensive investigations[111, 136-145]. The method is very easy and inexpensive, but the transfection efficiency is inferior to commercially available transfection agents which are based on liposomes[87, 88] and polymers[146].

The standard calcium phosphate method strongly depends on the experimental parameters such as concentration, pH, precipitation time, type of DNA and also on the experimentalist[137, 142, 147, 148]. Consequently, it has to be optimized for every cell line and for every laboratory setting. The transfection solutions cannot be stored because the calcium phosphate nanocrystals grow with time into ineffective microcrystals. It was shown that the successful transfection of cells strongly depends on the particle size[113, 116, 136]. Organic and inorganic additives were therefore used to preserve the small size of calcium phosphate particles and to inhibit their subsequent growth. Chowdhury *et al.* prepared calcium phosphate nanoparticles with the addition of magnesium, causing an inhibition of the particle grow and a higher transfection efficiency[149]. Kakizawa *et al.* prepared nanoparticles consisting of calcium phosphate, DNA and block-copolymers. A small size of the particles and good colloidal stability was

achieved by the steric effect of a poly(ethylene glycol) (PEG) layer surrounding the calcium phosphate core[145, 150].

Prabha *et al.* prepared PLGA nanoparticles by an emulsion evaporation technology. The smaller (70 nm) and larger nanoparticles (202 nm) were separately used for transfection. The small particles were 4-27 times more effective in the transfection than the large ones (depending on the cell line)[143].

Zhan *et al.* reported the preparation of superparamagnetic magnetite nanoparticles with a size of 10 nm, which were able to successfully penetrate the cell membrane[116].

Zhu *et al.* prepared oligonucleotide loaded microparticles with the size around 20 µm from poly(lactide-*co*-glycolide)-polyethylene glycol as a local active substance[151]. Nsereko and Amiji prepared chitin particles with a similar size for the delivery of paclitaxel[152].

The preparation of calcium phosphate nanoparticles especially for cell transfection was extensively carried out and investigated. Roy *et al.* reported the preparation of DNA incorporated calcium phosphate nanoparticles and the influence of DNA on the crystallinity of calcium phosphate[136]. The particles were crystalline without and amorphous with DNA. Jordan *et al.* varied in a systematic way the calcium and phosphate concentrations, the precipitation temperature and the precipitation time and studied the transfection efficiency. One minute of precipitation time gave the highest transfection efficiency. A longer time results in a decrease of the transfection efficiency. At a very high concentration of DNA the precipitation was completely inhibited, which suggests a clear interaction between DNA and calcium phosphate[139]. The time between precipitation solutions and their addition to the cells played a critical role. Depending on the precipitation method an increase or decrease of the transfection efficiency within 1 to 30 min was observed[148].

Yang and Yang studied the transfection efficiency of calcium phosphate precipitates as a function of cell medium, pH and time by transmission electron

microscopy. They observed a growth of the initially developed small crystallites. The crystallite sizes were approximately 50-100 nm. The pH was varied between 6.48 and 10.01 during the precipitation[140]. Seelos reported about time-dependent transfection experiments. If a freshly precipitated calcium phosphate developed into larger crystals, then the transfection was less effective. There is an inhibitory effect of proteins in the growth medium which has a strong influence on the crystal growth[148].

According to the current state of knowledge, calcium phosphate nanoparticles are incorporated into the cells by endocytosis (penetration of the cell membrane and uptake into an intracellular vesicle). DNA has to overcome several physical and chemical barriers before it can enter the nucleus (Figure 3.1.1), e.g. intracellular degradation in lysosomes in the cytoplasm[39, 153].

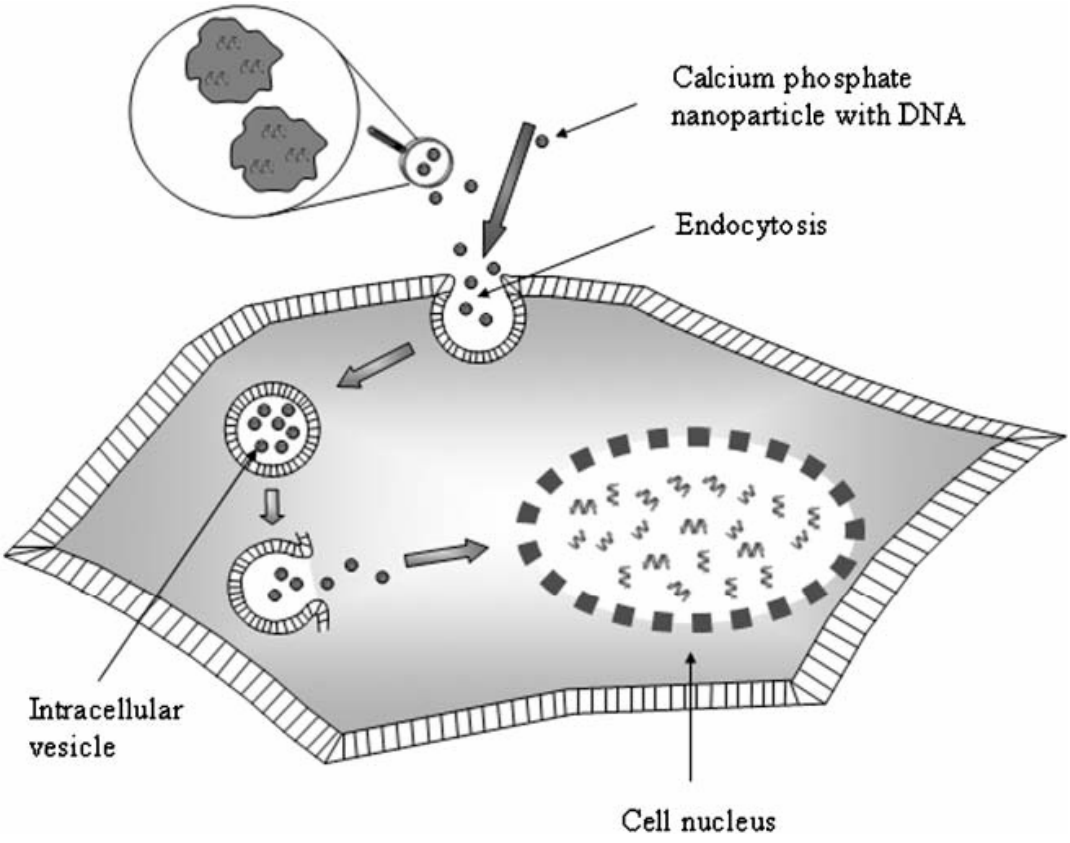

Figure 3.1.1: Schematic representation of the transfection mechanism[154].

Some studies were carried out to elucidate the pathway of DNA. Strain *et al.* found less than 7 % of the applied DNA inside the cells and less than 4 % in the

nucleus. Only 0.5 % of DNA was still undegraded and active[138]. Orrantia and Chang studied the way of ^{32}P-marked DNA into the cell and concluded that the morphology of the colloids and the protection from degrading enzymes played an important role for the transfection efficiency[147, 155]. Loyter *et al.* carried out investigations with ^{3}H-marked DNA to show the importance of the nanoparticle morphology (mainly the particle size)[153].

Taking into account all previously discussed, we can say that for a successful transfection it is important to have well-defined nanoparticles, which should be as small as possible. Nanoparticles have to incorporate the DNA, in order to prevent its intracellular degradation by enzymes.

Welzel *et al.* have shown how nanoparticles of calcium phosphate can be prepared with defined particles size[156] and how custom-made DNA-functionalized calcium phosphate nanoparticles can be used for cell transfection[154]. However, the colloid-chemical characterization of these nanoparticles was very preliminary, and there were some larger aggregates within the dispersions.

We demonstrate how stable dispersions can be prepared by variation of the inorganic part of the system, i.e. by substitution of cations within the calcium phosphate, and how DNA can be incorporated into the particles. This is a major goal for a potential biochemical application because DNA on the outside of particles is easily degraded within a cell and therefore cannot reach the nucleus.

3.1.1 Plasmid DNA, pcDNA3-EGFP, applied for transfection

Enhanced green fluorescent protein (EGFP) is a commonly used reporter system[157]. When this EGFP gene is successfully incorporated into the cell's genome, it causes the synthesis of enhanced green fluorescent protein, which can be detected by fluorescence microscopy. The emission of fluorescent light occurs, when EGFP exited at a wavelength of around 488 nm[157]. In this work plasmid DNA, pcDNA3-EGFP, was used. It was used for the stabilization of colloids and at the same time for the determination of the transfection efficiency. It is difficult to determine the size of plasmid DNA by electron microscopy, therefore the size of DNA was estimated as follows.

The information shown below was used for the calculation:

1. The size of pcDNA3 is 5441 bp;
2. The molar mass of the whole vector is 1 871 704 g mol^{-1}, which came from the multiplication of the average molar mass of one nucleotide (344 g mol^{-1}) by the size of the plasmid DNA (5441 bp)
3. The density of DNA is approximately 1.42 g cm^{-3} [158]

The volume of one mol is 1318101.4 cm^3 mol^{-1} which comes from the equation:

$V_m = M \rho^{-1}$ (M is the molar mass; ρ is the density of DNA)

If molar volume is divided by Avogadro constant (N_a), the volume of one DNA molecule is $2.19 \cdot 10^{-18}$ cm^3.

From

$$V = 4/3\ \pi r^3$$

the radius of a sphere of plasmid DNA is 8.04 nm, consequently its diameter is about 16 nm.

3.1.2. Optimization of calcium and phosphate concentration and the amount of DNA

Calcium phosphate nanoparticles were prepared by rapid mixing of aqueous solutions of calcium and phosphate, followed by addition of DNA to the formed dispersion. (Figure 3.1.2.1).

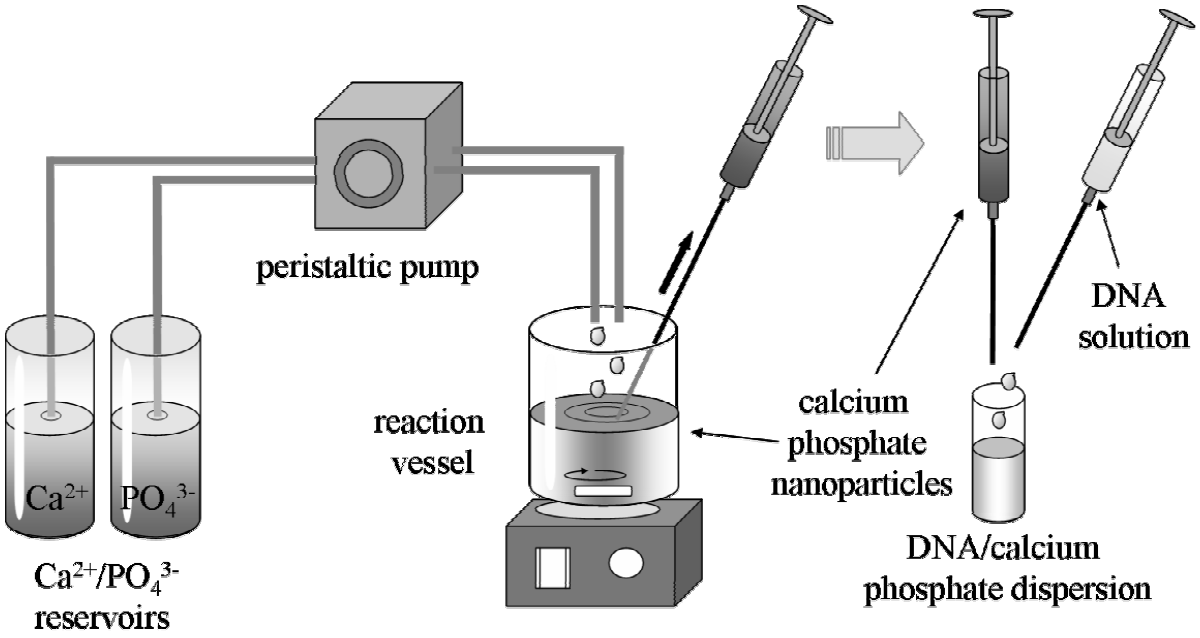

Figure 3.1.2.1: Schematic setup of the apparatus used for preparation of DNA-functionalized calcium phosphate nanoparticles. Calcium nitrate and diammonium hydrogen phosphate solutions are mixed in a vessel to form a precipitate. A part of the dispersion is taken with a syringe and mixed with DNA solution in an Eppendorf tube.

Our goal was to prepare stable colloids with small nanoparticles up to 100 nm in size. First of all we had to find the optimal concentration parameters to prevent the formation of larger particles and thereby precipitation. Two different concentrations of calcium (6.25 mM and 18 mM) and phosphate (3.74 mM and 10.8 mM) with the stoichiometric ration, corresponding to hydroxyapatite, $Ca_5(PO_4)_3OH$ ($Ca:PO_4=n:n=1.67$) were used. A solution with the concentration of calcium (6.25 mM) and phosphate (3.74 mM) gave the best results after addition of DNA for colloidal stabilization.

The amount of DNA on the surface of such nanoparticles influenced their charge which can be estimated by the zeta potential. The negatively charged DNA reversed the initially positive surface charge to negative values. In Figure 3.1.2.2 it can be seen that there is no change above about 0.2 mL DNA solution, i.e. we assume that the surface was fully covered with DNA at or above this concentration.

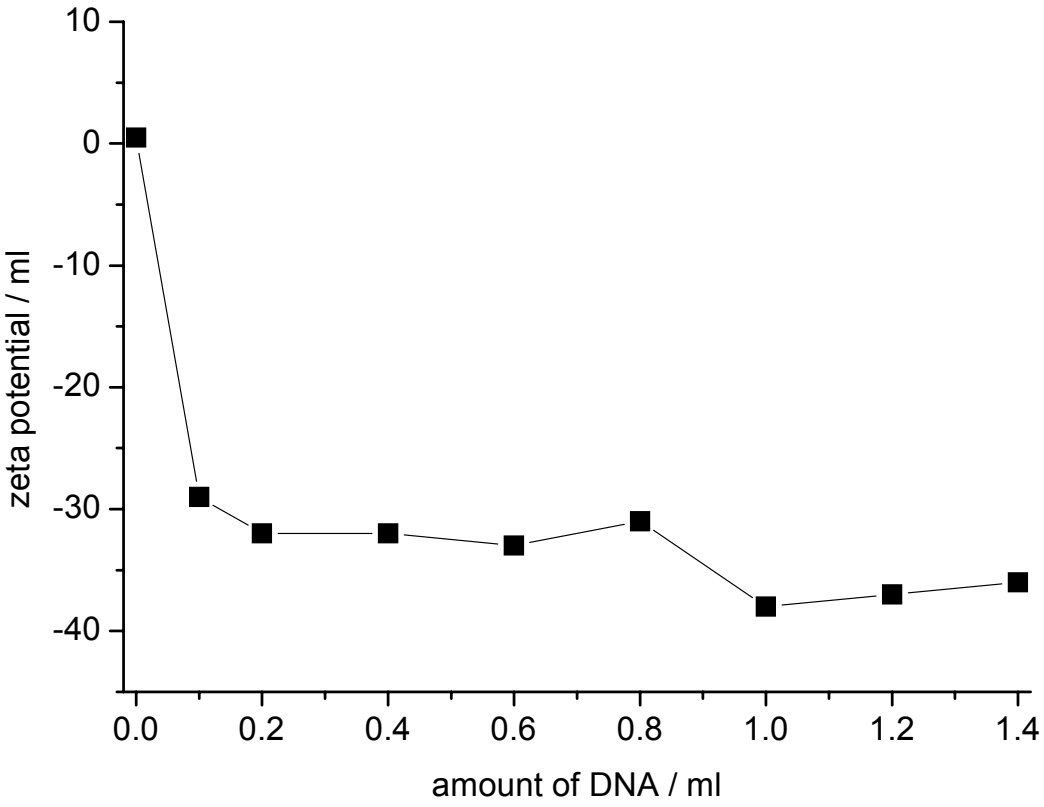

Figure 3.1.2.2: Effect of the amount of DNA solution ([DNA]=1 mg mL^{-1}) on the surface charge (expressed by the zeta potential) of the colloids (1 mL calcium phosphate dispersion with 6.25 mM Ca^{2+} and 3.74 mM PO_4^{3-} in all cases). There is no further adsorption of DNA above about 0.2 mL.

The influence of the amount of DNA on the particle size was also studied. The results from dynamic light scattering measurements are presented in Table 3.1.2.1. The optimal amount of DNA (0.2 mL) was found at which the colloid is monodisperse consisting of nanoparticles with diameter 36 nm. When the amount of DNA was lower than 0.2 mL, larger particles were observed. When

the amount of DNA was too high (0.3 mL and more), the polydispersity index (PDI) was very high, i.e. different fractions of particles were present.

Table 3.1.2.1: Colloid-chemical data of functionalized calcium phosphate nanoparticles with different amounts of DNA ([DNA]=1 mg mL^{-1}). The volume of calcium phosphate dispersion before mixing with DNA was always 1 mL. The percentages in the particle distributions give the volume distribution of the particles from dynamic light scattering. PDI denotes polydispersity index.

Sample	DNA / mL	PDI	Size of particles / nm	%	Zeta potential / mV
A	0.1	0.3	74	88	-29 (5)
B	**0.2**	**0.25**	**36**	**98**	**-33 (4)**
C	0.4	0.6	26	92	-32 (4)
D	0.6	0.5	22	99	-33 (7)
E	0.8	0.6	11	100	-31 (6)
F	1.0	0.5	37	100	-38 (3)
G	1.2	0.6	15	100	-37 (9)
H	1.4	0.6	13	99	-36 (5)

Analytical ultracentrifugation was used to see if all DNA was adsorbed on the surface or if there was free DNA in solution. Figure 3.1.2.3 shows typical distributions of the sedimentation coefficient for pure DNA and for the colloidal dispersion. From integration of the peak for DNA (s=1 to $5 \cdot 10^{-13}$ s) it can be derived that about 10 % of DNA was free in the colloidal dispersion and that consequently about 90 % were bound to the surface of the particles.

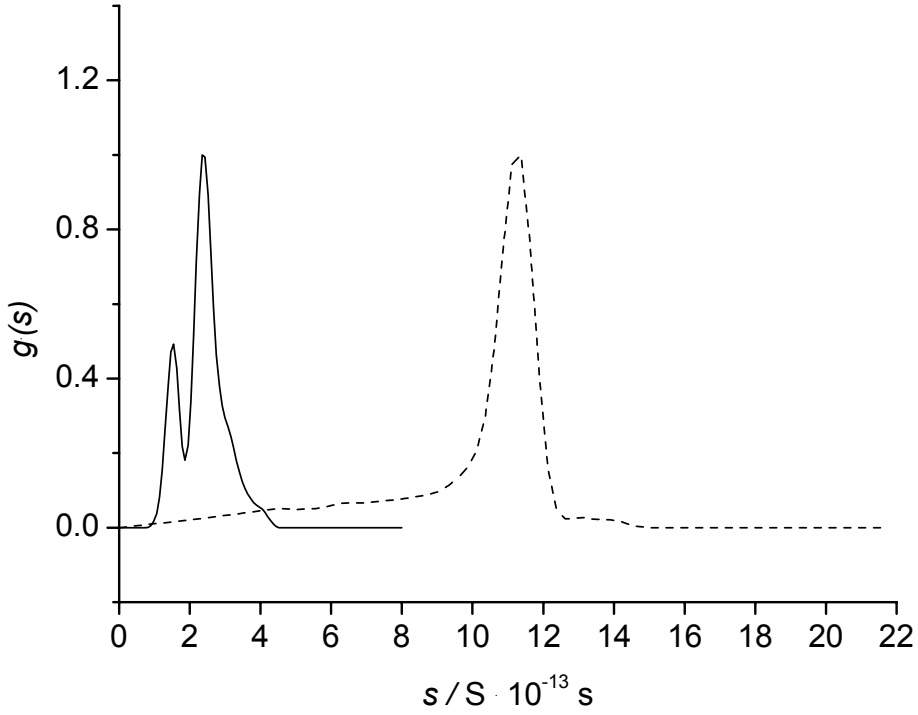

Figure 3.1.2.3: Sedimentation coefficient distribution of pure aqueous DNA solution (solid line; 0.5 mg mL^{-1}), and of calcium phosphate/DNA colloids (dashed line; 6.25 mM Ca^{2+} and 3.74 mM PO_4^{3-} with 1 mL of DNA of 1 mg mL^{-1}). The peaks at 1.5 and 2.5 correspond to free DNA and the peak at 12 corresponds to the DNA-coated calcium phosphate nanoparticles. There is almost no free DNA in the colloidal dispersion (Table 3.1.2.1 sample F).

3.1.3. Optimization and characterization of calcium phosphate/DNA nanoparticles with additions of magnesium and aluminum

To prevent the particle growth, magnesium and aluminum were tested as additives. Magnesium is a well known inhibitor of calcium phosphate crystal growth[149, 159]. The incorporation of the trivalent aluminum may introduce a higher positive charge when it substitutes for the divalent calcium. The addition of magnesium will be first discussed.

The initial concentration of magnesium (3 mM, 6 mM, 9 mM, 12 mM, 15 mM) was varied at a low concentration of calcium and phosphate (6.25 and 3.74 mM). Results from analytical ultracentrifugation are shown in Figure 3.1.3.1. It

can be clearly seen that the smallest sedimentation coefficient was found at magnesium concentration of 6 mM (*S*=10), i.e. the particles had the smallest size. If the concentration of magnesium was lower or higher than 6 mM, at this concentration the particle size is increased (Figure 3.1.3.1)

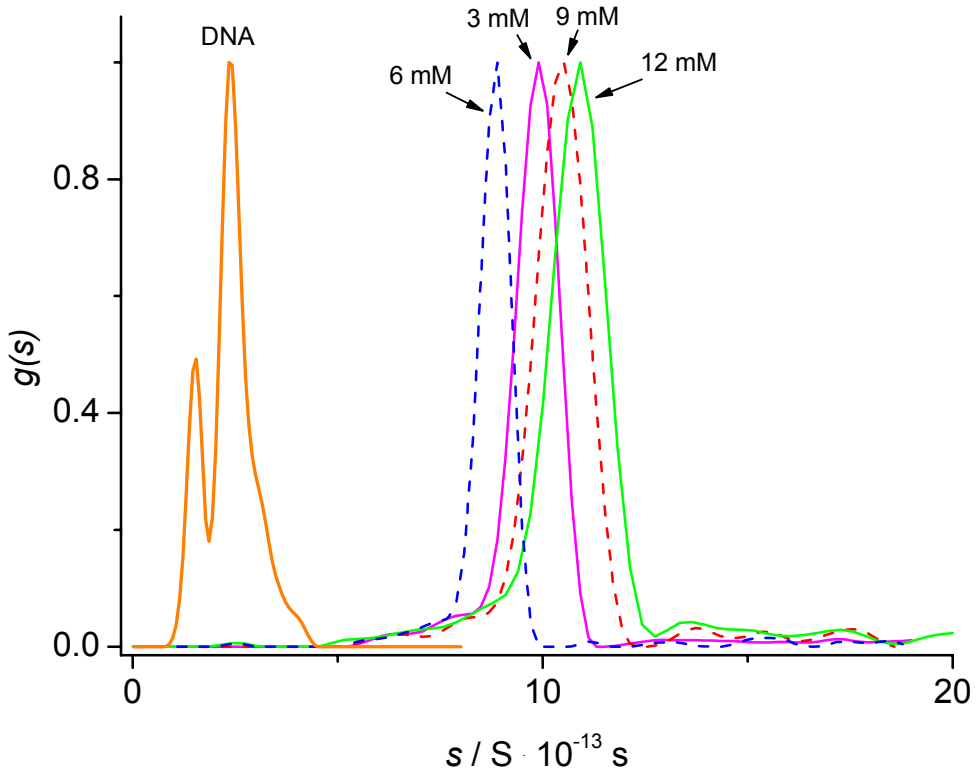

Figure 3.1.3.1: Sedimentation coefficient distribution of pure aqueous DNA solution (0.5 mg mL^{-1}) and of calcium phosphate/DNA colloids with addition of magnesium with different concentration (3 mM; 6mM; 9 mM; 12 mM). Arrows show the peaks at the corresponding concentration of magnesium. The peaks at 1.5 and 2.5 correspond to free DNA. There is no free DNA in the colloidal dispersion. Nanoparticles were prepared at the low concentration of calcium and phosphate (1mL; 6.25 mM and 3.74 mM) with 1.0 mL of DNA (1 mg mL^{-1}).

Particle size and DNA adsorption were studied by dynamic light scattering and analytical ultracentrifugation. The nanoparticles in the presence of magnesium were smaller in comparison to nanoparticles without magnesium. The optimal concentration of magnesium was 6 mM which led to two fractions with a particle size around 11 nm and 76 nm (Table 3.1.3.1; sample D). Analytical

ultracentrifugation again confirmed the almost complete adsorption of DNA on the surface of the particles, i.e. almost no free DNA was detected (comparable to Figure 3.1.2.3). If calcium was absent, i.e. if pure magnesium phosphate was precipitated, a particle size of about 32 nm was obtained (Table 3.1.3.1; sample E).

The initial concentration of aluminum was also varied (1 mM, 2 mM, 4 mM). Figure 3.1.3.2 shows the results from analytical ultracentrifugation for calcium phosphate nanoparticles with addition of aluminum. As aluminum can be toxic

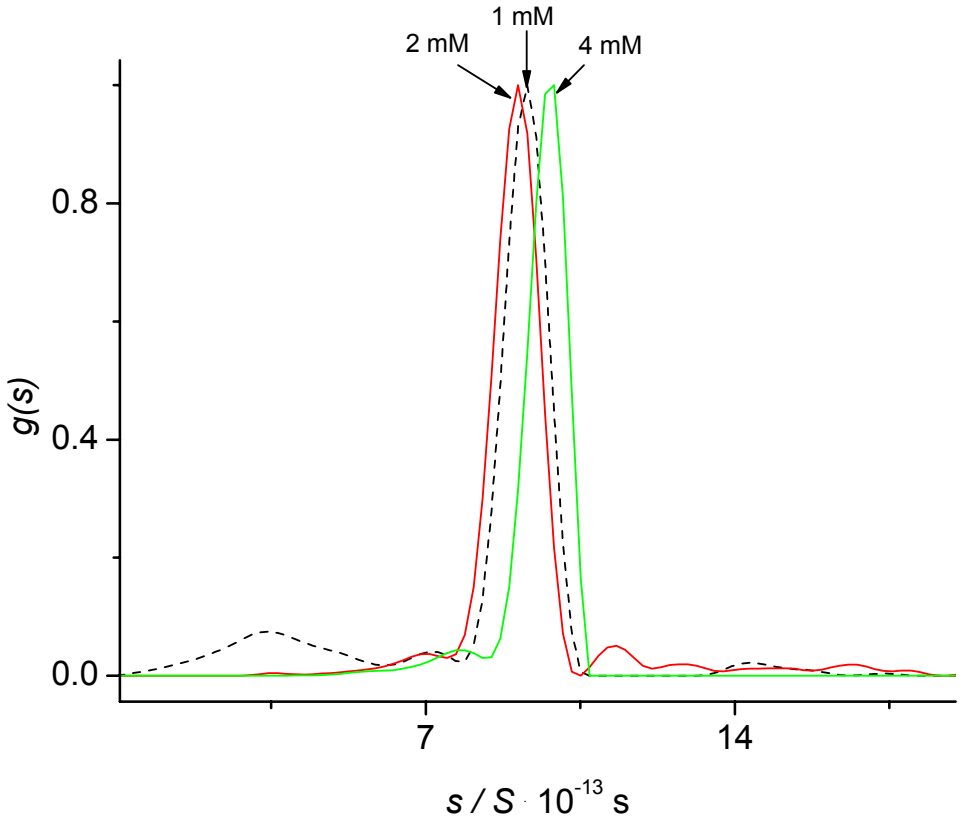

Figure 3.1.3.2: Sedimentation coefficient distribution of calcium phosphate/DNA colloids with addition of aluminum with different concentration (1 mM; 2 mM; 4 mM). Arrows show the peaks at the corresponding concentration of aluminum. Nanoparticles were prepared at the low concentration of calcium and phosphate (1 mL; 6.25 mM and 3.74 mM) with 1.0 mL of DNA (1 mg mL^{-1}) (Table 3.1.3.1; sample G).

for cells, e.g. in transfection studies, a small concentration of aluminum was chosen. Calcium phosphate/DNA nanoparticles with the addition of aluminum (2 mM) showed a good inhibitory effect on the particle size (*S*=8.7 compared to that of calcium phosphate/DNA without aluminum *S*=11.3). By analytical ultracentrifugation was found that the optimal concentration of aluminum was 2 mM at the low concentration of calcium and phosphate (6.25 and 3.74 mM) (see Figure 3.1.3.2).

Aluminum and magnesium both inhibited the growth of the nanoparticles. Small particles with about 21 nm in diameter were obtained according to dynamic light scattering. This corresponded well to TEM results (Figure 3.1.3.3).

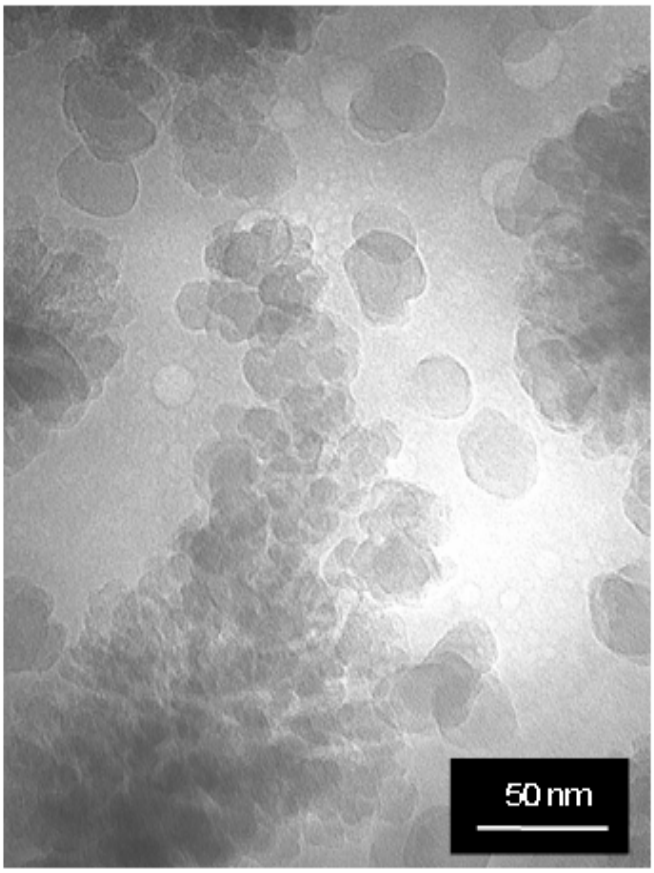

Figure 3.1.3.3: Transmission electron micrograph of calcium phosphate nanoparticles with addition of aluminum, functionalized by 1.0 mL DNA. The particles had a typical size of 15 to 30 nm (Table 3.1.3.1; sample G).

In contrast, we found larger particles when we prepared aluminum phosphate colloids, i.e. without calcium (Table 3.1.3.1; sample H). In this case, the particle size was up to 306 nm with aggregates. However, DNA adsorbed with high efficiency if aluminum was present as shown by the strongly negative zeta potential. This might be ascribed to an initially more positive surface charge if Al^{3+} substituted for Ca^{2+} which in turn increased the adsorption of the negatively charged DNA.

To compare the morphology and size of pure calcium phosphate nanoparticles to those with addition of magnesium and aluminum different methods of analysis were used. It is possible to compare the size of three types of

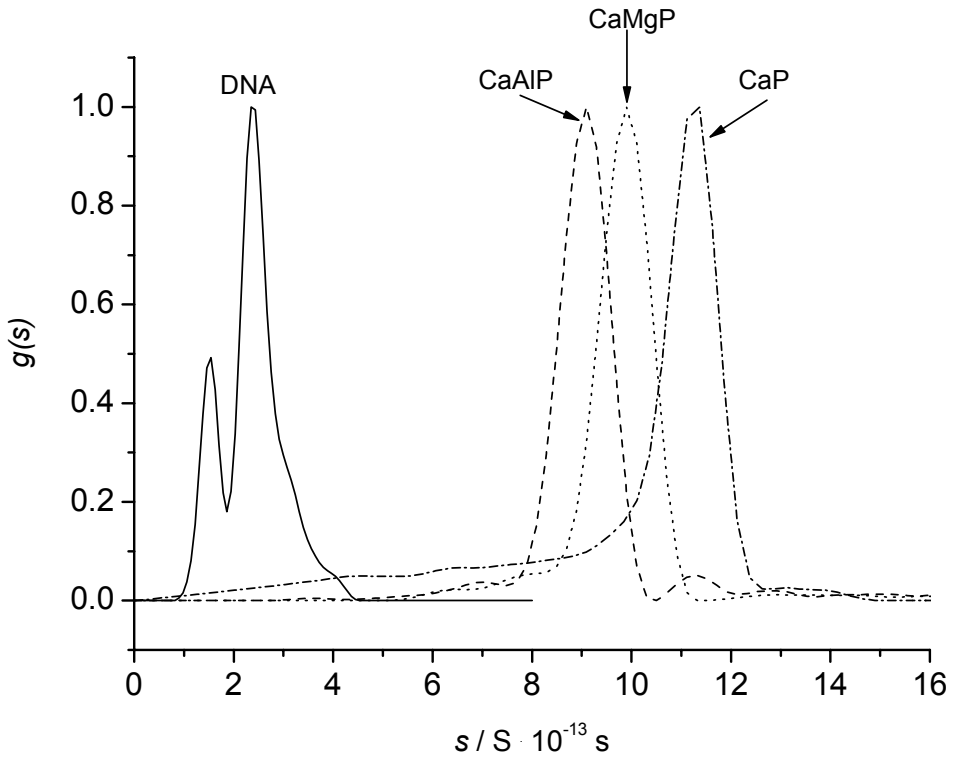

Figure 3.1.3.4: Sedimentation coefficient distribution of pure aqueous DNA solution (0.5 mg mL^{-1}). Arrows denote the peaks corresponding to DNA, calcium phosphate/DNA colloids without and with additions of aluminum and magnesium. Nanoparticles were prepared at the low concentration of calcium (6.25 mM), phosphate (3.74 mM), magnesium (6 mM) and aluminum (2 mM) with 1.0 mL of DNA (1 mg mL^{-1}).

nanoparticles, calcium phosphate/DNA (CaP), calcium phosphate/DNA with aluminum (CaAlP) and calcium phosphate/DNA with magnesium (CaMgP). The results from analytical ultracentrifugation measurements are represented in Figure 3.1.3.4. The nanoparticles with addition of magnesium or aluminum were smaller in comparison to nanoparticles without those.

SEM pictures show the morphology of the calcium phosphate nanoparticles with the addition of magnesium; magnesium phosphate and aluminum phosphate nanoparticles (Figure 3.1.2.5). All types of particles have a spherical morphology.

The schematic representation of the particle size is shown in Figure 3.1.3.6.

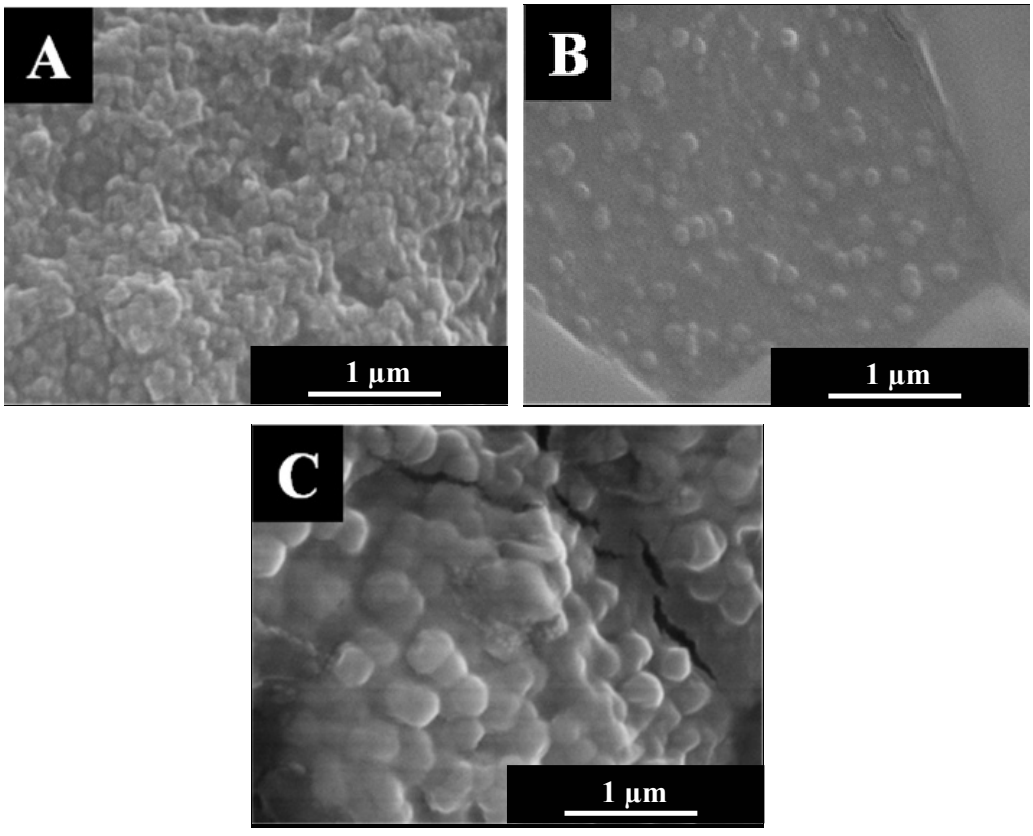

Figure 3.1.3.5: Scanning electron micrographs of calcium phosphate nanoparticles with additions of magnesium (A); magnesium phosphate (B) and aluminum phosphate nanoparticles (C). Nanoparticles were prepared at the low concentration of calcium (6.25 mM), phosphate (3.74 mM), magnesium (6 mM) and aluminum (4 mM) with 0.2 mL of DNA (1 mg mL^{-1}) (Table 3.1.3.1; samples D, E, H).

Calcium phosphate/DNA nanoparticles showed a particle size around 36 nm, with addition of aluminum the size decreased to 21 nm and with magnesium two different fractions with the size 11 nm and 76 nm were observed (Figure 3.1.3.6). Magnesium phosphate/DNA nanoparticles were also small (32 nm).

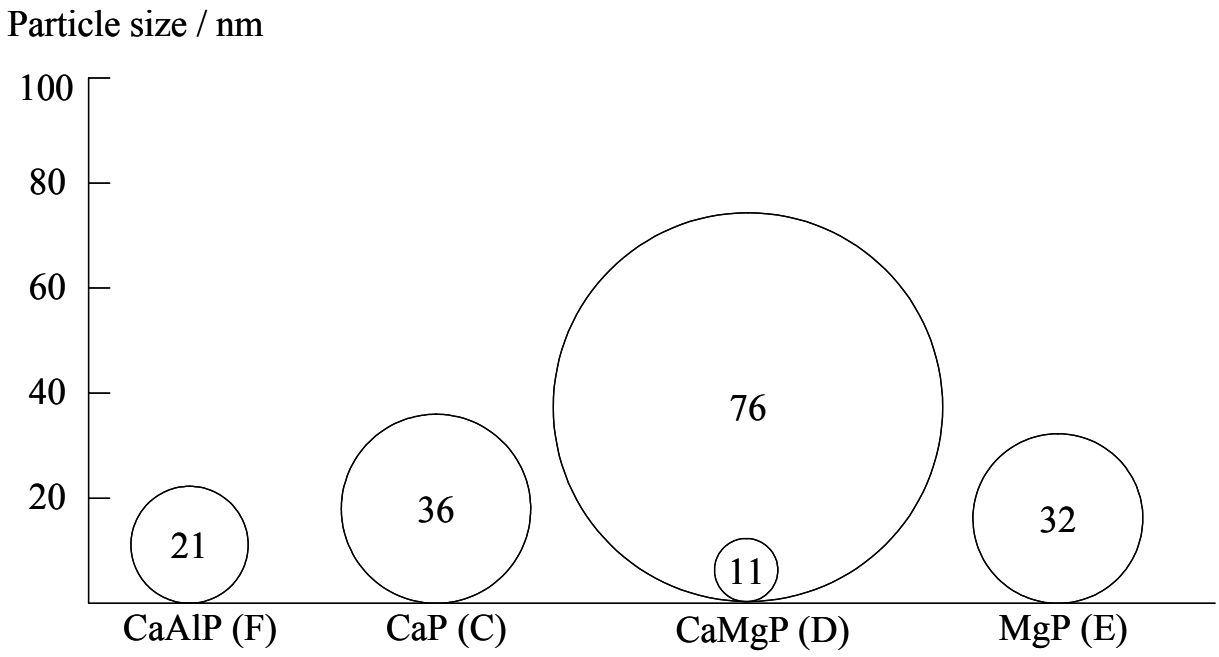

Figure 3.1.3.6: Schematic representation of the particle size for pure calcium phosphate and for calcium phosphate precipitated in the presence of aluminum or magnesium by dynamic light scattering. All colloids were stabilized with 0.2 mL DNA (1 mg mL^{-1}); sample numbers (Table 3.1.3.1). given in parentheses.

At the high concentration of calcium and phosphate (18 mM and 10.8 mM) we also obtained small nanoparticles with a hydrodynamic diameter of 35 nm (Table 3.1.3.1; sample I).

Table 3.1.3.1: Colloid-chemical data of functionalized calcium phosphate nanoparticles. The volume of calcium phosphate dispersion before mixing with DNA (1 mg mL^{-1}) was always 1 mL (*s**=sedimentation coefficient from analytical ultracentrifugation). The percentages in the particle distributions give the volume distribution of the particles from light scattering.

Sample						Zeta potential / mV	Size of small particles / nm	%	Size of large particles / nm	%	*s* / S · 10^{-13} s
	$[Ca^{2+}]$ / mM	$[HPO_4^{2-}]$ / mM	DNA / mL	$[Mg^{2+}]$ / mM	$[Al^{3+}]$ / mM						
A	18	10.8	-	-	-	3(3)	346	30	1961	70	-
B	6.25	3.74	-	-	-	0.5(3)	-	-	1320	100	-
C	6.25	3.74	0.2	-	-	-33(4)	36	99	-	-	16
D	6.25	3.74	0.2	6.0	-	-25(4)	11	63	76	33	-
E	-	3.74	0.2	6.0	-	-25(4)	32	99	-	-	-
F	6.25	3.74	0.2	-	2.0	-28(4)	21	99	-	-	-
G	6.25	3.74	1.0	-	2.0	-35 (4)	40	90	225	2	8.7
H	-	3.74	0.2	-	4.0	-66(5)	82	47	306	22	-
I	18	10.8	0.2	-	-	-32(5)	35	92	272	5	19

3.1.4 Transfection experiments with calcium phosphate/DNA nanoparticles

The DNA-loaded calcium phosphate nanoparticles were prepared by a straightforward precipitation method (Figure 3.1.2.1). The transfection was carried out with the DNA-loaded calcium phosphate nanoparticles with the fluorophor protein coding for plasmid DNA, pcDNA3-EGFP. As control, the standard calcium phosphate method and a commercial dendrimer-based transfection agent (Polyfect®) were used. The amounts of DNA in the different transfection experiments were comparable (see Experimental chapter 4.5).

For the preliminary experiments, T-HUVEC (transformed human umbilical vein endothelial cells) were used. T-HUVEC were obtained after spontaneous transformation of primary HUVEC[160] which are good *in vitro* models for understanding the mechanism of angiogenesis which plays a critical role in many physiological processes[161]. Furthermore, they are models for endothelial cell-derived tumors.

The results are summarized in Table 3.1.4.1. The transfection efficiency using Polyfect® (9.9 %) was the highest as expected, and was used as reference. Using the standard calcium phosphate method we obtained about 2.5 % transfected cells while the calcium phosphate/DNA nanoparticles gave up to 3.1 % (at the low concentration of calcium and phosphate of 6.25 mM and 3.74 mM) and 3.5 % (at the high concentration of 18 mM and 10.8 mM). The transfection efficiency of calcium phosphate/DNA nanoparticles with additions of magnesium (6 mM) and aluminum (2 mM) was 2.1 % and 2.6 % respectively. For magnesium phosphate/DNA (at the concentration of magnesium of 6 mM) and aluminum phosphate/DNA nanoparticles (at the concentration of aluminum of 4 mM) the transfection efficiency was below 1 % and could not be quantified.

Table 3.1.4.1: Results of all transfection experiments with T-HUVEC in serum-free RPMI 1640 medium (average of several experiments; 0.2 mL DNA with 1 mg mL^{-1} calcium phosphate solution; 3.3 µg DNA per transfection). Nanoparticles were prepared at the low concentration of calcium and phosphate (6.25 mM and 3.74 mM). For the calcium phosphate/DNA nanoparticles dispersion at a high concentration of calcium and phosphate (18 mM and 10.8 mM) the transfection efficiency is given in parentheses (Table 3.1.3.1; samples C, D, E, F, H).

Method	**Transfection efficiency / %**
Polyfect®	9.9 ± 3.8
Standard calcium phosphate precipitation method	2.5 ± 2.1
Calcium phosphate/DNA nanoparticles	3.1 ± 1.3 (3.5 ± 0.8)
Calcium phosphate/DNA nanoparticles with the addition of magnesium (6 mM)	2.1 ± 0.4
Calcium phosphate/DNA nanoparticles with the addition of aluminum (2 mM)	2.6 ± 0.5
Magnesium phosphate/DNA nanoparticles (6 mM)	< 1 %
Aluminum phosphate/DNA nanoparticles (4 mM)	< 1 %

It is important to note that at a high concentration of calcium and phosphate (18 mM, 10.8 mM) the transfection efficiency was higher compared to the low concentration (6.25 mM and 3.74 mM) and easier to reproduce. Therefore, for further experiments the high concentration was used.

Futher transfection experiments were carried out with T-HUVEC and two other cell lines (HeLa and LTK) in different media. These cell lines were a representative choice out of cell lines typically used in cell biology: T-HUVEC (human, endothelial cells), HeLa (human, epithelial cells), and LTK (mouse, fibroblasts). HeLa and LTK cells were easier to transfect with Polyfect® or other non-viral vectors than T-HUVEC (Table 3.1.4.2). However, for DNA-loaded calcium phosphate nanoparticles, the transfection efficiency was somewhat higher for HeLa cells (4-10 %, depending on the medium) and almost the same

for LTK and T-HUVEC (2-4 %). The transfection efficiency also depended on the cultivation medium (Table 3.1.4.2). The efficiency increased when serum-free (i.e. protein-free) medium was used as solvent for the DNA-coated nanoparticles. This is probably due to an interaction between protein and nanoparticles. The reason for this behaviour is not known, but there may be an interaction between the DNA-coated surface and the chemically affine proteins that leads to bridging and agglomeration.

Table 3.1.4.2: Results of all transfection experiments with HeLa, LTK and T-HUVEC (average of several experiments; 0.2 mL DNA with 1 mg mL^{-1} calcium phosphate solution; 3.3 µg DNA per transfection). Nanoparticles were prepared at the high concentration of calcium and phosphate (18 mM and 10.8 mM).

Cell line	Method	Transfection efficiency / %		
		Quantum® medium	RPMI 1640 with FCS	Serum-free RPMI 1640
HeLa	Polyfect®	19.4 ± 0.6	18.3 ± 3.8	31.6 ± 5.4
	Standard calcium phosphate precipitation method	4.5	11.7	22
	Calcium phosphate/DNA nanoparticles	4.0 ± 0.3	4.2 ± 1.6	10.0 ± 2.4
LTK	Polyfect®	17.4 ± 0.2	9.9 ± 2.3	21.9 ± 5.4
	Standard calcium phosphate precipitation method	6.2	8.3	9.5
	Calcium phosphate/DNA nanoparticles	2.4 ± 0.6	2.2 ± 0.2	3.9 ± 0.6
T-HUVEC	Polyfect®	9.9 ± 4.0	10.9 ± 3.0	9.9 ± 3.8
	Standard calcium phosphate precipitation method	2.8 ± 2.5	5.2 ± 0.2	2.5 ± 2.1
	Calcium phosphate/DNA nanoparticles	2.9 ± 0.6	2.7 ± 1.2	3.5 ± 0.8

In all cases, the transfection efficiency was smaller with the calcium phosphate nanoparticles than with the commercial agent (Polyfect®). Consequently, we tried to increase the efficiency of the nanoparticles by variation of the accessible parameters such as the amount of DNA and pH. First we studied the effect of the amount of DNA in the dispersion on the transfection efficiency. Only insignificant differences were observed with T-HUVEC, even with a fivefold amount of DNA (Figure 3.1.4.1).

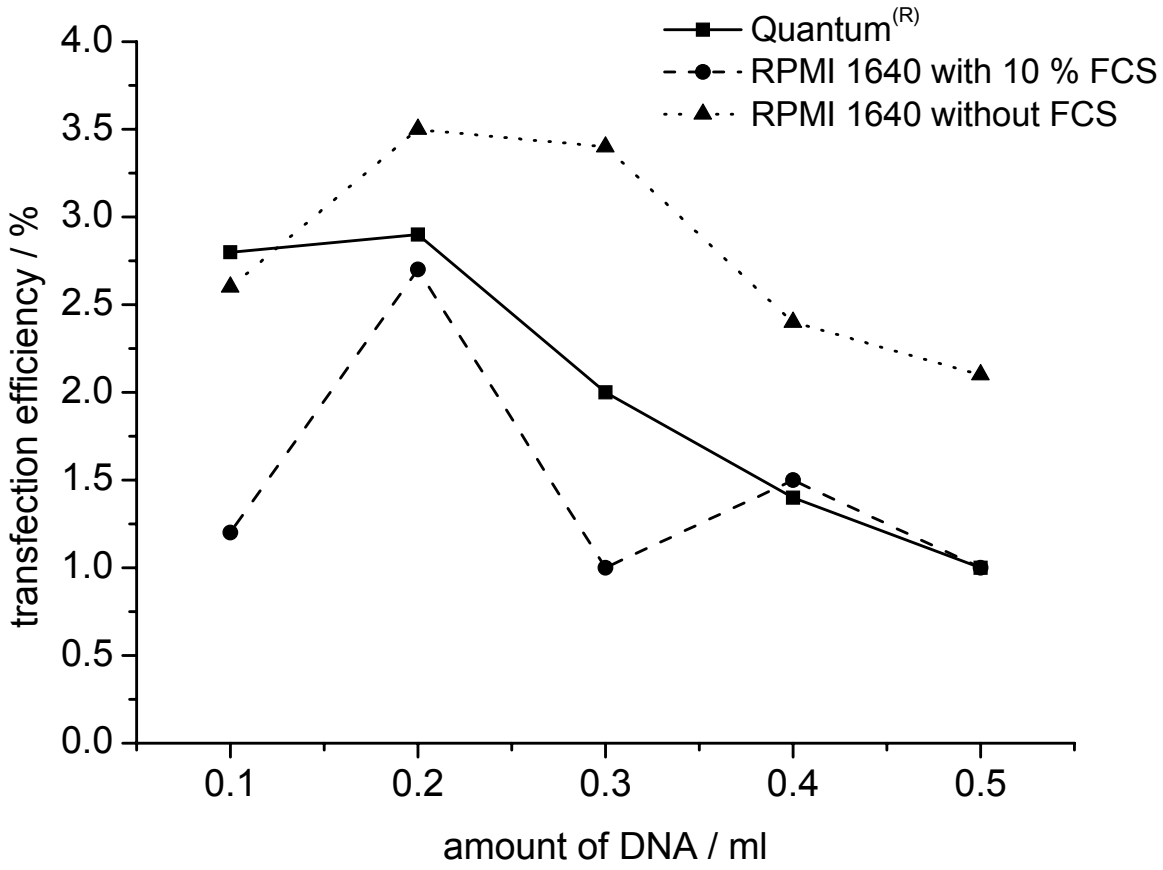

Figure 3.1.4.1: Effect of the amount of DNA ([DNA]=1 mg mL^{-1}) in the colloids on the transfection efficiency of T-HUVEC cultured in different media. The corresponding amounts of DNA per transfection were 1.8 µg (0.1 mL), 3.3 µg (0.2 mL), 4.6 µg (0.3 mL), 5.7 µg (0.4 mL), and 6.7 µg (0.5 mL). The variation in the transfection efficiency was not significant.

The scatter in the results is probably statistically insignifican. We conclude that a simple increase of the amount of DNA (going from 1.8 µg to 6.7 µg) does not increase the transfection efficiency. However, it is also not clear whether all DNA was really adsorbed on the particles or whether it was merely dissolved in the solution.

It is well known that DNA itself, i.e. without a nanoparticle as carrier, is not active in transfection[38, 78]. A variation of the pH during precipitation of calcium phosphate also did not noticeably influence the transfection efficiency in contrast to the common experience with the classical method where the deviation from pH 7.1 showed dramatically decrease in the transfection efficiency[147, 162]. Using the calcium phosphate/DNA nanoparticles precipitated at pH 7 we could obtain 3 % transfected cells in Quantum® medium and up to 5.7 % transfected cells in serum-free RPMI 1640 medium. The transfection efficiency of calcium phosphate/DNA nanoparticles in transfection mixtures containing FCS was below 1 % and could not be quantified.

Presumably, the reason for the low transfection efficiency is the attack of nucleases within the cytoplasm which prevents the transfer of calcium phosphate/DNA nanoparticles into the nucleus[39]. Therefore an encapsulation of DNA could increase the efficiency, similar to the action of liposomes or polymers[87, 88, 146].

3.1.5 Conclusion

It was demonstrated how nanodisperse calcium phosphate/DNA nanoparticles with a size below 100 nm can be prepared by a comparatively easy and well reproducible process, especially if calcium is partially substituted by magnesium or aluminum. These ions obviously have an inhibitory effect on the particle growth of calcium phosphate.

The cell experiments (T-HUVEC) showed that the transfection efficiency of the calcium phosphate/DNA nanoparticles yielded up to 3.1 % or 3.5 % (depending on the concentration of calcium and phosphate) and is comparable with the results from the standard calcium phosphate method (2.5 %). The transfection efficiency of calcium phosphate/DNA nanoparticles with additions of magnesium and aluminum was not as high as we expected (2.1 % and 2.6 %), although in these colloids the nanoparticles had the smallest size. In fact, the reason of the low transfection efficiency may be the degradation of DNA by nucleases in the cells.

These functionalized nanoparticles formed a stable colloid and did not lose their properties after several weeks of storage in contrast to the standard calcium phosphate method.

3.2 Multi-shell calcium phosphate/DNA nanoparticles as carriers for the transfection

In the previous chapter it was shown that custom-made nanoparticles of calcium phosphate can be efficiently coated and colloidally stabilised by DNA and then used for cell transfection[163]. The advantage of this preparation in comparison to the common *in-situ* precipitation method is a much better control over size and composition of these particles. However, it turned out that the transfection efficiency of such nanoparticle dispersions could not be increased further even by variation of the amount of DNA or the nature of the nanoparticles (precipitation conditions).

Before the DNA successfully enters the nucleus, it has to overcome several physical and chemical barriers, e.g. intracellular degradation in lysosomes[39, 153]. We assumed that the particles were taken up by the cells but then internally digested by nucleases. Therefore the DNA needs to be protected from such an attack by incorporation into the particle. In the following we demonstrate how this can be accomplished by preparing multi-shell particles.

3.2.1 Characterization of multi-shell calcium phosphate/DNA nanoparticles

Multi-shell nanoparticles with a calcium phosphate core and DNA/calcium phosphate shells can be prepared by subsequent precipitation/functionalization (Figure 3.2.1.1). The goal was to protect the DNA from degradation within the cell by incorporating it into the particle. We used two different concentrations of the calcium (6.25 mM and 18 mM) and phosphate (3.74 mM and 10.8 mM) solutions to prepare multi-shell calcium phosphate nanoparticles (Table 3.2.1.1).

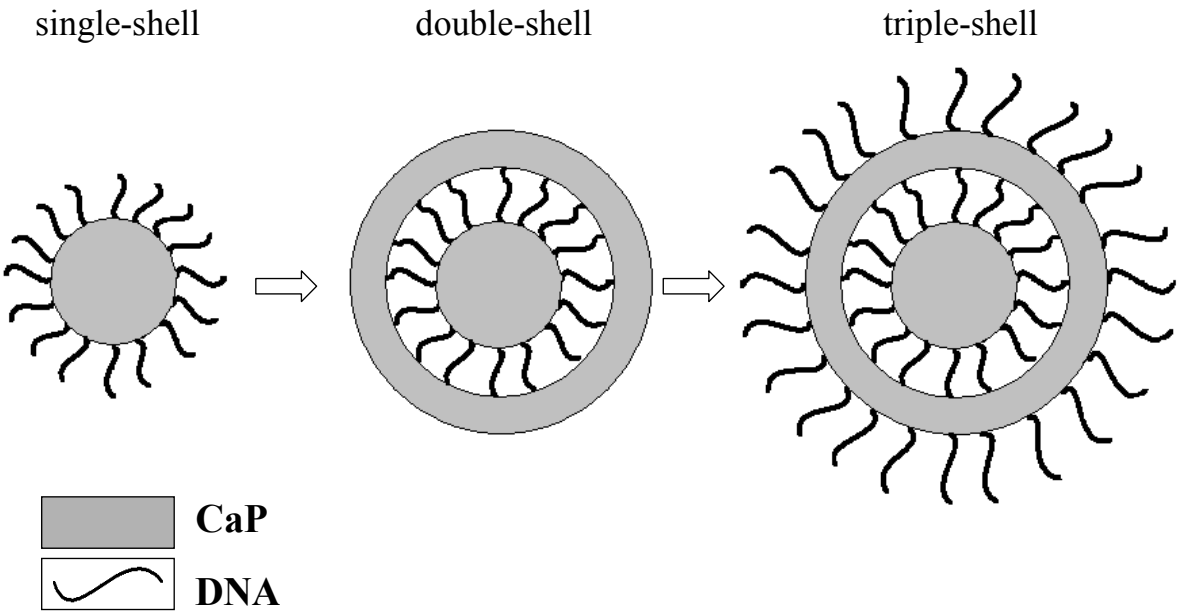

Figure 3.2.1.1: Schematic representation of the three types of calcium phosphate/DNA nanoparticles.

The particle size was smaller if the outer layer consisted of DNA (single- and triple-shell; see Figures 3.2.1.2 and 3.2.1.3 and Table 3.2.1.1). If calcium phosphate was on the outside, aggregation occurred, probably due to the absence of electrostatic and steric stabilization (see below). The zeta potential of single- and triple-shell nanoparticles was very similar (-32 and -30 mV), and their density should also be comparable, therefore we tentatively assume that there was an increase in size when going from single-shell to triple-shell particles.

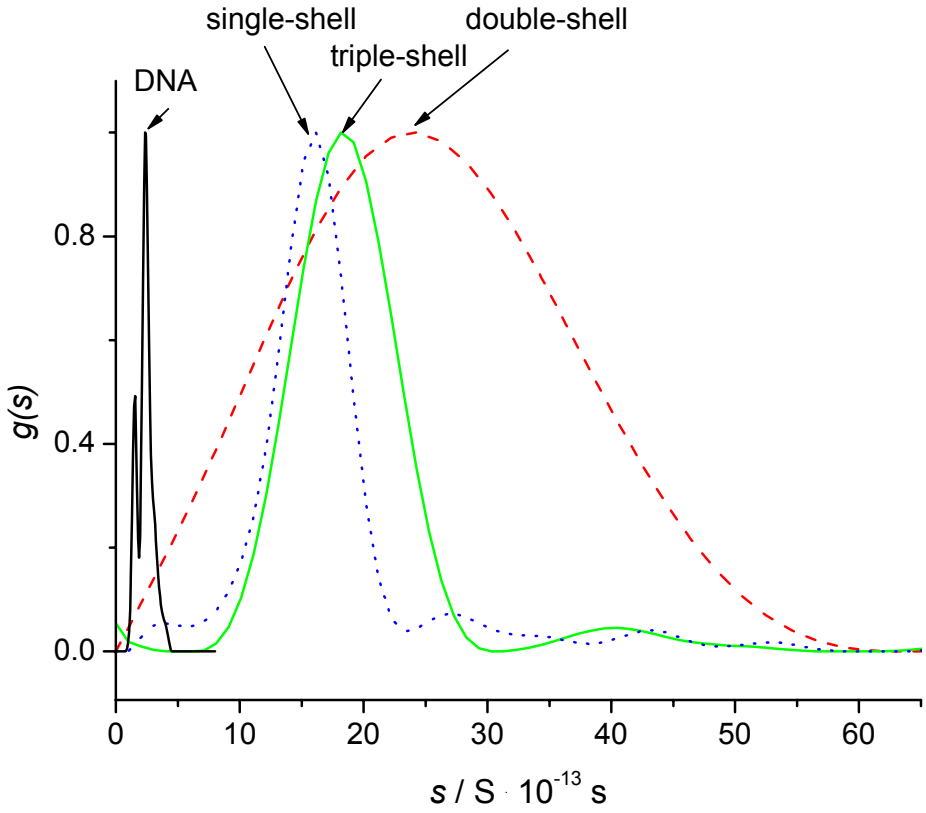

Figure 3.2.1.2: Sedimentation coefficient distributions of calcium phosphate/DNA colloids with single-shell, double-shell and triple-shell nanoparticles. Arrows show the peaks corresponding to DNA (0.5 mg mL^{-1}), single-shell, double-shell and triple-shell calcium phosphate/DNA nanoparticles (Table 3.2.1.1; samples D, E, F). Nanoparticles were prepared at the low concentration of calcium (6.25 mM) and phosphate (3.74 mM) with 0.2 mL of DNA (1 mg mL^{-1}).

For samples which contained DNA, we frequently observed a large peak in dynamic light scattering. This was also present if only DNA was dissolved in water. Because the dispersions did not show sedimentation and because no large aggregates were found in ultracentrifugation, we tentatively ascribed this phenomenon to DNA-water aggregates that do not contain calcium phosphate. The peaks in light scattering could not be removed by filtration. Visually, the samples did not show large aggregates (in contrast to the samples B, E in Table 3.2.1.1, which were not colloidally stabilised and showed sedimentation).

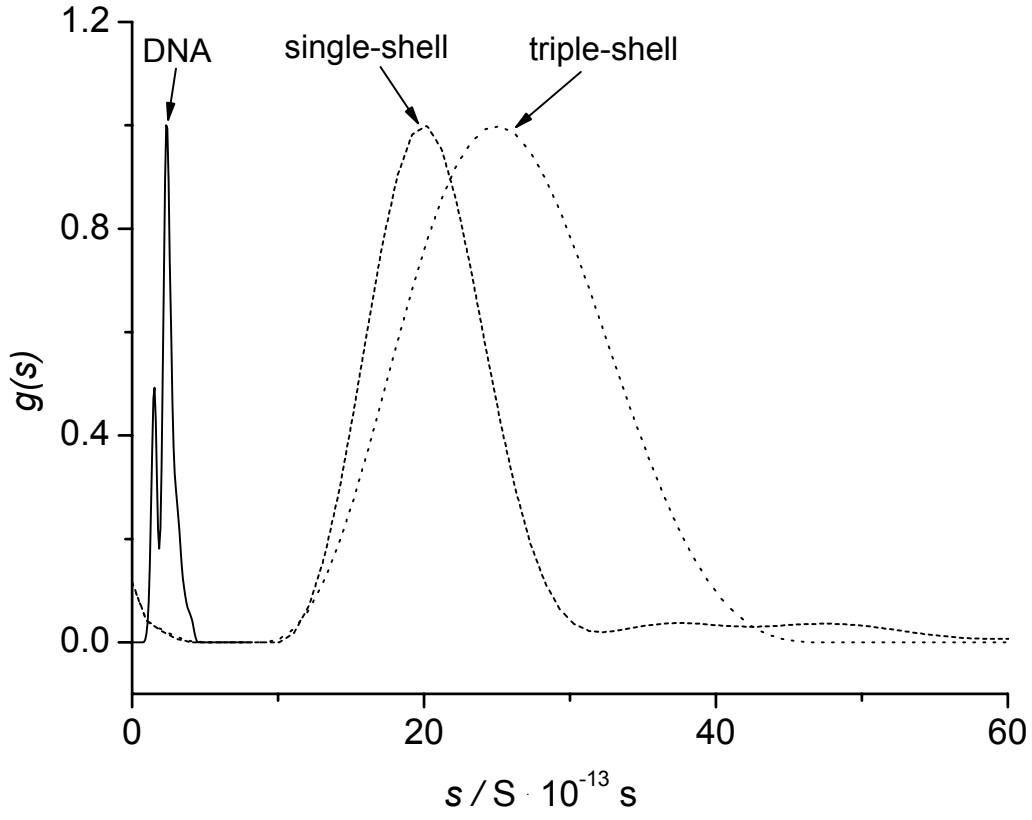

Figure 3.2.1.3: Sedimentation coefficient distributions of calcium phosphate/DNA colloids with single-shell and triple-shell nanoparticles. Arrows show the peaks corresponding to DNA (0.5 mg mL^{-1}), single-shell and triple-shell calcium phosphate/DNA nanoparticles (Table 3.2.1.1; samples A, B, C). Nanoparticles were prepared at the high concentration of calcium (18 mM) and phosphate (10.8 mM) with 0.2 mL of DNA (1 mg mL^{-1}).

The alternating layer structure of the multi-shell particles was demonstrated by their zeta potential which is a qualitative measure of the particle charge. Calcium phosphate particles without DNA carry almost no charge ("CaP"). A coating with DNA renders the particles strongly negative ("single-shell"). The addition of another external layer of calcium phosphate ("double-shell") compensates most of this negative charge, and the outer layer of DNA makes the particles negatively charged again (Fig. 3.2.1.4). This effect depends on the amount of calcium phosphate which is used to prepare the second layer.

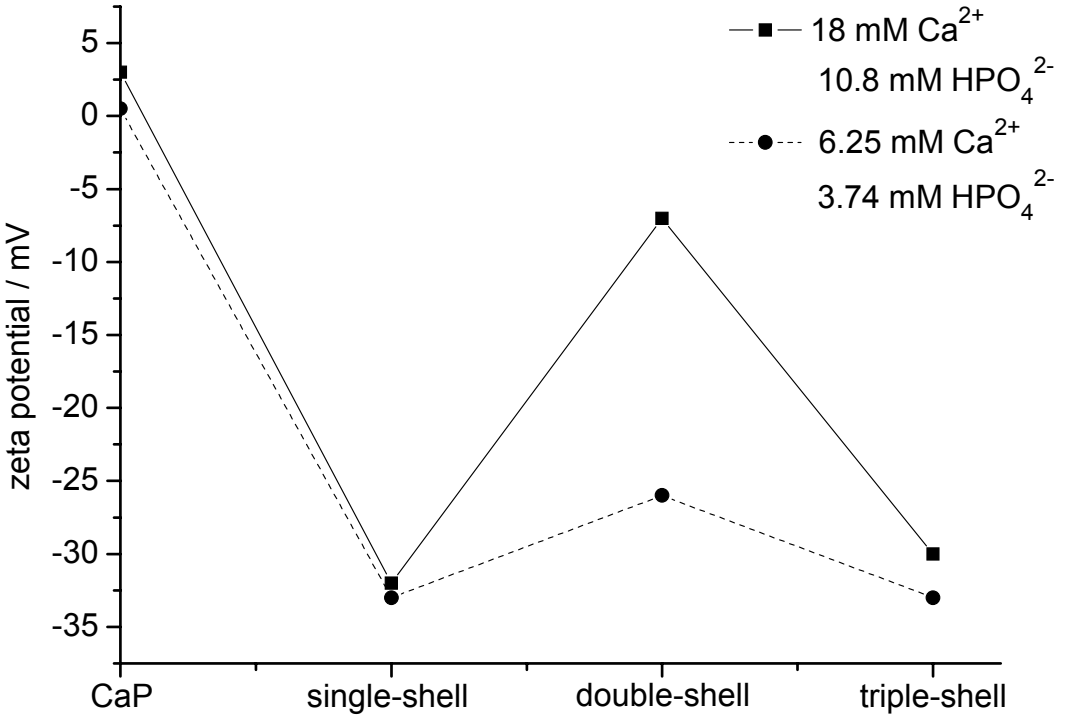

Figure 3.2.1.4: Dependence of the zeta potential from the type of nanoparticles. Solid line: Nanoparticles at high concentration of calcium and phosphate (18 mM and 10.8 mM) with 0.2 mL of DNA (1 mg mL^{-1}); dashed line: Nanoparticles at low concentration of calcium and phosphate (6.25 mM and 3.74 mM) with 0.2 mL of DNA (1 mg mL^{-1}) (Table 3.2.1.1; samples A/D, B/E, C/F).

If there is not enough calcium phosphate present (e.g. 6.25 mM/3.74 mM), it is not sufficient to fully cover the surface and some DNA groups are left exposed, thereby giving the particle a still considerably negative charge. The double-shell particles with calcium phosphate on the outside were not stable towards aggregation, probably due to the absence of steric and electrostatic stabilization (Table 3.2.1.1, samples B and E). Unfortunately, it was not possible to visualize the internal structure of the multi-shell particles by transmission electron microscopy due to strong radiation damage at high magnification.

As shown in Figure 3.2.1.5, multi-shell nanoparticles had the same spherical shape, but a different size. The average particle diameter (z-average) from dynamic light scattering was almost the same at high and low concentrations of

calcium and phosphate: around 35 nm (PDI=0.2) for single-shell particles, around 75 nm (PDI=0.4) for double-shell particles and around 45 nm (PDI=0.6) for triple-shell particles (Table 3.2.1.1; samples A-F). The particle diameter increased with the number of shells, but the simultaneously increasing polydispersity index (PDI) showed that we probably had a mixture of smaller and larger particles with an increasing number of shells. This supports the assumption that the particles had a core-shell-structure.

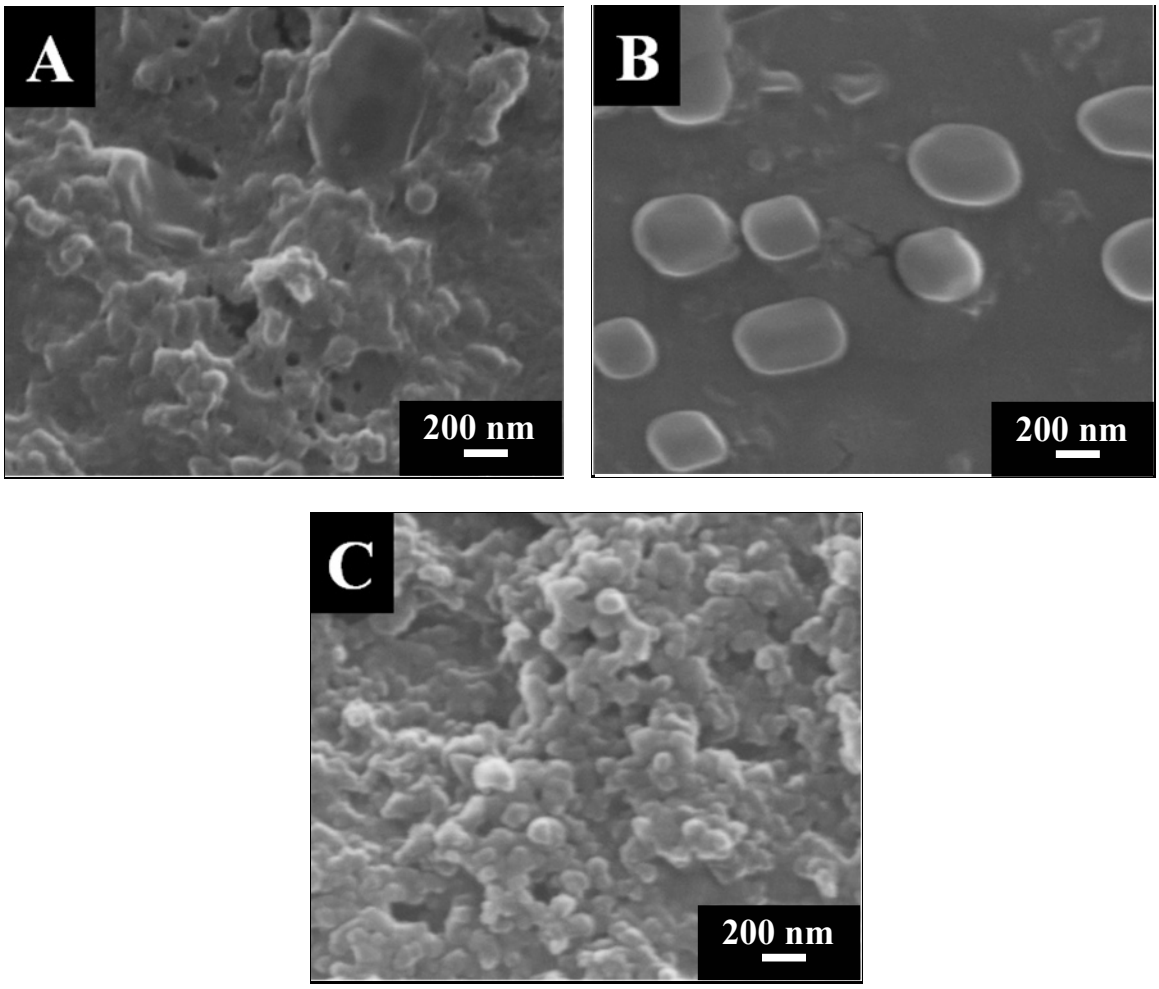

Figure 3.2.1.5: Scanning electron micrograph of single-shell (A), double-shell (B) and triple-shell (C) calcium phosphate/DNA nanoparticles (Table 3.2.1.1; samples D, E, F). Nanoparticles were prepared at the low concentration of calcium and phosphate (6.25 mM and 3.74 mM) with 0.2 mL of DNA (1 mg mL^{-1}).

Table 3.2.1.1: Colloid-chemical data of functionalized calcium phosphate nanoparticles. The volume of calcium phosphate dispersion before mixing with DNA was always 1 mL (*s**=sedimentation coefficient from analytical ultracentrifugation). The percentages in the particle distributions give the volume distribution of the particles from light scattering. The large aggregates in some samples containing DNA on the outside ("single" and "triple") are probably due to DNA-water aggregates and not to large calcium phosphate particles (see text).

Sample					Zeta potential / mV	Size of small particles / nm	%	Size of large particles / nm	%	*s* / S · 10^{-13} s
	No. of shells	$[Ca^{2+}]$ / mM	$[HPO_4^{2-}]$ / mM	DNA / mL						
A	single	18	10.8	0.2	-32(5)	35	92	272	5	
B	double	a) 18 b) 18	a) 10.8 b) 10.8	a) 0.2 -	-7(11)	76	11	736	83	-
C	triple	a) 18 b) 18	a) 10.8 b) 10.8	a) 0.2 c) 0.2	-30(4)	45	48	788	50	24
D	single	6.25	3.74	0.2	-33(4)	36	99	-	-	16
E	double	a) 6.25 b) 6.25	a) 3.74 b) 3.74	a) 0.2 -	-26(6)	75	70	295	20	23
F	triple	a) 6.25 b) 6.25	a) 3.74 b) 3.74	a) 0.2 c) 0.2	-33(5)	46	54	1046	45	17

3.2.2. Transfection efficiency of multi-shell nanoparticles

There are a number of carriers of organic and inorganic nature which incorporate DNA, thereby protecting it from degrading enzymes[118, 146, 164]. Therefore, three types of nanoparticles were developed to investigate the effect of DNA protection and the role of small particles for a successful transfection (Figure 3.2.1.1)

For transfection experiments with multi-shell nanoparticles, T-HUVEC was selected, because this cell line showed the lowest transfection efficiency and therefore any improvement would be better seen in this case. For DNA protection an external layer of calcium phosphate on DNA-coated calcium phosphate nanoparticles was prepared by crystallization (denoted "double-shell" in Figure 3.2.1.1). This results in the formation of core-shell particles with a calcium phosphate core, a layer of DNA causing the expression of EGFP, and an outer calcium phosphate shell. Because such a system is not stable for long towards agglomeration (no protective DNA layer), we prepared triple-shell particles with another layer of DNA for colloidal stabilization. The main idea was to prevent the crystal growth by the adsorption of the outer layer of DNA on the nanoparticle surface which leads to electrostatic stabilization of the colloid (denoted "triple-shell" in Figure 3.2.1.1). These three kinds of particles were used for transfection experiments with T-HUVEC. Depending on the transfection method T-HUVEC show large differences in transfection efficiencies which helps to detect even small improvements of the method.

Multi-shell nanoparticles at different concentrations of calcium (6.25 mM and 18 mM) and phosphate (3.74 mM and 10.8 mM) were tested on the cells. The results from transfection experiments are discussed here.

Table 3.2.2.1: Results of transfection experiments with T-HUVEC from numerical analysis of the laser fluorescence micrographs. The efficiencies are given as average ± standard deviation (*N*=3). Nanoparticles were prepared at the low concentration of calcium and phosphate (6.25 mM and 3.74 mM).

Method	**Transfection efficiency / %**		
	Quantum® medium	**RPMI 1640 with FCS**	**Serum-free RPMI 1640**
Polyfect®	9.9 ± 4.0	10.9 ± 3.0	9.9 ± 3.8
Standard calcium phosphate precipitation method	2.8 ± 2.5	5.2 ± 0.2	2.5 ± 2.1
Single-shell calcium phosphate/DNA-nanoparticles	3.2 ± 1.8	3.2 ± 2.1	3.1 ± 1.3
Double-shell calcium phosphate/DNA-nanoparticles	2.5 ± 0.8	2.4 ± 1.0	3.4 ± 0.7
Triple-shell calcium phosphate/DNA-nanoparticles	4.6 ± 0.6	3.3 ± 1.1	4.3 ± 0.2

In Table 3.2.2.1 the results of transfection experiments with T-HUVEC at a low concentration of calcium and phosphate are shown. We obtained transfection efficiency between 2 to 4 % for all type of calcium phosphate/DNA nanoparticles. The reason for this low efficiency can be a lack of the particles in the solution or not enough calcium and phosphate for the shell formation.

It is important to note that at a high concentration of calcium and phosphate the results from transfection experiments were significantly better. We observed a continuous increase of the transfection efficiency when going from single-shell to triple-shell nanoparticles from 3.5 % up to 10 % in serum-free RPMI1640. With the standard calcium phosphate method we achieved about 5 % of transfected cells and with the commercial transfection agent Polyfect® about 10 %. The results are summarized in Table 3.2.2.2. Figure 3.2.2.1 shows the cell morphology and EGFP fluorescence after transfection (T-HUVEC).

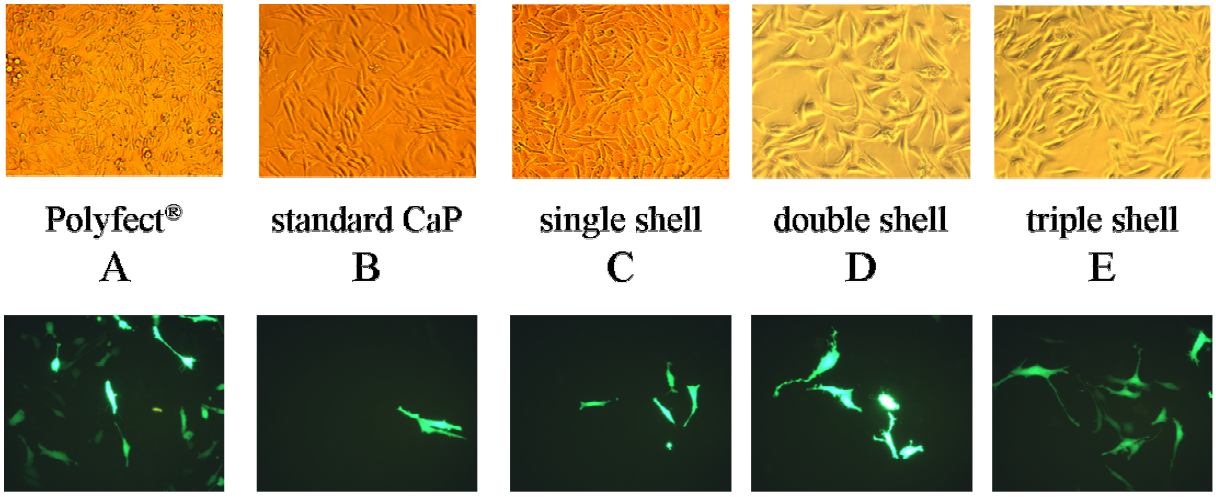

Figure 3.2.2.1: Transmission light microscopy (upper row) and EGFP fluorescence microscopy (lower row; magnification 200 x in all cases) of T-HUVEC that were transfected with the commercial transfection agent Polyfect® (A), with standard calcium phosphate precipitation method (B), and with calcium phosphate/pcDNA3-EGFP nanoparticles in serum-free RPMI medium (C: single-shell nanoparticles, D: double-shell, E: triple-shell; according to Figure 3.2.1.1). Transfected cells appear green as a whole due to EGFP fluorescence. The increase in transfection efficiency from C to E is obvious.

The transfection efficiency did not depend strongly on the type of medium within the limits of reproducibility. Single-shell particles were comparable to the classical precipitation method, demonstrating that the principle is the same in both kinds. The addition of another layer of calcium phosphate considerably increased the transfection efficiency, supporting our concept. The efficiency of calcium phosphate-mediated transfection with triple-shell particles was comparable to that of Polyfect®. For all three media, the results are graphically represented in Figures 3.2.2.2-3.2.2.4.

Table 3.2.2.2: Results of transfection experiments with T-HUVEC from numerical analysis of the laser fluorescence micrographs. The efficiencies are given as average ± standard deviation (*N*=3). For the nanoparticle dispersions, the transfection efficiencies are also given in parentheses after 2 weeks of storage at 4°C (*N*=1). There was no significant decrease in the transfection efficiency after storage. Nanoparticles were prepared at the high concentration of calcium and phosphate (18 mM and 10.8 mM)

Method	**Transfection efficiency / %**		
	Quantum® medium	**RPMI 1640 with FCS**	**Serum-free RPMI 1640**
Polyfect®	9.9 ± 4.0	10.9 ± 3.0	9.9 ± 3.8
Standard calcium phosphate precipitation method	2.8 ± 2.5	5.2 ± 0.2	2.5 ± 2.1
Single-shell calcium phosphate/DNA nanoparticles	2.9 ± 0.6 (2.4)	2.7 ± 1.2 (3.9)	3.5 ± 0.8 (3.9)
Double-shell calcium phosphate/DNA nanoparticles	5.6 ± 2.8 (6.7)	4.9 ± 1.7 (4.9)	6.2 ± 2.4 (7.0)
Triple-shell calcium phosphate/DNA nanoparticles	9.4 ± 3.3 (10.1)	6.1 ± 2.6 (5.5)	9.8 ± 6.5 (5.0)

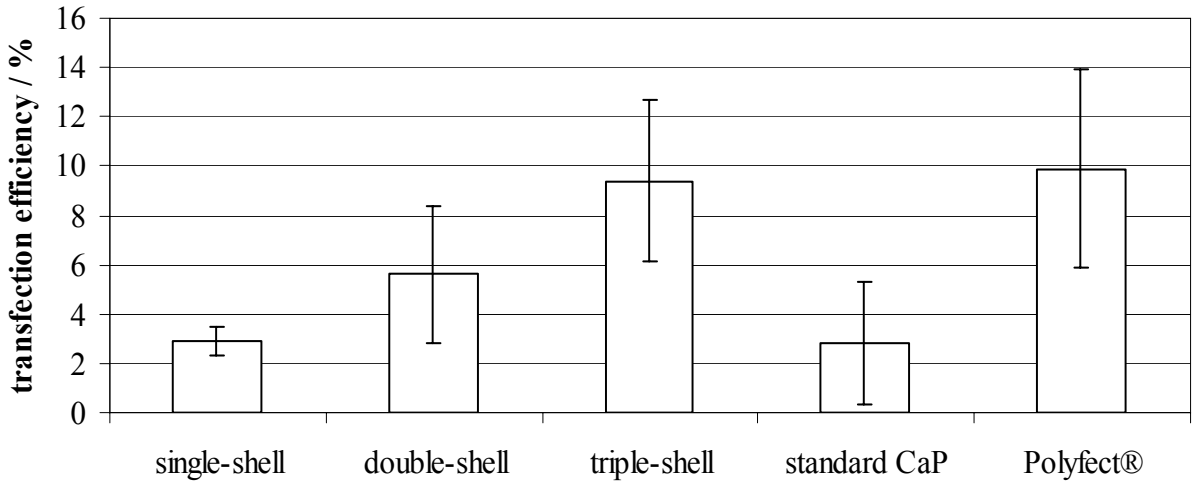

Figure 3.2.2.2: Comparison of the transfection efficiency of T-HUVEC in Quantum® medium by different methods. The error bars represent the standard deviation (*N*=3). There were significant differences between single-shell and triple-shell ($P<0.01$) and triple-shell and the standard calcium phosphate method ($P<0.05$)

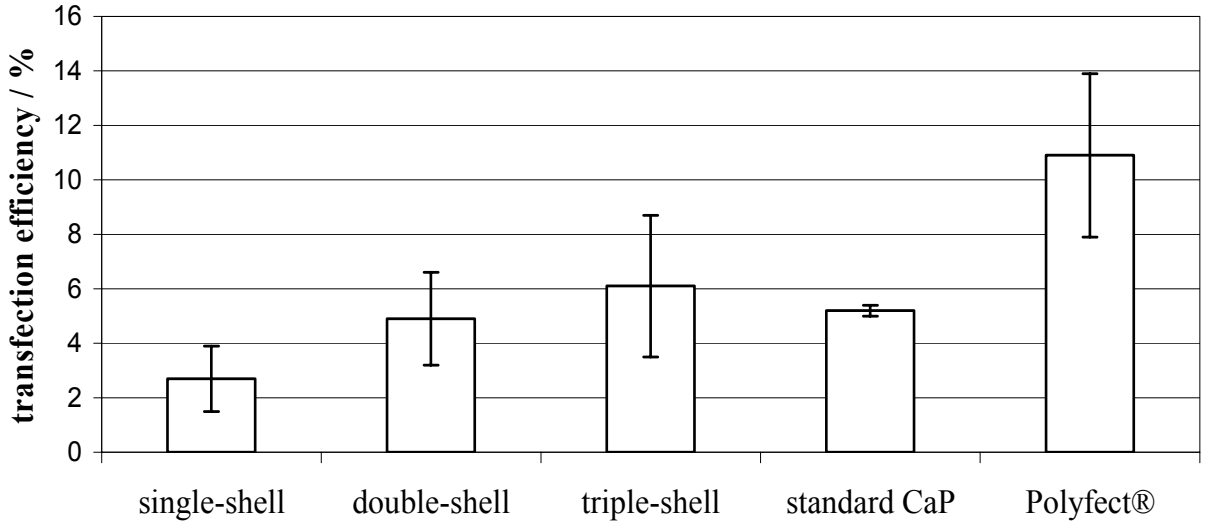

Figure 3.2.2.3: Comparison of the transfection efficiency of T-HUVEC in RPMI 1640 medium with FCS by different methods. The error bars represent the standard deviation (*N*=3).

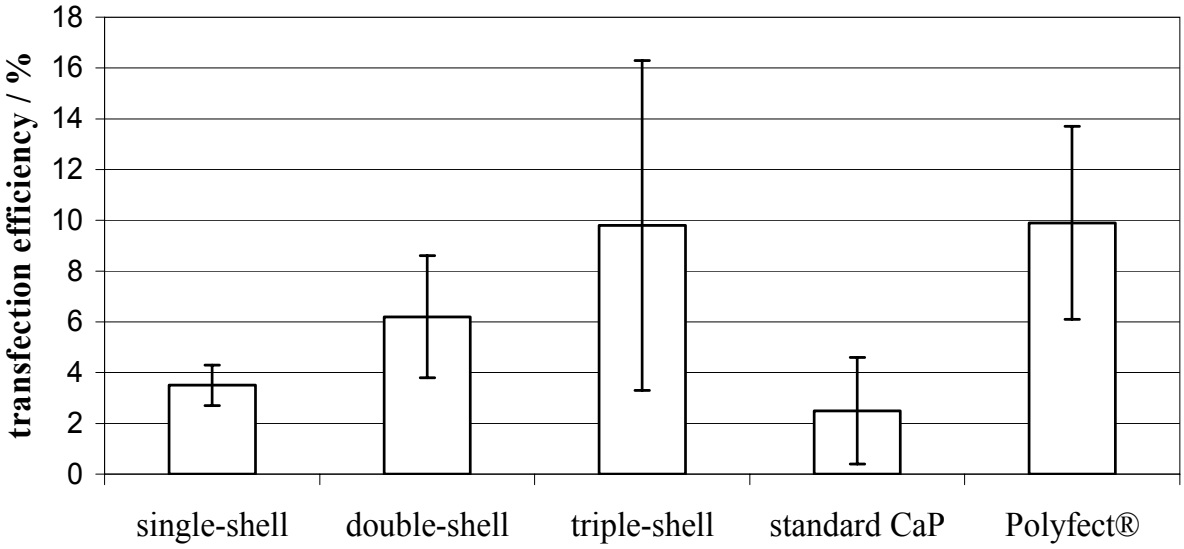

Figure 3.2.2.4: Comparison of the transfection efficiency of T-HUVEC in RPMI 1640 medium without FCS by different methods. The error bars represent the standard deviation (*N*=3).

As it was shown in chapter 3.2.1, the particles have a core-shell structure and at least in this case, the charge does not play a critical role for the transfection efficiency, otherwise we would not observe a continuous increase in transfection efficiency with the number of shells.

We also tried to extend the procedure and to add more shells of calcium phosphate and DNA, in order to further increase the transfection efficiency. Unfortunately, the efficiency does not increase after the addition of more layers, probably because of an increasing polydispersity and simultaneous crystallisation-reprecipitation processes (no detailed light scattering experiments were carried out with these systems).

The particle dispersions could be stored at 4°C for two weeks and all dispersions (single-, double- and triple-shell) kept their transfection efficiency (T-HUVEC; Table 3.2.2.2). The storage was not continued thereafter, but we assume that the storage time could in principle be even longer.

3.2.3 Conclusion

By a comparatively easy and well reproducible process we prepared multi-shell calcium phosphate/DNA-nanoparticles with a calcium phosphate core and DNA/calcium phosphate shells. Such shells help to protect DNA from the degradation by enzymes (nucleases) inside the cytoplasm of cultured endothelial cells, reaching the efficiency of Polyfect®. In principle, different layers can sequentially deliver different agents[165]. Calcium phosphates should be advantageous due to their high biocompatibility and good biodegradability compared to other types of nanoparticles used for cell transfection such as iron oxide (magnetite)[166], silica[113] or gold[115]. In contrast to the classical calcium phosphate method, the particle/DNA dispersions can be stored for weeks without loss of their transfection efficiency. It was shown by the high transfection efficiency that the DNA remained intact in the multi-shell particles. It may be assumed that the DNA inside the particle is the most active and that it should be possible to substitute the DNA on the outside (which is mainly used for colloidal stabilization) by other agents like double-hydrophilic block-copolymers[167].

3.3 Calcium phosphate colloids containing protamine: Colloidal and biochemical properties

Many advancements were made over the past several years in the field of non-viral gene therapy to improve gene delivery and expression to the cells both *in vitro* and *in vivo*. The uptake of isolated genes by tissue culture cells was used widely to test for gene function, for treating genetic diseases[168].

Calcium phosphate nanoparticles are good carriers due to such characteristics as non-toxicity, high biocompatibility, good biodegradability, and simplicity of large-scale production and use. Our purpose was to make them more efficient in cell transfections and targetable to become cell-specific.

The cell membrane generally represents an impenetrable barrier for the transport of biomolecules like DNA or polypeptides[169], therefore, a drug delivery system is required.

In recent years, the knowledge of the unique property of viruses to penetrate into cells and to deliver their genetic material was applied and studied in non-viral gene delivery systems. Viral proteins, so-called TAT proteins (TAT=trans-activating transcriptional activator), play a very important role in the trafficking of nanoparticles into the cell and especially in the overcoming of DNA the nuclear membrane barrier. As reported by Pante *et al.,* the maximum size of the macromolecules for the passage through the nuclear pore complex is about 39 nm[170]. Larger molecules must possess a nuclear localization sequence (NLS) to pass through the nuclear pores. The use of TAT proteins and derived peptides for the intracellular delivery of drug carriers can dramatically increase the transfection efficiency.

Some researchers have reported the increase of the transfection efficiency of magnetic nanoparticles in the presence of TAT peptides[171-173]. Torchilin *et al.* demonstrated the successful delivery of large liposomes (with a size of 200 nm) with attached TAT-peptide molecules[174].

In our studying protamine was chosen to expert a specific role in our DNA delivery system. Protamine is a basic protein with a molecular weight of approximately 4000 to 10000. Protamine has four possible nuclear localization sequences consisting of basic amino acids and proline or serine residues[168, 175, 176] (for details see chapter 2.2.4.1).

3.3.1 Mechanism of the transfer of calcium phosphate/DNA/protamine nanoparticles

Figure 3.3.1.1 represents the schematic illustration of the DNA delivery pathway. As a first step, calcium phosphate nanoparticles should be formed. Positively charged protamine[177] can neutralize a negative charge of DNA and provide an approach of nanoparticles to negatively charged cell membrane via electrostatic interaction (Figure 3.3.1.1, I). Then nanoparticles move into the cytoplasm by endocytosis.

After calcium phosphate/DNA/protamine nanoparticles escape from endosomes and are released into the cytoplasm, they meet importins there. Protamine, which is adsorbed on the surface of nanoparticles, binds with importins by NLS (Figure 3.3.1.1, IV). These nanoparticles with importins approach the external nuclear membrane and attach on the cytoplasmatic filaments of the pore complex. It is not yet clearly understood whether whole nanoparticles enter the nucleus or only the plasmid DNA[178].

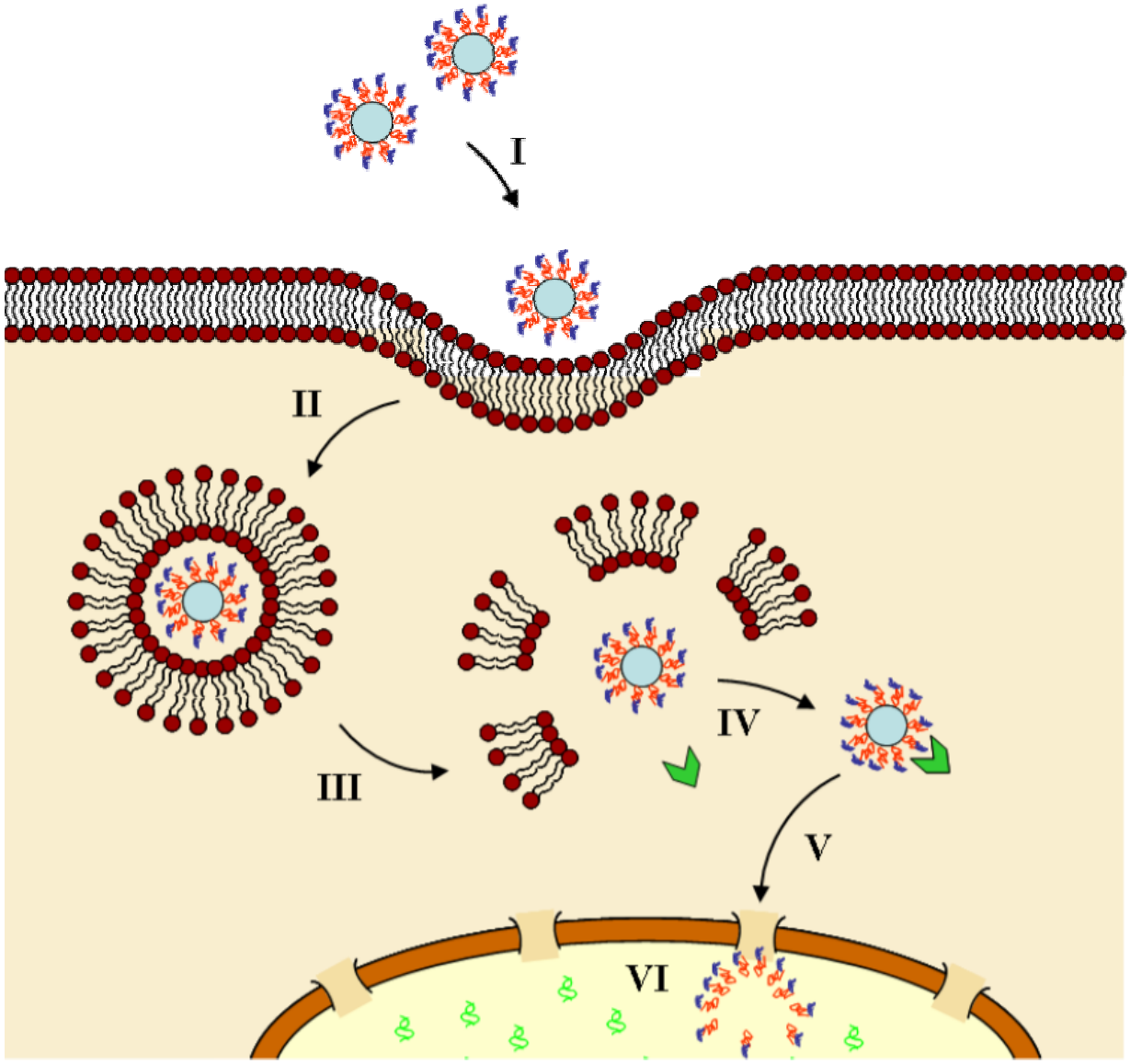

Figure 3.3.1.1: Schematic illustration of transfer mechanism of calcium phosphate/DNA nanoparticles in addition of protamine into a cell. I: Formation of calcium phosphate/DNA/protamine nanoparticles and their uptake. II: Endocytosis. III: Escape from endosomes and intracellular release. IV: Binding to importin. V: Nuclear targeting. VI: Nuclear entry and gene expression.

3.3.2 Characterization of colloids with protamine

The calcium phosphate/DNA nanoparticles were functionalized at protamine concentrations from 0.5 to 20 mg mL^{-1}. The colloidal properties were studied in dependence of the concentration of protamine.

It was observed that by increasing the concentration of protamine the size of particles became smaller. This tendency is clearly seen from 1.0 to 10 mg mL^{-1}. The solution with a protamine concentration of 10 mg mL^{-1} gave the smallest particles and the highest transfection efficiency. Further addition of protamine in the solution led to an increasing particle size (Table 3.3.2.1). The average particle diameter (z-average) from dynamic light scattering was 288 nm (PDI=0.3) for single-shell particles, 177 nm (PDI=0.2) for double-shell particles, and 80 nm (PDI=0.7) for triple-shell particles. The particle diameter decreased with the number of shells, but the simultaneously increasing polydispersity index (PDI) showed that we probably had a mixture of smaller and larger particles with an increasing number of shells.

Protamine is a positively charged molecule which is interacting with the negative charge of the phosphate groups in DNA molecule. The interaction behaviour of calcium phosphate/DNA nanoparticles with protamine is elucidated by zeta potential measurements. By an addition of protamine (1 mg mL^{-1}) the nanoparticles assumed a positive charge (Figure 3.3.2.1). The single- and triple-shell nanoparticles were less negatively charged compared to the nanoparticles without protamine (-30 mV). At a protamine concentration of 5 mg mL^{-1}, the charge of DNA was fully neutralized and the zeta potential of nanoparticles became slightly positive (around +5 mV) (Table 3.3.2.1).

For characterization, we also used transmission and scanning electron microscopy.

Table 3.3.2.1: Colloid-chemical data of functionalized calcium phosphate/DNA/protamine nanoparticles. The volume of the calcium phosphate dispersion before mixing with DNA was always 1 mL. The percentages in the particle distributions give the intensity distribution of the particles from light scattering.

	Sample	Z-Average (nm)	PDI	Zeta potential /mV
A	Single-shell calcium phosphate/DNA/protamine nanoparticles (1 mg mL^{-1})	379	0.3	-20
B	Double-shell calcium phosphate/DNA/protamine nanoparticles (1 mg mL^{-1})	578	0.2	-7
C	Triple-shell calcium phosphate/DNA/protamine nanoparticles (1 mg mL^{-1})	493	0.4	-11
D	Single-shell calcium phosphate/DNA/protamine nanoparticles (5 mg mL^{-1})	221	0.4	0
E	Double-shell calcium phosphate/DNA/protamine nanoparticles (5 mg mL^{-1})	355	0.4	7
F	Triple-shell calcium phosphate/DNA/protamine nanoparticles (5 mg mL^{-1})	543	0.5	2
G	**Single-shell calcium phosphate/DNA/protamine nanoparticles (10 mg mL^{-1})**	**288**	**0.3**	**1**
H	**Double-shell calcium phosphate/DNA/protamine nanoparticles (10 mg mL^{-1})**	**177**	**0.2**	**5**
I	**Triple-shell calcium phosphate/DNA/protamine nanoparticles (10 mg mL^{-1})**	**80**	**0.7**	**1**
J	Single-shell alcium phosphate/DNA/protamine nanoparticles (20 mg mL^{-1})	236	0.3	4
K	Double-shell calcium phosphate/DNA/protamine nanoparticles (20 mg mL^{-1})	213	0.4	5
L	Triple-shell calcium phosphate/DNA/protamine nanoparticles (20 mg mL^{-1})	391	0.4	6

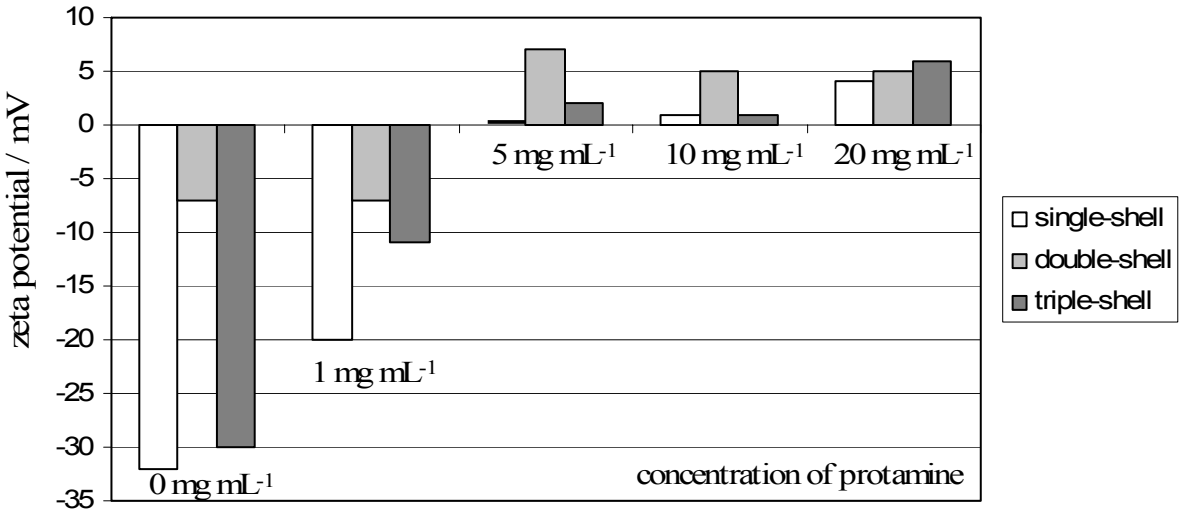

Figure 3.3.2.1: Dependence of the zeta potential from the concentration of protamine in single-, double- and triple-shell calcium phosphate/DNA/protamine nanoparticles.

Figure 3.3.2.2 shows typical electron micrographs of triple-shell nanoparticles functionalized with protamine. The particles had a spherical shape with a size of about 50 to 80 nm.

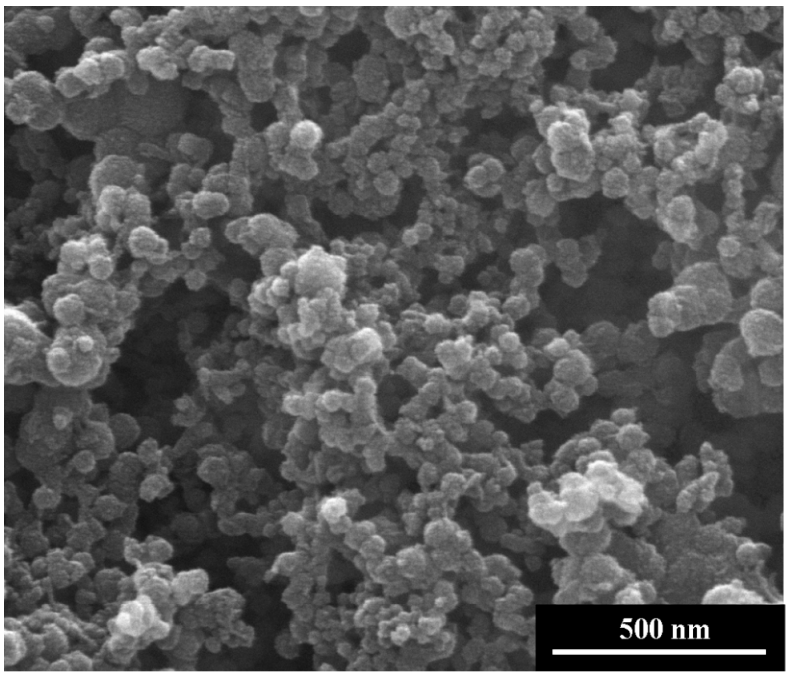

Figure 3.3.2.2: Scanning electron micrograph of triple-shell calcium phosphate/DNA/protamine nanoparticles (10 mg mL^{-1}) (Table 3.3.2.1; sample I).

3.3.3 Transfection efficiency of calcium phosphate/DNA/protamine nanoparticles

Transfection experiments were carried out with T-HUVEC in three different media. The influence of the content of protamine on the transfection efficiency was studied. The experiments with 0.5 to 5 mg mL^{-1} and 20 mg mL^{-1} of protamine showed no significant variation in transfection efficiency (Table 3.3.3.1). Up to 5 % of transfected cells were observed. However, the transfection efficiency was somewhat higher for double-shell nanoparticles with 5 mg mL^{-1} of protamine (5.1 to 8.6 % of transfected cells depending on the cell culture medium).

As expected, single-shell nanoparticles with different concentrations of protamine in all three media showed a low transfection efficiency (up to 5 %). The reason is an attack of nucleases within the cytoplasm, which destroy DNA and prevent its transfer and incorporation into the nucleus. Protamine in single-shell nanoparticles cannot protect DNA from the degradation like the calcium phosphate shells in double- and triple-shell nanoparticles. The optimal concentration of protamine was 10 mg mL^{-1} which showed the highest transfection efficiency. The transfection efficiency was 7-8 % for double-shell nanoparticles and 9-14 % for triple-shell nanoparticles.

For all three media, the results from Table 3.3.3.1 are graphically represented in Figures 3.3.3.1-3.3.3.3.

Table 3.3.3.1: All results of transfection experiments carried out with functionalized calcium phosphate/DNA/protamine nanoparticles.

Methode	**Transfektion efficiency / %**		
	Quantum® medium	**RPMI 1640 with FCS**	**Serum-free RPMI 1640**
Single-shell calcium phosphate/DNA nanoparticles	2.3	1.4	1.2
Double-shell calcium phosphate/DNA nanoparticles	3.2	1.9	3.8
Triple-shell calcium phosphate/DNA nanoparticles	4	3.7	5.1
Single-shell calcium phosphate/DNA/protamine nanoparticles (0.5 mg mL^{-1})	4.9	3.3	2.9
Double-shell calcium phosphate/DNA/protamine nanoparticles (0.5 mg mL^{-1})	4.7	2.4	3.7
Triple-shell calcium phosphate/DNA/protamine nanoparticles (0.5 mg mL^{-1})	3.7	2.6	4.0
Single-shell calcium phosphate/DNA/protamine nanoparticles (1 mg mL^{-1})	1.8	1.2	2.2
Double-shell calcium phosphate/DNA/protamine nanoparticles (1 mg mL^{-1})	2.7	2.5	5.5
Triple-shell calcium phosphate/DNA/protamine nanoparticles (1 mg mL^{-1})	2.1	1.3	1.4
Single-shell calcium phosphate/DNA/protamine nanoparticles (5 mg mL^{-1})	2.1	1.8	1.9
Double-shell calcium phosphate/DNA/protamine nanoparticles (5 mg mL^{-1})	6.7	8.6	5.1
Triple-shell calcium phosphate/DNA/protamine nanoparticles (5 mg mL^{-1})	2.9	5.4	4.5
Single-shell calcium phosphate/DNA/protamine nanoparticles (10 mg mL^{-1})	**5.0**	**3.8**	**3.0**
Double-shell calcium phosphate/DNA/protamine nanoparticles (10 mg mL^{-1})	**7.2**	**8.0**	**6.8**
Triple-shell calcium phosphate/DNA/protamine nanoparticles (10 mg mL^{-1})	**14.4**	**10.6**	**8.9**
Single-shell calcium phosphate/DNA/protamine nanoparticles (20 mg mL^{-1})	5.0	2.0	3.0
Double-shell calcium phosphate/DNA/protamine nanoparticles (20 mg mL^{-1})	5.0	3.5	4.0
Triple-shell calcium phosphate/DNA/protamine nanoparticles (20 mg·mL^{-1})	9.0	10.0	4.0

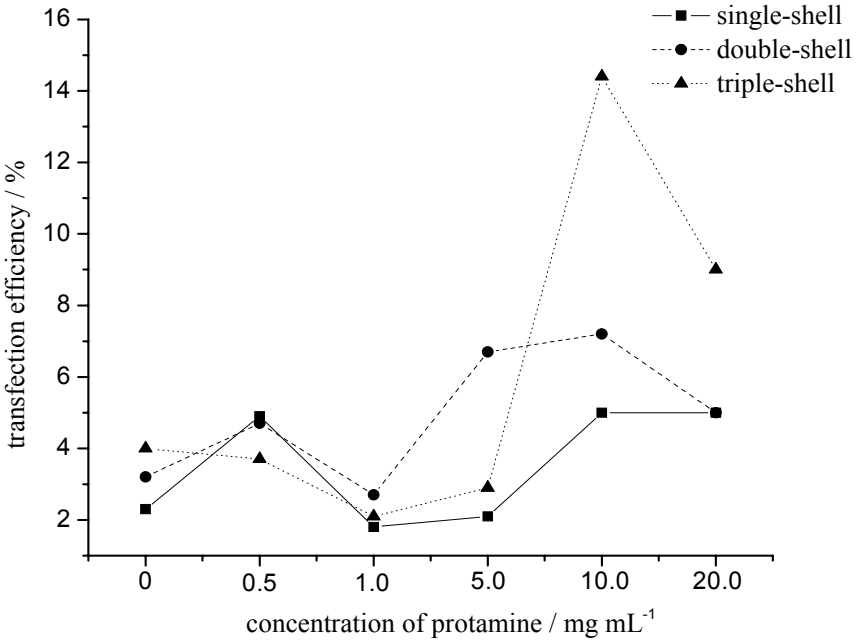

Figure 3.3.3.1: Effect of the concentration of protamine in single-, double- and triple-shell calcium phosphate nanoparticles on the transfection efficiency of T-HUVEC in Quantum® medium.

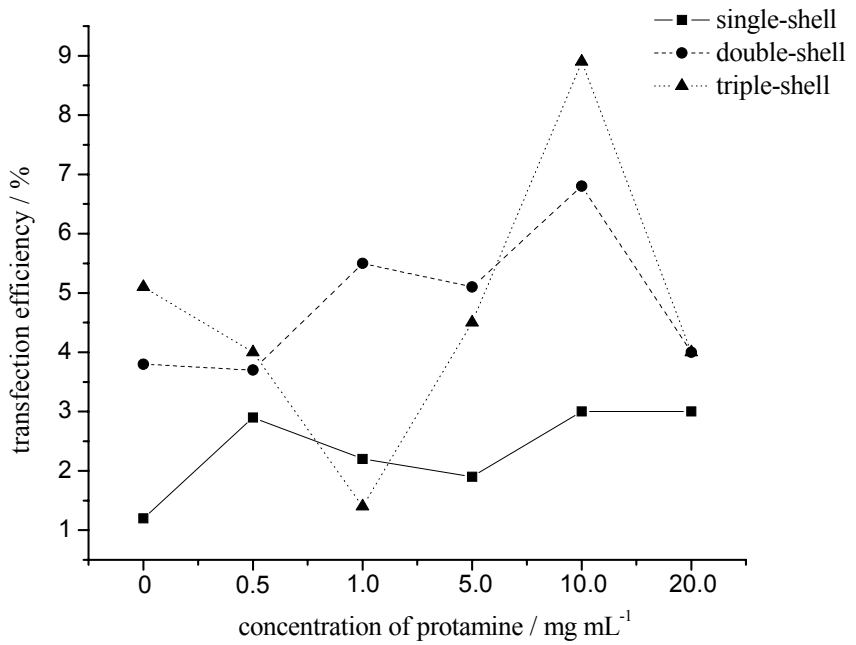

Figure 3.3.3.2: Effect of the concentration of protamine in single-, double- and triple-shell calcium phosphate nanoparticles on the transfection efficiency of T-HUVEC in RPMI 1640 medium without FCS.

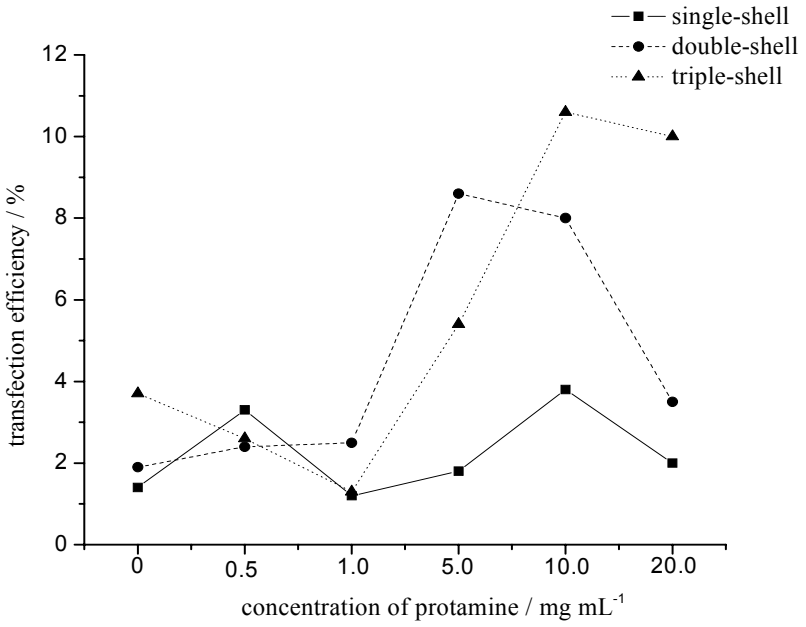

Figure 3.3.3.3: Effect of the concentration of protamine in single-, double- and triple-shell calcium phosphate nanoparticles on the transfection efficiency of T-HUVEC in RPMI 1640 medium with FCS.

Such results are corresponding to the mechanism proposed by Masuda *et al.*[179]. The protamine molecule possesses different functions: As a condenser of DNA by its arginine residues and as a nuclear localization signal. At a low concentration of protamine (below 10 mg mL^{-1}), all basic amino acids of protamine may be consumed in the condensation of DNA. Therefore, the recognition of the NLS by the nuclear transport-associating proteins (importins) is limited. At the optimal concentration of protamine (10 mg mL^{-1}), the protamine with NLS is displayed on the surface of the particles, allowing the particles to be recognized by nuclear transport-associating proteins.

The transfection efficiency was lower at a protamine concentration of 20 mg mL^{-1}. The reason could be that free protamine may interact with nuclear transport-associating proteins[179] and, therefore, inhibit the nuclear transfer of DNA.

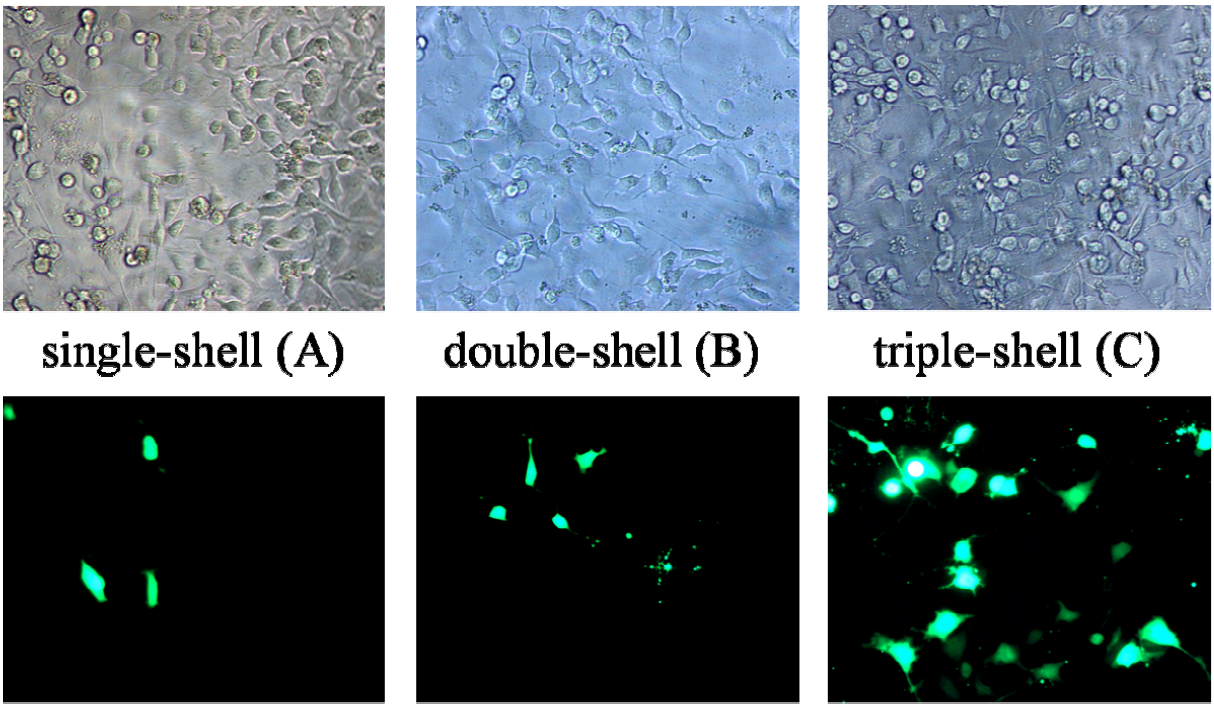

Figure 3.3.3.4: Transmission light microscopy (upper row) and EGFP fluorescence microscopy (lower row; magnification 200 x in all cases) of T-HUVEC that were transfected with calcium phosphate/pcDNA3-EGFP nanoparticles with addition of protamine (10 mg mL^{-1}) in RPMI medium with FCS (A: single-shell, B: double-shell, C: triple-shell nanoparticles). Transfected cells appear green as a whole due to EGFP fluorescence.

Figure 3.3.3.4 shows the transfection efficiency observed by microscopy. All cells are presented in transmission light microscopy and only transfected cells appear as green cells in fluorescence microscopy. As a control we used calcium phosphate/DNA nanoparticles without protamine to show the effect of protamine on the transfection efficiency.

At the optimal concentration of protamine, the transfection efficiency was better than in control experiments. There was no significance, but the tendency of the increasing transfection efficiency can be clearly seen (Figure 3.3.3.5-3.3.3.7).

Protamine supplied sufficient positive charge to completely neutralize the phosphodiester backbone of DNA. As a consequence of this neutralization, the DNA was condensed into a compact particle[168].

The reason of a more effective transfection with calcium phosphate/DNA/protamine nanoparticles can also be the compensation of the negative charge of DNA by positively charged protamine molecules, thereby improving the uptake by cells. Protamine/DNA nanoparticles (i.e. without calcium phosphate) showed no transfection efficiency in control experiments.

Table 3.3.3.2: Results of transfection experiments with T-HUVEC by numerical analysis of laser fluorescence micrographs. The efficiencies are given as average ± standard deviation (*N*=3).

Method	**Transfektion efficiency, %**		
	Quantum® medium	**RPMI 1640 with FCS**	**Serum-free RPMI 1640**
Polyfect®	9.9 ± 4.0	10.9 ± 3.0	9.9 ± 3.8
Standard calcium phosphate precipitation method	2.8 ± 2.5	5.2 ± 0.2	2.5 ± 2.1
Single-shell calcium phosphate/DNA nanoparticles	2.9 ± 0.6	2.7 ± 1.2	3.5 ± 0.8
Double-shell calcium phosphate/DNA nanoparticles	5.6 ± 2.8	4.9 ± 1.7	6.2 ± 2.4
Triple-shell calcium phosphate/DNA nanoparticles	9.4 ± 3.3	6.1 ± 2.6	9.8 ± 6.5
Single-shell calcium phosphate/DNA/ protamine nanoparticles (10 mg mL^{-1})	4.3 ± 1.5	4.6 ± 1.3	3.5 ± 0.6
Double-shell calcium phosphate/DNA/ protamine nanoparticles (10 mg mL^{-1})	9.7 ± 4.6	8.3 ± 2.6	8.3 ± 2.1
Triple-shell calcium phosphate/DNA/ protamine nanoparticles (10 mg mL^{-1})	9.5 ± 0.8	12.7 ± 8.4	11.5 ± 4.4

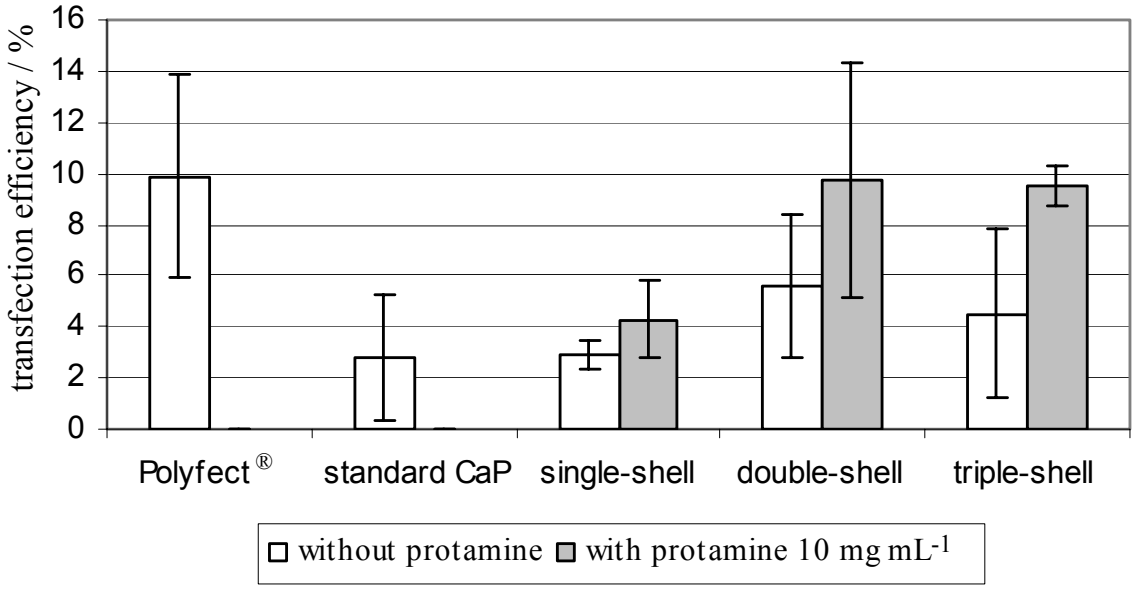

Figure 3.3.3.5: Comparison of the transfection efficiency of T-HUVEC in RPMI 1640 medium without FCS by different methods. The error bars represent the standard deviation (*N*=3).

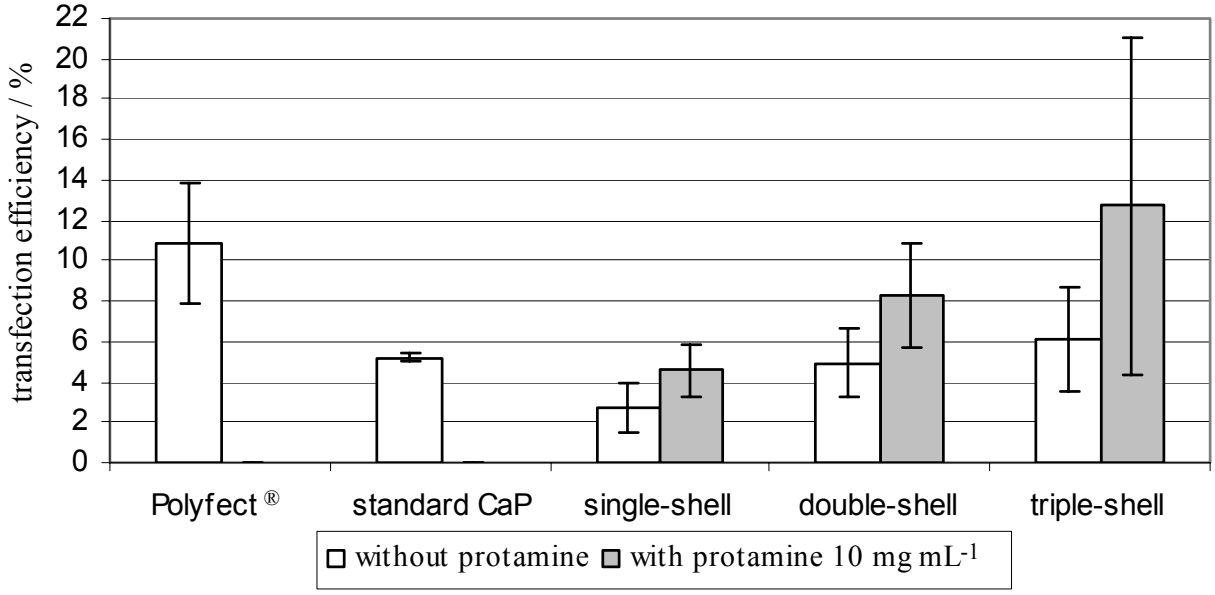

Figure 3.3.3.6: Comparison of the transfection efficiency of T-HUVEC in RPMI 1640 medium with FCS by different methods. The error bars represent the standard deviation (*N*=3).

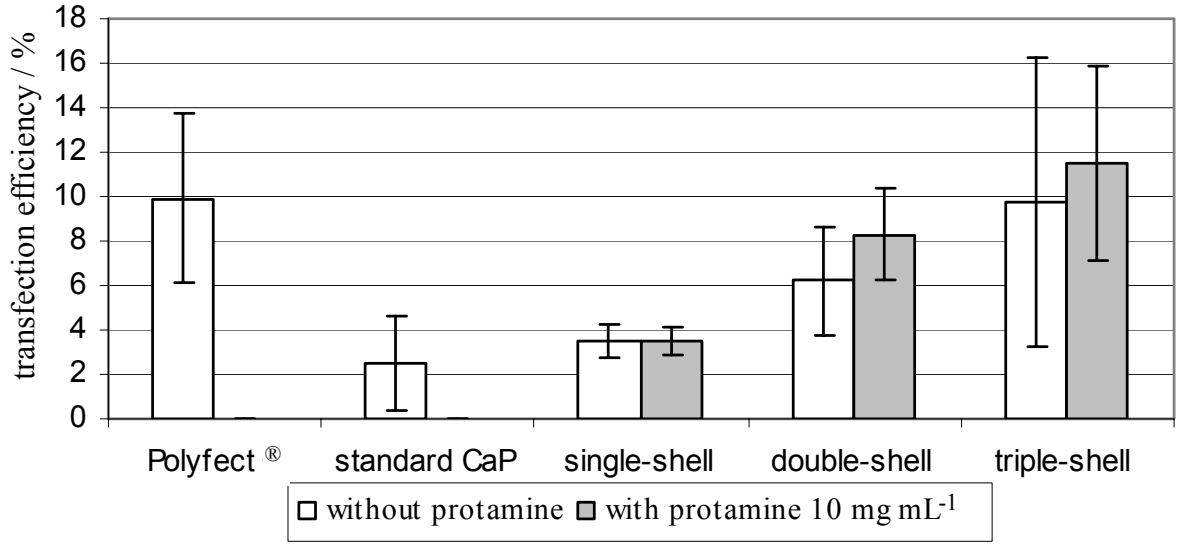

Figure 3.3.3.7: Comparison of the transfection efficiency of T-HUVEC in Quantum® medium by different methods. The error bars represent the standard deviation (*N*=3).

The highest transfection efficiencies were found for nanoparticles in RPMI 1640 with FCS medium (up to 13 %) (Figure 3.3.3.6). The efficiency for triple-shell nanoparticles with protamine was almost two times better compared to those without protamine (12.7 % vs. 6.1 %). In all these cases we can talk only about the tendency of improvement in transfection efficiency, but not about true significance of the results, because the standard deviation is large.

3.3.4 Conclusion

Calcium phosphate/DNA/Protamine nanoparticles were prepared and characterized. Protamine was used to improve the efficiency of DNA delivery into cells. *In vitro* transfection studies showed that calcium phosphate/DNA/protamine nanoparticles had a higher transfection efficiency compared to calcium phosphate/DNA nanoparticles without protamine and as high as a commercially available transfection agent (Polyfect®).

Protamine plays an important role in neutralization of negatively charged DNA molecules and their condensation, which cause an easier interaction of the nanoparticles with negatively charged membrane and their successful penetration into cells. Protamine also provides the direct nuclear import of DNA. However, statistically significant effect of protamine was not found.

3.4 Tracking the pathway of calcium phosphate/DNA

Over the past few years, the intracellular trafficking of plasmid DNA was extensively studied, because it is one of the major challenges for efficient gene delivery[139, 140]. For successful cell transfection (the non-viral introduction of DNA into eukaryotic cells), a variety of extracellular and intracellular barriers must be overcome. There are some major physical barriers: The plasma membrane, the cytoskeletal network and the nuclear membrane[38, 180, 181]. In previous chapters the development of DNA-coated calcium phosphate nanoparticles for cell transfection was shown. Transfection rates comparable to commercial transfection agents (Polyfect®) were achieved with multi-shell nanoparticles. The dispersions could be stored for weeks without loss of transfection efficiency.

General questions remain as to the way of the nanoparticles into the cell and their route within the cell. To address this question, we used the red-fluorescencing marker tetramethylrhodamine isothiocyanate (TRITC) bound to bovine serum albumin (BSA) as a marker. Nanoparticles functionalized with pcDNA3-EGFP for transfection and TRITC-BSA for labeling were prepared. As control, we prepared calcium phosphate nanoparticles functionalized with TRITC-BSA only, and also nanoparticles (aggregates) of pcDNA3-EGFP and TRITC-BSA, i.e. without a calcium phosphate core.

By fluorescence microscopy and laser confocal microscopy we followed the way of the three types of nanoparticles in contact with T-HUVEC cells. Thereby, the efficiency of transfection (green fluorescence) as well as the distribution of the nanoparticles (red fluorescence) could be compared.

3.4.1 Particle characterization

The results of dynamic light scattering are shown in Table 3.4.1.1. In the colloidal dispersion of CaP/BSA, two fractions with a particle size around 11 nm and 268 nm were found, as well as for CaP/DNA/BSA with sizes of 12 nm and 276 nm and for DNA/BSA with sizes of 9 nm and 329 nm. Scanning and transmission electron microscopies confirmed the presence of two fractions of nanoparticles (Figure 3.4.1.1-3.4.1.2). All particles carry a strongly negative charge, as evidenced by the zeta potential, due to the negatively charged phosphate groups of adsorbed DNA. The particle size distributions of all samples were very similar.

Table 3.4.1.1: Colloid-chemical data of functionalized calcium phosphate nanoparticles. PDI=Polydispersity index from dynamic light scattering. The size ratio refers to intensity distributions.

Sample	PDI	Size of small particles / nm	%	Size of large particles / nm	%	Zeta potential / mV
CaP/DNA	0.2	35	92	272	5	-32
CaP/BSA	0.3	11	56	268	35	-40
CaP/DNA/BSA	0.7	12	46	276	51	-30
DNA/BSA	0.4	9	22	329	40	-38

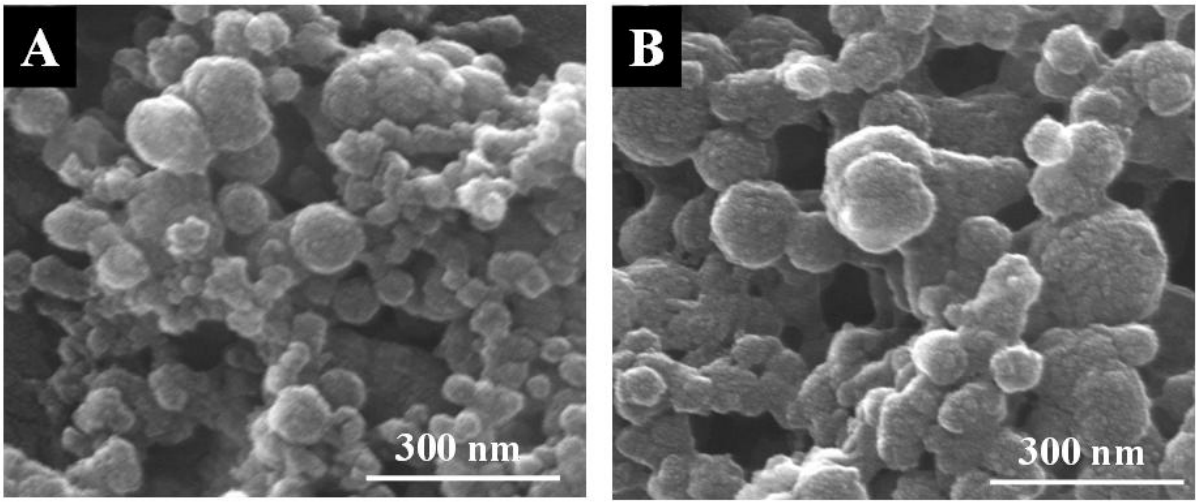

Figure 3.4.1.1 Scanning electron micrographs of CaP/BSA (A) and CaP/DNA/BSA nanoparticles (B). The particle size confirms the results from dynamic light scattering.

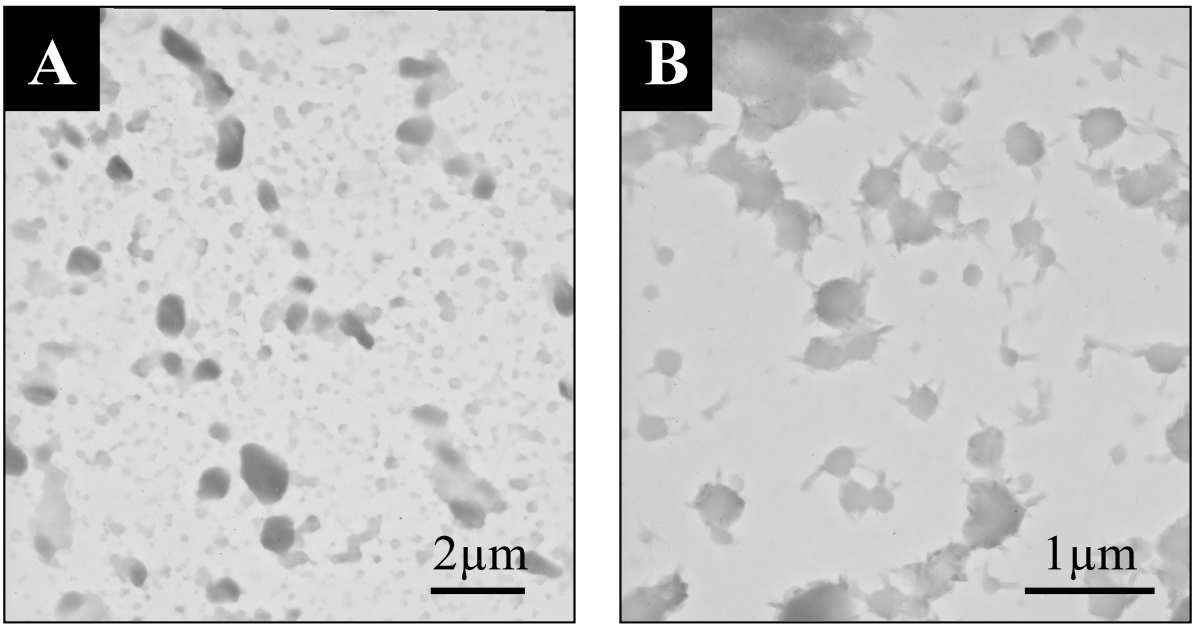

Figure 3.4.1.2: Transmission electron micrographs of CaP/DNA/BSA (A) and CaP/BSA nanoparticles (B). The particle size confirms the results from dynamic light scattering.

3.4.2 Experiments with cells

3.4.2.1 Calcium phosphate/BSA nanoparticles (CaP/BSA)

Fluorescence microscopy and laser confocal microscopy were used to follow the trafficking of fluorescence-labeled nanoparticles into T-HUVEC in vitro (Figure 3.4.2.1). Within the first hour of transfection with CaP/BSA nanoparticles, the nanoparticles accumulated on the plasma membrane. After two hours, the nanoparticles were observed in the cytoplasm. During the next hours, the nanoparticles were transported towards the nucleus. After 24 hours all nanoparticles were found near the nuclear membrane.

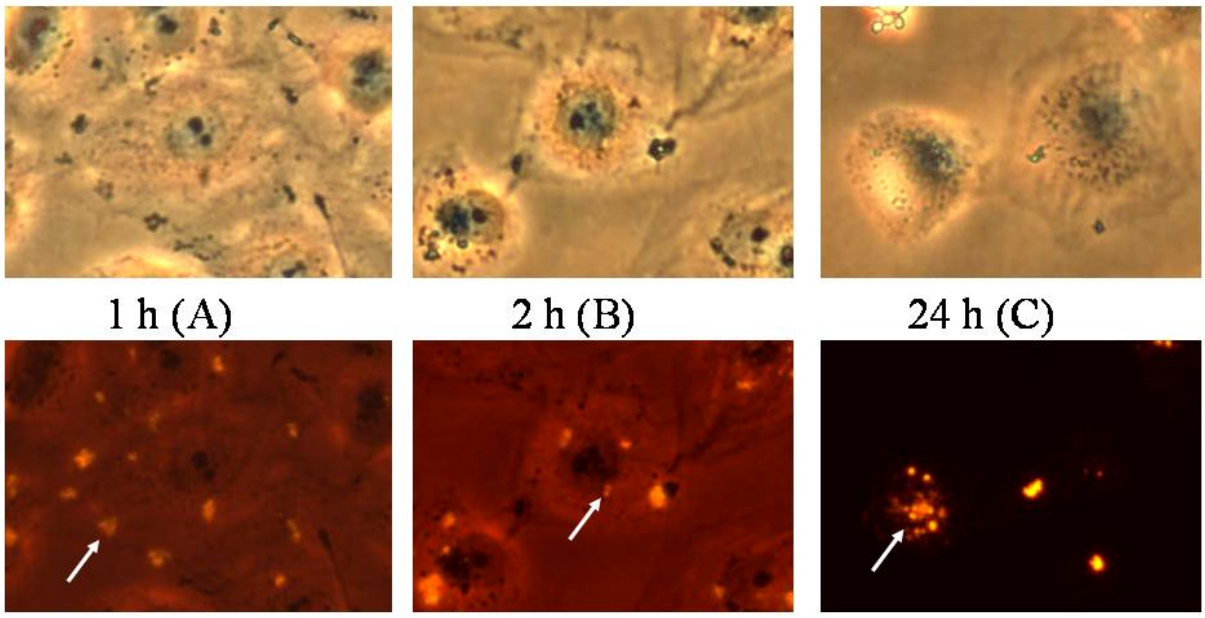

Figure 3.4.2.1: The endocytosis of CaP/BSA nanoparticles in T-HUVEC was monitored using transmission light microscopy (top) and fluorescence microscopy (bottom). In the upper row, cells and nanoparticles (black dots) can be seen. Arrows on fluorescent microscopy images in the lower row show the CaP/BSA nanoparticles as fluorescing dots in the cells.

3.4.2.2 Calcium phosphate/DNA/BSA nanoparticles (CaP/DNA/BSA)

The intracellular fate of CaP/DNA/BSA nanoparticles was similar to that of CaP/BSA nanoparticles in the absence of DNA. In this case we could also see whether DNA was successfully incorporated into the nucleus. i.e. whether or not a transfection occurred. In Figure 3.4.2.2, the way of nanoparticles into the cells is shown. Nanoparticles were accumulated on the plasma membrane and went into the cells after 2 hours of transfection.

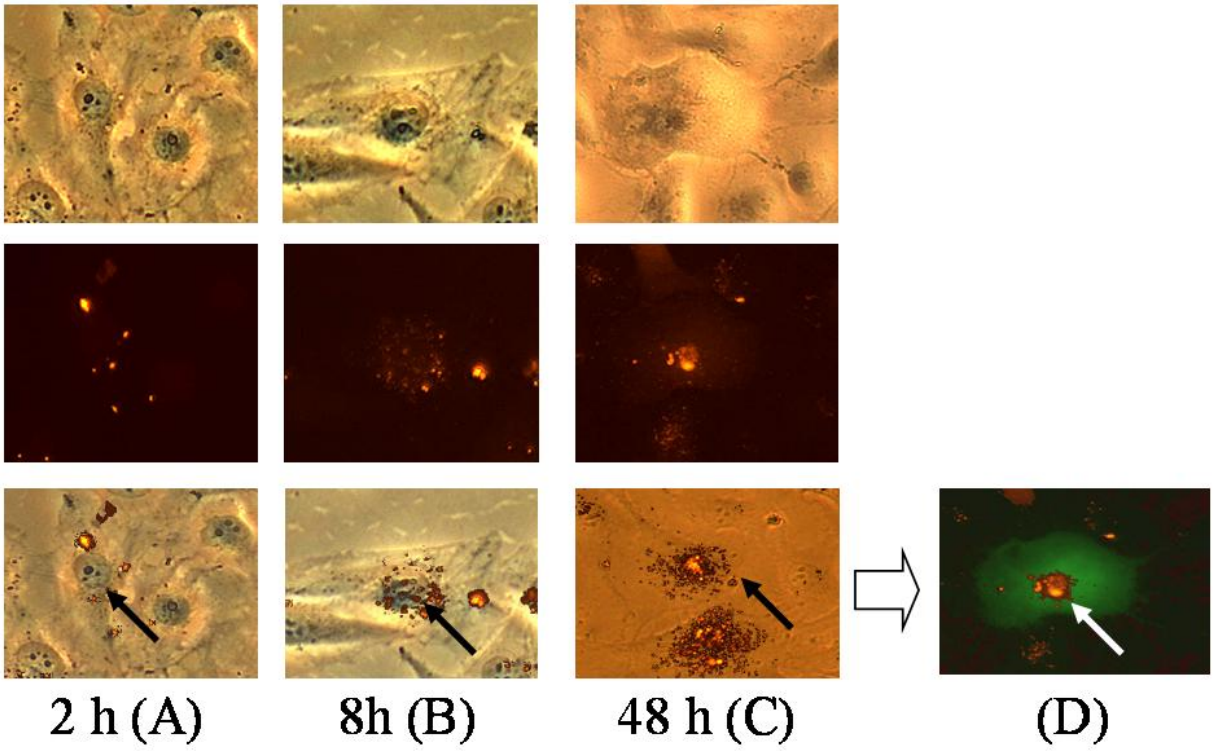

Figure 3.4.2.2: Transmission light microscopy (top row), fluorescence microscopy (center row) and overlay of both pictures (bottom row) of T-HUVEC transfection experiments. In light microscopy, all cells and their nuclei are visible. In the central row, the CaP/DNA/BSA nanoparticles appear as bright red dots. Arrows indicate binding of nanoparticles to the cell surface after 2 h (A), penetration into the cytoplasm after 8 h (B), and accumulation on the nuclear membrane after 48 h (C). After 48 hours, the transfected cells appear green with incorporated red-fluorescing nanoparticles (D).

Already after 8 hours many nanoparticles were attached to the nuclear membrane. The successful incorporation of plasmid DNA into the nucleus was detected using pcDNA3-EGFP which coded for EGFP. Only the transfected cells show the green fluorescence of EGFP (Figure 3.4.2.2, D). Laser confocal microscopy showed that the nanoparticles were accumulated inside the cells in the case of successfully transfected cells (Figure 3.4.2.3).

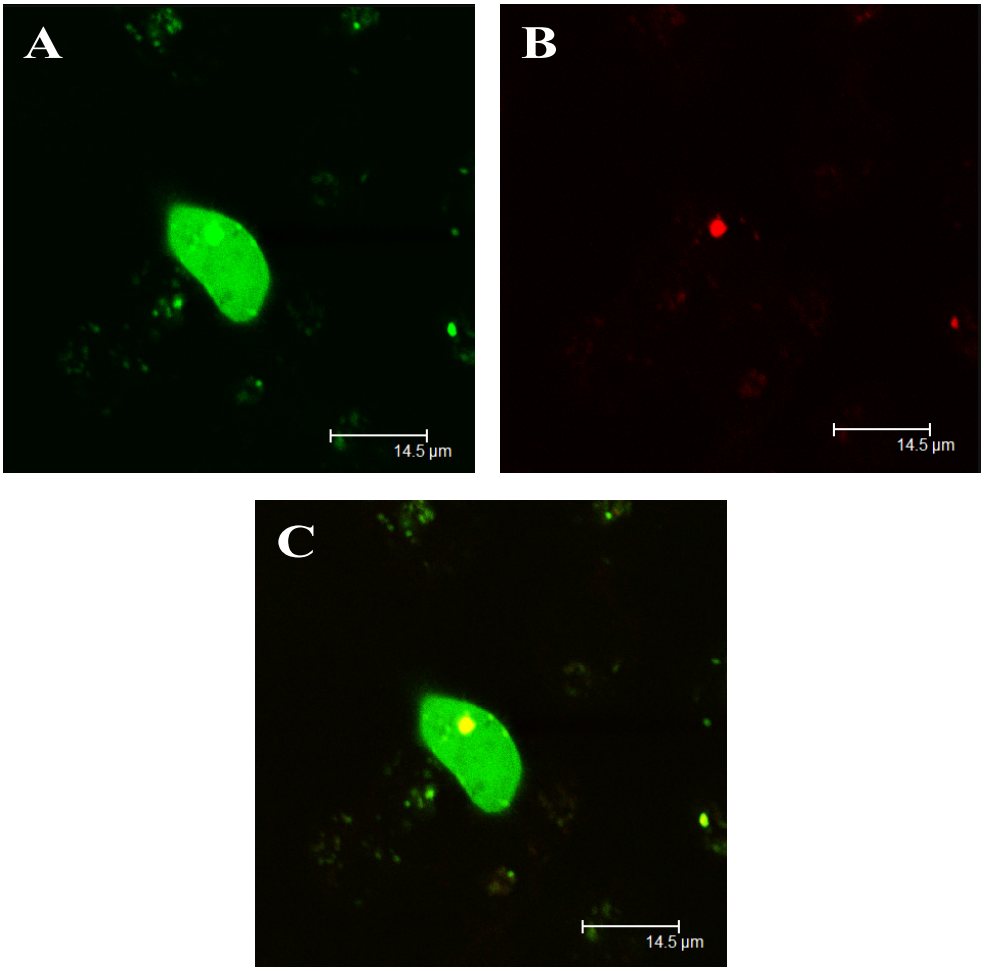

Figure 3.4.2.3: Laser confocal microscopy of T-HUVEC transfection experiments. A green fluorescing transfected cell after 48 hours is shown (A). The CaP/DNA/BSA nanoparticles appear as red fluorescing dots (B). The particles are localized inside the cell (C; overlay of A and B).

3.4.2.3 DNA/BSA nanoparticles (DNA/BSA)

In contrast, the cells treated with DNA/BSA (i.e. without calcium phosphate) remained dark regardless of the incubation time because the cells could not take up TRITC or BSA even at high concentration (Figure 3.4.2.4). The fluorescing aggregates of DNA/BSA neither entered the cells nor adhered to the cell membrane and were completely removed by washing.

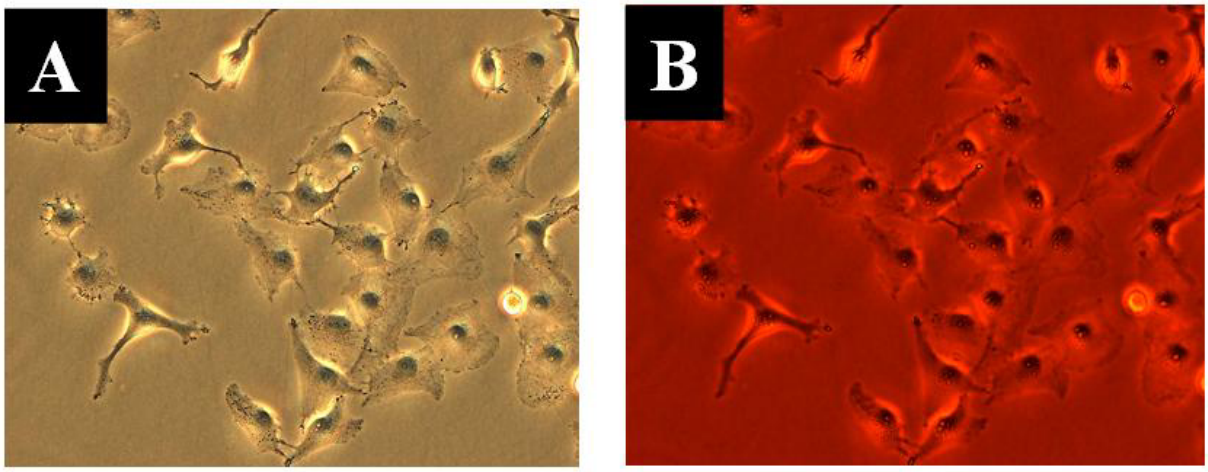

Figure 3.4.2.4: Transmission light microscopy and fluorescence microscopy of T-HUVEC after 2 hours of transfection with DNA/BSA nanoparticles. In light microscopy all cells can be seen (A); by fluorescence microscopy no bright dots were found, i.e. all red-fluorescing particles were removed by washing and no transfection occurred (B).

Our results correspond well to the literature: Choy *et al.* showed that the marker FITC alone can not pass into the cells[119]. It is obvious that calcium phosphate plays an important role in mediating the cellular uptake of TRITC-BSA and DNA. Plasmid DNA routing is a very complicated process consisting of many physico-chemical barriers which have to be overcome for efficient gene expression. The current literature gives a number of studies on the mechanism of intracellular trafficking of nucleic acids after crossing the cell membrane. Lukacs *et al.* examined DNA mobility through the cytoplasm and found that larger DNA fragments were unable to diffuse through the cytoplasm. No

diffusion through the cytoplasm was observed for DNA fragments > 2000 base pairs in length [182]. It was assumed that DNA within endosomes after endocytosis is traveling towards the nucleus by a yet unknown process[153, 183]. Unprotected DNA is degraded within minutes by nucleases presented in cytoplasm[38, 39, 184, 185].

There are three major intracellular processes that can influence on the successful trafficking of plasmid DNA into the nucleus: Endocytosis, endosome escape and nuclear targeting.

To summarize the results from the experiments and the literature the illustration of DNA trafficking can be set up following (Figure 3.4.2.5).

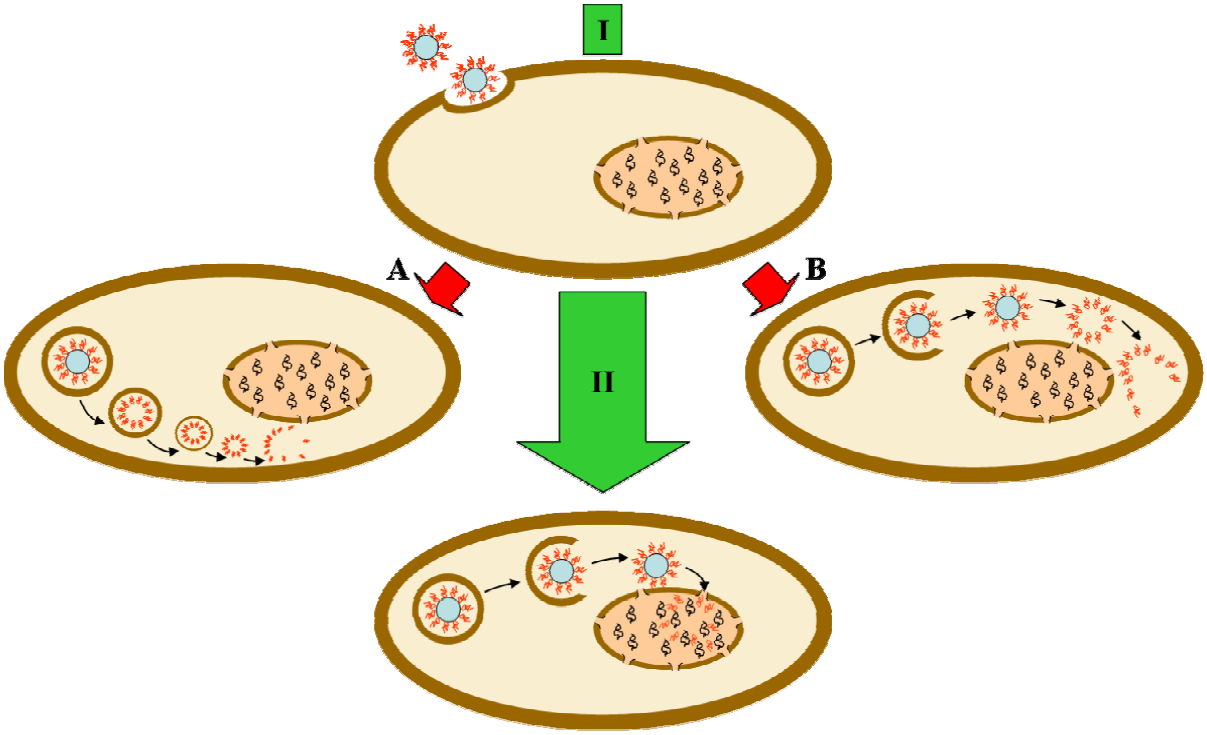

Figure 3.4.2.5: Representation of DNA trafficking into the cell. I-II: A successful trafficking of DNA directly into the nucleus and its expression. Two ways of DNA degradation are shown: A: Degradation in endosomes. Endosome, containing DNA, fuses with lysosome. The degradation of DNA occurs under influence of variety of hydrolytic enzymes inside the lysosome. B: Degradation in the cytoplasm by nucleases.

Nanoparticles are usually too large to pass through ion channels into the plasma membrane, therefore they enter the cell by endocytosis[153, 183]. Endocytosis involves the deformation of the plasma membrane and the formation of endosomal vesicles, containing the nanoparticles.

Plasmid degradation can occur during endocytosis inside endosomes. Endosomal degradation is a multi-step process. Carrier vesicles transfer the nanoparticles with DNA from the early endosomes compartment (with pH 6.3-6.8) to the late endosomes compartment (with pH 5-5.5). If DNA does not escape from endosomes before the fusion with lysosomes (with pH > 5) [186], then endosomal degradation takes place (Figure 3.4.2.5, A). When the nanoparticles with DNA are successfully released into the cytoplasm from endosomes before their fusion with lysosomes, they can suffer an attack by nucleases, which can degrade the DNA (Figure 3.4.2.5, B).

For efficient transfection DNA has to survive the attack of cytoplasmic nucleases and to enter the nucleus. During the trafficking of plasmid DNA in the cytoplasm, DNA must escape from the endosome prior to fusion with lysosomes and be liberated into the cytoplasm before nuclear targeting[178, 181, 187].

Nuclear targeting was studied by many researchers [64, 188-190]. However, it is still not clear when DNA is detached from the nanoparticles. One of the possibilities is that calcium phosphate nanoparticles are slowly dissolved by acid in the endosomal vesicle and DNA is released into the cytoplasm. Another possibility is that nanoparticles with DNA go to the nucleus where the import of DNA can occur. In this case, DNA can be protected until its incorporation into the nucleus which causes an increase in transfection efficiency[163].

3.4.3 Conclusions

We have demonstrated the comparatively easy preparation of calcium phosphate nanoparticles functionalized with DNA and fluorescence-marked with TRITC-BSA. SEM observations and dynamic light scattering analysis showed that all nanoparticles had spherical morphology with sizes between 10 nm and 300 nm. Fluorescence microscopy and laser confocal microscopy studies were used to follow the pathway of these nanoparticles into the cells. The nanoparticles were adsorbed on cellular membrane after 2 h and could be found in the cytoplasm after 8 h where they accumulated then near the nuclear membrane. The transfection efficiency correlates with the distribution of the nanoparticles in the cells. DNA/BSA aggregates alone are not able to penetrate the cell membrane, i.e. the inorganic nanoparticles (calcium phosphate) are necessary as carriers to enter the cell.

3.5 Functionalization of calcium phosphate nanoparticles by oligonucleotides and their application for gene silencing

A promising approach for the treatment of inherited and acquired diseases are gene silencing techniques[191] which can selectively inhibit the synthesis of proteins in a cell. Short fragments of nucleic acids (DNA or RNA) with typical lengths of 15-30 nucleotides must be introduced into a cell[192-194]. These oligonucleotides are able to interact with the mRNA transcripts of a mutant or an over-expressed gene inside the cell (in the cytoplasm), thereby preventing their translation into disease-related proteins.

The major challenge of this approach is to find an efficient delivery method system for oligonucleotides into the cell. Generally, oligonucleotides can only exert their inhibitory role when they have entered the cell[180], i.e. after passing through the cell membrane. Effective viral systems were developed to achieve this goal, but this approach is potentially dangerous due to the risk of recombination of the virus, strong immunogenicity and carcinogenicity[195]. Most alternative methods make use of the fact that nanoparticles are taken up by living cells, and can therefore be used as carriers for biomolecules like DNA, RNA, or oligonucleotides. Generally, the uptake of “naked” oligonucleotides or DNA into cells is not possible[73]; therefore a suitable carrier is needed. The problem with the non-viral delivery of oligonucleotides into cells in gene therapy is similar to the delivery of DNA. However, it may be assumed that short oligonucleotides are taken up easier than full-size DNA[196]. Generally, the uptake of "naked" oligonucleotides or DNA into cells is not possible[196]; therefore a suitable carrier is needed. A promising approach that has been developed in the last years is the use of nanoparticles as carriers for these biomolecules. Provided that the nanoparticles are small enough, different substances can be used, like polymers[197, 198], liposomes[199], peptides, or inorganic nanoparticles like silica[200, 201], magnetite[200, 201], gold[115, 202], and calcium phosphate[118, 154, 163].

It was shown in previous chapters that custom-made DNA-functionalized calcium phosphate nanoparticles can be used for cell transfection. Calcium phosphate is advantageous to other types of nanoparticles due to its easy preparation (also inexpensive), its high affinity to DNA[203], its high biocompatibility, and its good biodegradability in biological systems[12]. In this chapter we report the preparation and stabilization of such nanoparticles with oligonucleotides of defined length and sequence. As proof of principle, we also show that double-stranded RNA (22 nucleotides) can induce gene-specific inhibition of the expression of enhanced green fluorescent protein (EGFP) in HeLa-EGFP cells.

3.5.1 Characterization of calcium phosphate/oligonucleotide colloids

Calcium phosphate nanoparticles were prepared by rapid mixing of aqueous solutions of calcium and phosphate (with the concentration 6.25 mM and 3.74 mM), followed by addition of oligonucleotides to the formed dispersion to coat the inorganic nanoparticles and to prevent their aggregation. As with DNA, we expected the negatively charged oligonucleotides to interact with the calcium phosphate surface[203]. The high degree of adsorption can be immediately derived from the strongly negative zeta potential (pure calcium phosphate has a zeta potential of about +7 mV)[156]. The oligonucleotides on the surface should stabilize the dispersions both by electrostatic repulsion as well as by steric stabilization (Figure 3.5.1.1).

Table 3.5.1.1: Colloid-chemical data of oligonucleotide-functionalized calcium phosphate at a concentration of the oligonucleotides of 5 μM.

Sample	Oligo 5'-3' (single-stranded)	Zeta potential / mV	Size of small particles / nm	Size of large particles / nm
10-1	AGTCCCCTCT	-2	578	>5000
18-2	GGAGCTGGTGTTTACGGC	-23	233	935
18-3	GAGCCAACCTGGCTCTGA	-14	-	1831
25-5	TTAGCCATGGGTGCACTT GAGCGGC	-25	176	516
30-6	CCCTGGATCCCATATGCT ATTACCAGAACA	-18	313	944

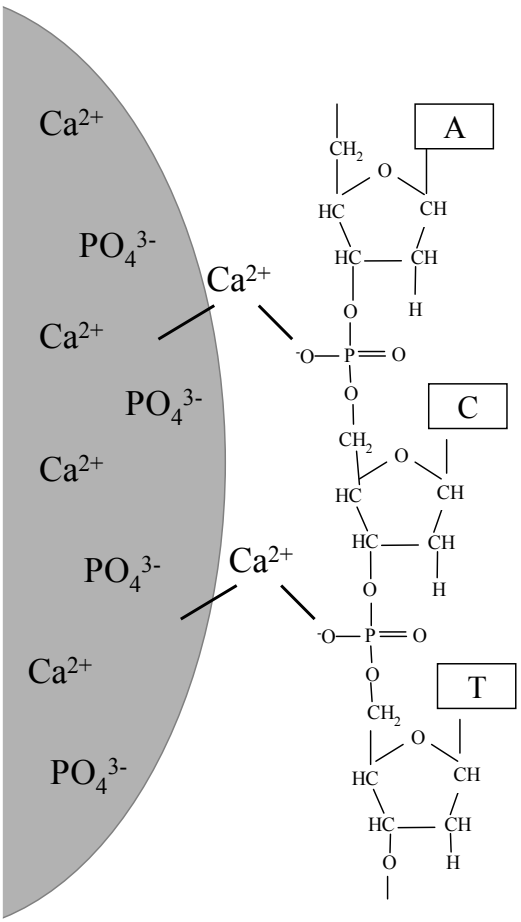

Figure 3.5.1.1: Schematic model of the interaction between a calcium phosphate particle and an oligonucleotide.

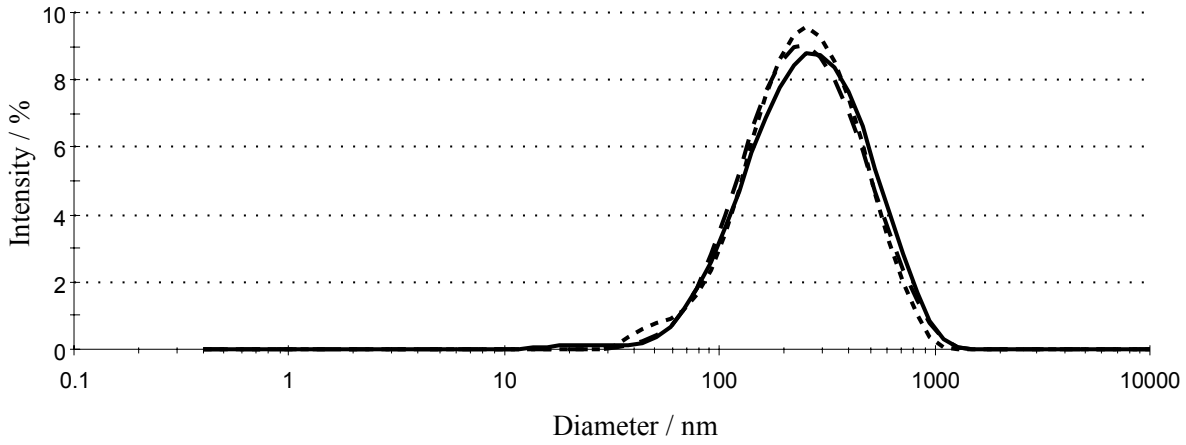

Figure 3.5.1.2: Results of dynamic light scattering of calcium phosphate nanoparticles, functionalized by single-stranded oligonucleotides (concentration 9 μM). The particles had an average size around 200 nm (solid line: sample A; dashed line: sample D; dotted line: sample F; Table 3.5.1.2).

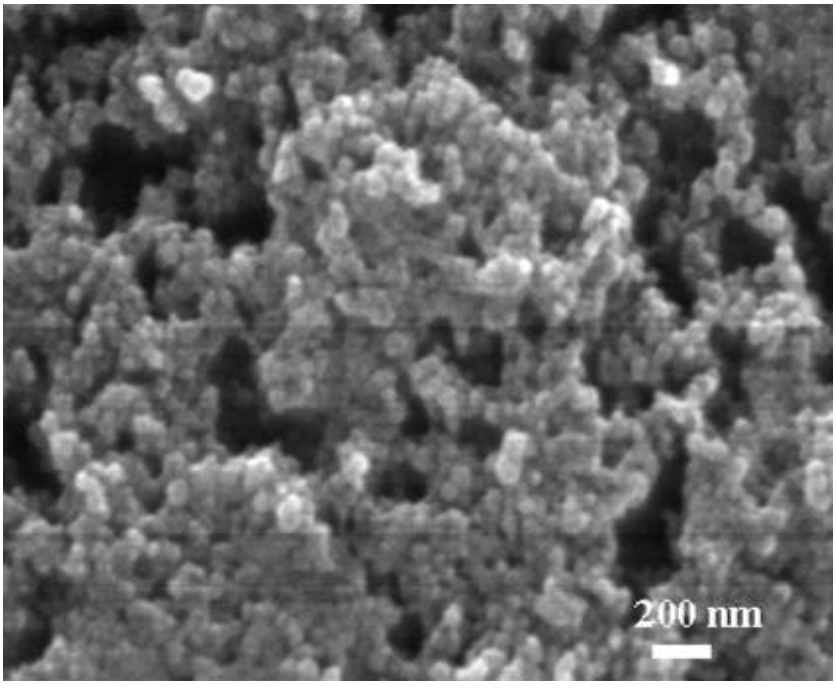

Figure 3.5.1.3: Scanning electron micrograph (SEM) of calcium phosphate nanoparticles, functionalized with the single-stranded oligonucleotide 25-G at a concentration 9 μM (Table 3.5.1.2; sample C). Note that the particle size in SEM is smaller than by dynamic light scattering because in the latter method, the hydrodynamic radius is measured.

Table 3.5.1.2: Colloid-chemical data of functionalized calcium phosphate nanoparticles (standard deviations given after the average in parantheses). The initial concentrations were $[Ca^{2+}]$=6.25 mM and $[HPO_4^{2-}]$=3.74 mM. PDI=Polydispersity index from dynamic light scattering.

	Name	Sequence (from 5' to 3')	[Oligo] / µM	Zeta potential / mV	PDI	Particle size (Z-average) / nm
A	25-5	TTAGCCATGGGTGCACTTGAGCGGC	9	-29 (7)	0.3	212
B	25-comp	GCCGCTCAAGTGCAC CCATGGCTAA	9	-29 (6)	0.3	194
C	25-G	CGGTAGAGGGGACTTTCCGAGTGGC	9	-30 (8)	0.2	184
D	25-C	GCCACTCGGAAAGTCCCCTCTACCG	9	-28 (8)	0.3	202
E	25-polyC	CCCCCCCCCCCCCCCCCCCCCCCCC	9	-29 (6)	0.3	256
F	37-V	AGAGGGGACTTTCCGAGACGCTCGGAAAGTCCCCTCT	9	-29 (6)	0.3	210
G	25-5	TTAGCCATGGGTGCACTTGAGCGGC	45	-44 (12)	0.5	437
H	25-comp	GCCGCTCAAGTGCAC CCATGGCTAA	45	-37 (8)	0.3	250
I	25-G	CGGTAGAGGGGACTTTCCGAGTGGC	45	-30 (10)	0.5	581
J	25-C	GCCACTCGGAAAGTCCCCTCTACCG	45	-36 (7)	0.3	271
K	25-polyC	CCCCCCCCCCCCCCCCCCCCCCCCC	45	-20 (7)	0.5	552
L	V-37	AGAGGGGACTTTCCGAGACGCTCGGAAAGTCCCCTCT	45	-31 (7)	0.4	237
M	25-5/25-comp	double strand of 25-5 and 25-comp	5	-22 (7)	0.2	352
N	25-5/25-comp	double strand of 25-5 and 25-comp	9	-21 (5)	0.3	297
O	25-5/25-comp	double strand of 25-5 and 25-comp	45	-33 (10)	0.2	113
P	25-G/25-C	double strand of 25-G and 25-C	5	-22 (7)	0.2	307
Q	25-G/25-C	double strand of 25-G and 25-C	9	-20 (6)	0.4	367
R	25-G/25-C	double strand of 25-G and 25-C	45	-36 (12)	0.3	231

A good colloidal stabilization of single-stranded oligonucleotides was possible at a concentration of 9 µM as shown by dynamic light scattering and electron microscopy (Figures 3.5.1.2 and 3.5.1.3). At a lower concentration (5 µM), only larger aggregates were observed (>500 nm) (Table 3.5.1.1) and at a higher concentration (45 µM), also larger aggregates (>1000 nm) besides the 100-200 nm particles were observed in some cases by dynamic light scattering (Table 3.5.1.2).

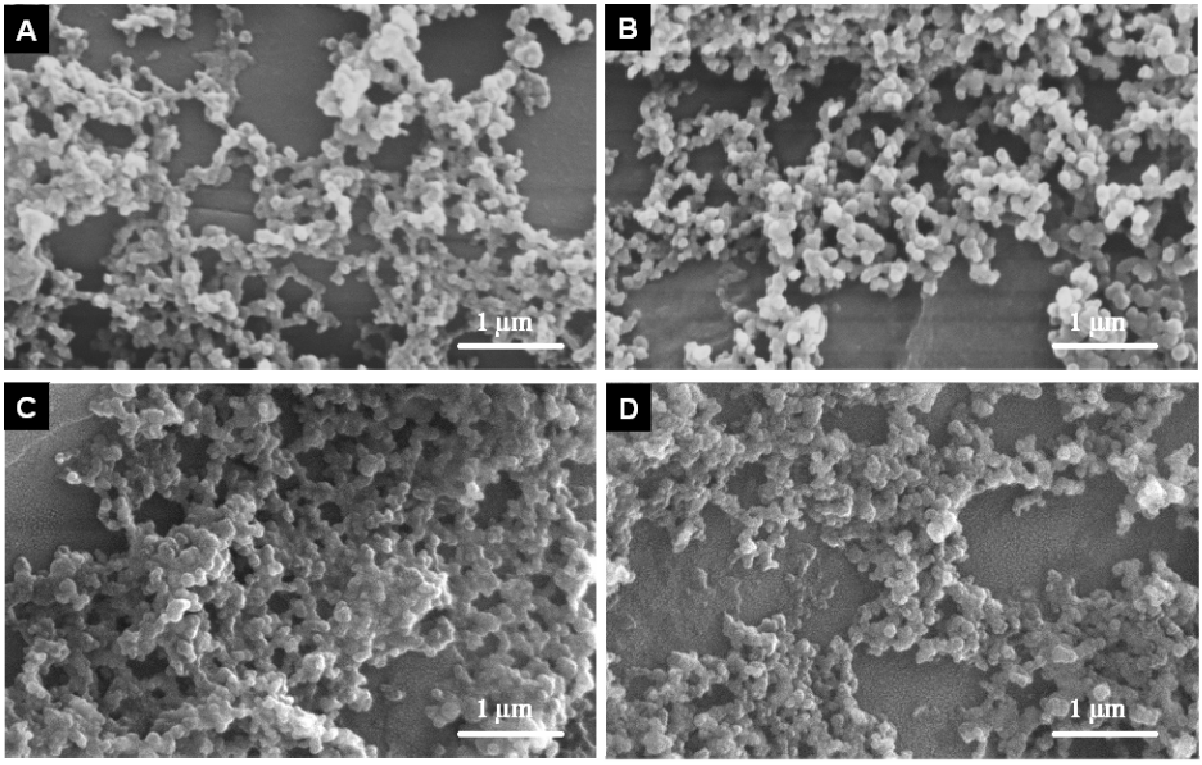

Figure 3.5.1.4: Scanning electron micrograph of calcium phosphate nanoparticles, functionalized with the single-stranded oligonucleotide 25-5 (A) and 25-5comp (B), 25-C (C), and 25-polyC (D) with the concentration 45 µM. (Table 3.5.1.2; samples G, H, J, K).

We assume that at the lower concentration, the surface was not sufficiently covered to prevent crystal growth, and that at the higher concentration, agglomeration of the primary particles occurred. This agglomeration may be driven by the interaction of complementary nucleobases.

At the optimal concentration (9 µM), we observed no significant differences in particle size (around 200 nm) and zeta potential (around -30 mV) for the different single-stranded oligonucleotides. However, the sequence and ratio of the nucleobases in the single-stranded oligonucleotides had an influence on the particle size at the higher concentration (45 µM). A strong tendency to agglomeration was observed for the oligonucleotides 25-5, 25-G, 25-polyC where the particle size reached 400-500 nm. However, the change in size was not significant for the other oligonucleotides (Table 3.5.1.2).

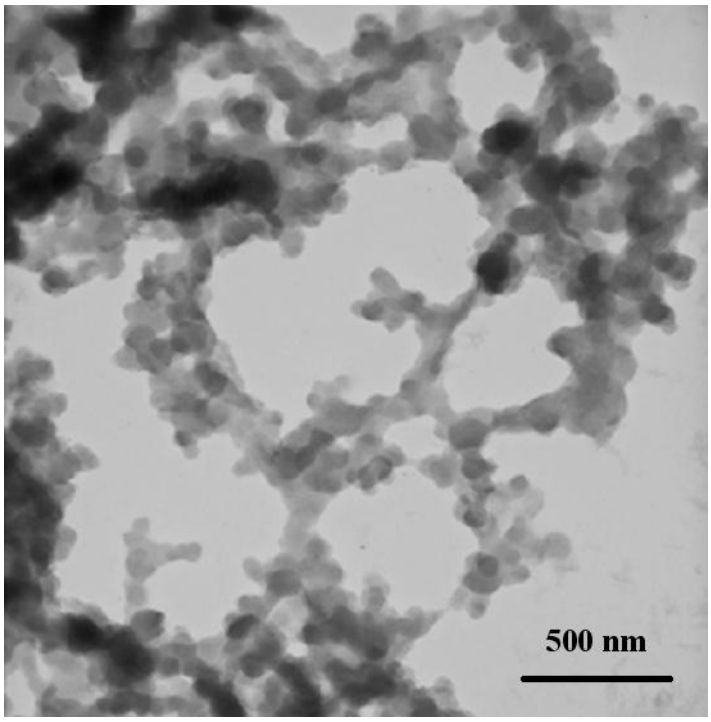

Figure 3.5.1.5: Transmission electron micrograph of calcium phosphate nanoparticles, functionalized by the oligonucleotide 25-G with the concentration 45 µM. The particles had a typical size around 70 nm (Table 3.5.1.2; sample I).

Electron microscopy revealed that the larger particles at the higher concentration (45 µM) consisted of agglomerated primary nanoparticles and not of large individual crystals (Figures 3.5.1.4 and 3.5.1.5). This supports the assumption that the oligonucleotides effectively prevented the crystal growth, but also caused some kind of bridging of neighboring particles.

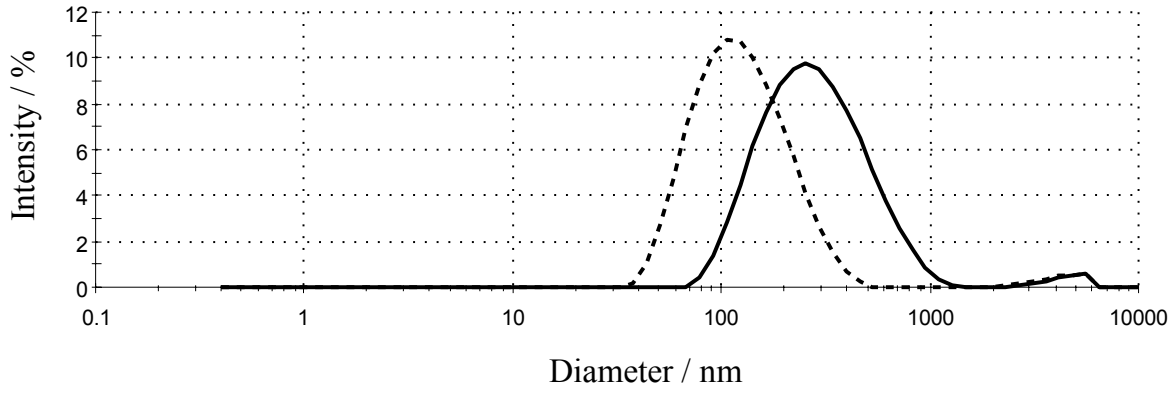

Figure 3.5.1.6: Results of dynamic light scattering of calcium phosphate nanoparticles, functionalized with double-stranded oligonucleotides at theconcentration 45 µM (solid line: 25-G/25-C; dashed line: 25-5/25-comp). (Table 3.5.1.2; samples R, O).

We used the same concentrations as for single-stranded oligonucleotides to stabilize calcium phosphate nanoparticles with double-stranded oligonucleotides (25-5/25-comp and 25-G/25-C). In this case, a higher concentration was needed for effective stabilization. The optimal concentration was 45 µM with a particle size around 110 nm for 25-5/25-comp and 230 nm for 25-G/25-C (Figure 3.5.1.6). The concentrations of 5 µM and 9 µM are too small for an effective stabilization, and the particles showed an increase in the hydrodynamic diameter up to 350 nm (Table 3.5.1.2).

In this case not only the concentration of double-stranded oligonucleotides but also the type of oligonucleotides played an important role in the formation of nanoparticles. As shown in Figure 3.5.1.7, calcium phosphate nanoparticles functionalized by double-stranded oligonucleotides had a different size and morphology.

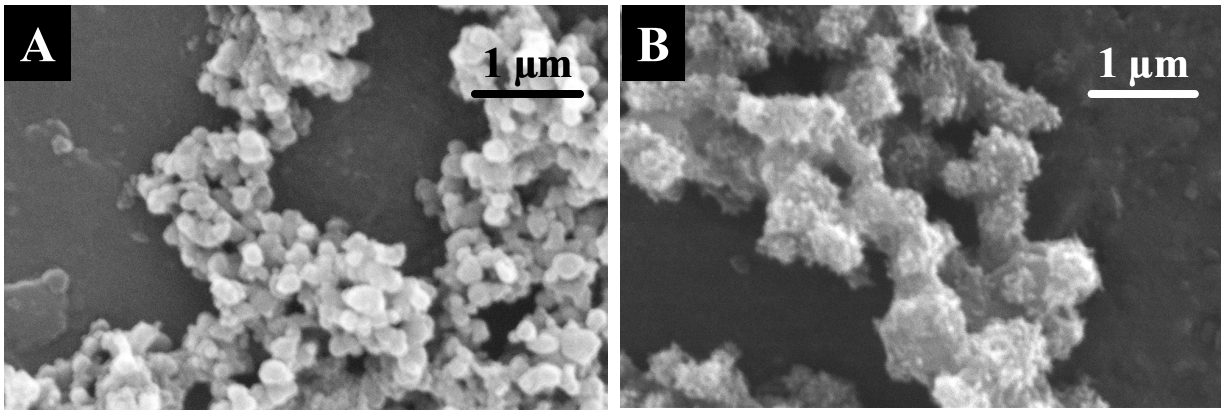

Figure 3.5.1.7: Scanning electron micrograph of calcium phosphate nanoparticles, functionalized with the double-stranded oligonucleotides 25-5/25-comp and 25-G/25-C (Table 3.5.1.2, samples O, R).

Colloids with the 25-5/25-comp duplex consisted of spherical smooth nanoparticles with hydrodynamic diameters of about 110 nm. On the other hand, the double-stranded oligonucleotides 25-G/25-C with calcium phosphate formed fluffy nanoparticles with a size of 230 nm (Figure 3.5.1.7, Table 3.5.1.2). In the latter case, the growth of the calcium phosphate nanocrystals was not effectively inhibited.

3.5.2. Gene silencing experiments on HeLa-EGFP cells

Gene silencing was tested according to Refs[93, 204-206] on EGFP-HeLa cells with double-stranded siRNA, encoding the inhibition of EGFP synthesis. siRNA with 22 nucleobases (22-nt) was shown earlier to induce the greatest decrease in GFP expression[93]. We used a concentration of 45 µM dsRNA which was found optimal for double-stranded oligonucleotides (see above). The resulting calcium phosphate/siRNA nanoparticles also had a particle size around 100 nm and a spherical morphology (Figure 3.5.2.1). siRNA was used to down-regulate the expression of an EGFP reporter pre-mRNA which is stably expressed in HeLa cells. Once the mRNA has been cleaved, the synthesis of the fluorescing protein

EGFP cannot occur anymore. Thus, the extent of EGFP inhibition in the cells (cells which show no green fluorescence anymore) is proportional to the antisense activity of the tested delivery system.

The efficiency can then be easily computed from the ratio of still fluorescing cells to the total number of cells. Figure 3.5.2.2 and Table 3.5.2.1 show the corresponding results. The efficiency of gene silencing was between 40 and 60 %, with no significant dependence on the medium. The efficiency of the dispersion did not decrease after two weeks of storage at 4 °C, indicating a high stability of the colloidal dispersions. The results of EGFP knockdown efficiency of HeLa-EGFP in DMEM with FCS and in Quantum® medium are graphically represented in Figure 3.5.2.3

Note that such calcium phosphate nanoparticles are not toxic as shown earlier by Welzel *et al.* by an MTT test[154]. In addition, the morphology of the cells in light microscopy showed that they were still alive, therefore it cannot be argued that the decrease in the number of green fluorescing cells was due to an adverse action of the nanoparticles. The kind of cell culture medium did not play a significant role.

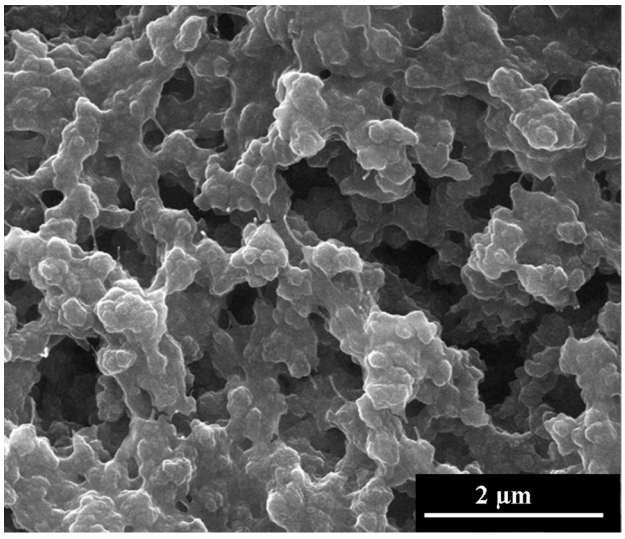

Figure 3.5.2.1: Scanning electron micrograph of calcium phosphate nanoparticles, functionalized by siRNA (concentration 45 µM).

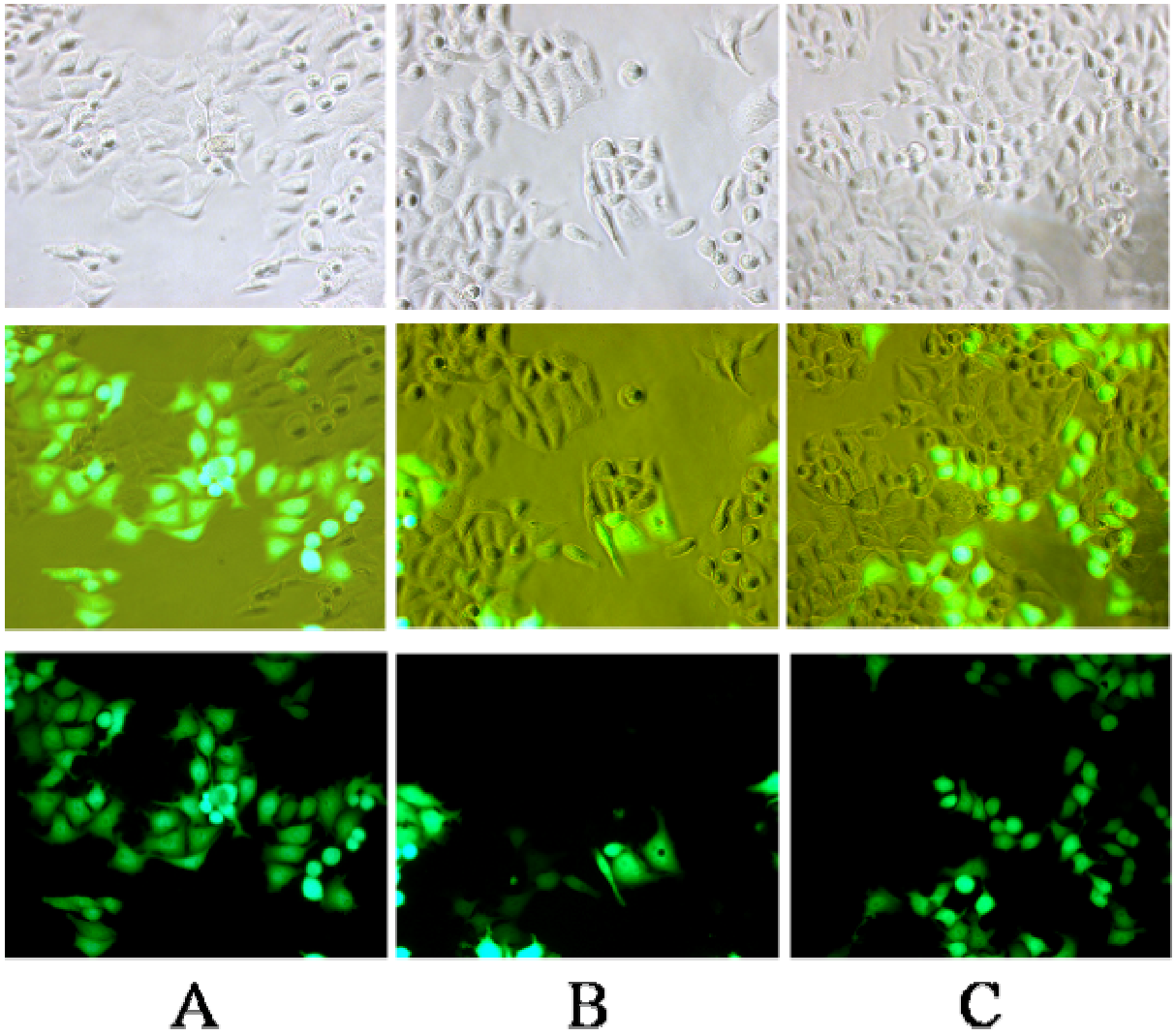

Figure 3.5.2.2: Transmission light microscopy (top row) and EGFP fluorescence microscopy (center and bottom rows; different contrast) of HeLa-EGFP antisense experiments after transfection. In the two upper rows, all cells can be seen. In the two lower rows, the cells which still express EGFP appear green. A: Control (no transfection); B: Cell culture in DMEM medium with FCS; C: Cell culture in Quantum® medium (magnification 200x in all cases).

Table 3.5.2.1: Results of transfection experiments with HeLa-EGFP by numerical analysis of the laser fluorescence micrographs. The percentage of green fluorescing cells is given as average ± standard deviation (*N*=3 for freshly prepared dispersions; *N*=1 for dispersions stored at 4 °C). There is no significant decrease in the transfection efficiency after storage.

Method	**Percentage of green fluorescing cells**	**Percentage of not fluorescing cells**	**Percentage of successful gene silencing**	**Efficiency of gene silencing**
Control	82±4 %	100–82 = 18 %	18–18 = 0 %	0/82 = 0.00
Calcium phosphate/oligo-nucleotide nanoparticles in DMEM/FCS, freshly prepared	48±13 %	100–48 = 52 %	52–18 = 34 %	34/82 = 0.41
Calcium phosphate/oligo-nucleotide nanoparticles in DMEM/FCS, after 14 d storage at 4 °C	40 %	100–40 = 60 %	60–18 = 42 %	42/82 = 0.51
Calcium phosphate/oligo-nucleotide nanoparticles in Quantum®, freshly prepared	38±12 %	100–38 = 62 %	62–18 = 44 %	44/82 = 0.54
Calcium phosphate/oligo-nucleotide nanoparticles in Quantum®, after 14 d storage at 4 °C	34 %	100–34 = 66 %	66–18 = 48 %	48/82 = 0.59

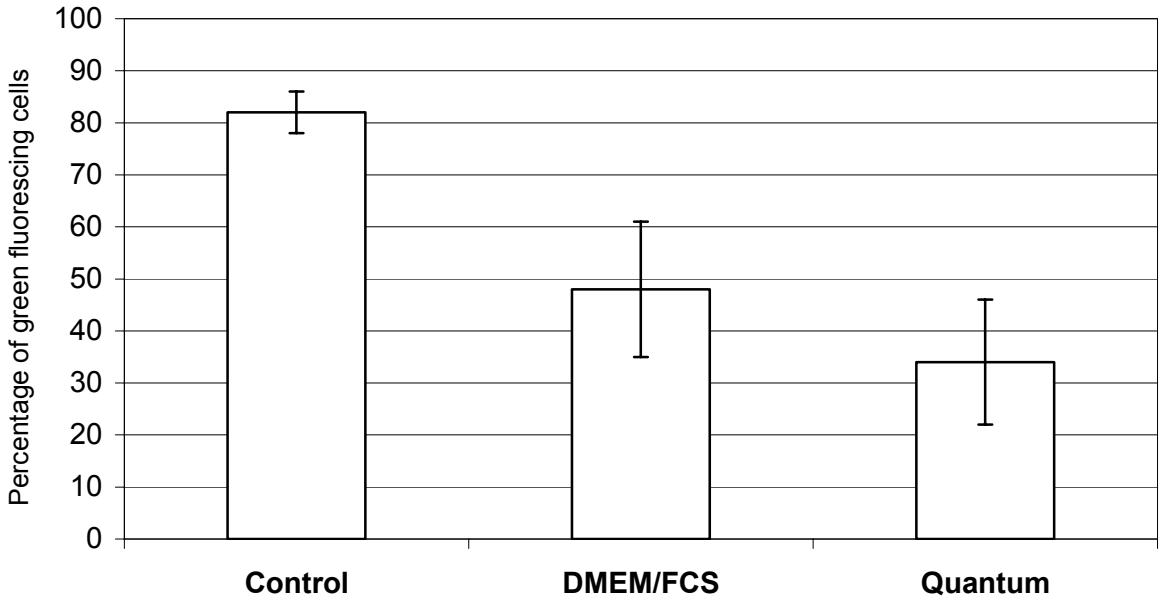

Figure 3.5.2.3: EGFP knockdown efficiency of HeLa-EGFP in DMEM with FCS and in Quantum® medium, expressed as the ratio of the number of not fluorescing cells to the total number of cells with not transfected cells as control. The error bars represent the standard deviation (N=3). There were significant statistical differences between the transfection experiments and the control (P<0.001).

Calcium phosphate nanoparticles as oligonucleotide delivery system have several advantages over other non-viral and viral delivery system. Such nanoparticles can be easily and cost-efficiently prepared, they are highly biocompatible and not cytotoxic, and they are not infectious like viral vectors.

3.5.3 Conclusion

In the current study, we have shown the preparation of stable calcium phosphate/oligonucleotide dispersions and their biological application *in vitro* to HeLa-EGFP cells. Calcium phosphate nanoparticles can be stabilized with a shell of oligonucleotides. To obtain a stable colloid, both the oligonucleotide concentration and the nature of oligonucleotides (single- or double-stranded) must be considered. Monodisperse colloids could be prepared with single-stranded oligonucleotides at a concentration of 9 µM and with double-stranded oligonucleotides at a concentration of 45 µM. The size of the stabilized nanoparticles is in the range of 100 nm, i.e. well-suited for cellular uptake. The dispersions showed a good physicochemical stability and could be stored at 4°C without agglomeration or precipitation for several weeks.

We have developed this into a delivery system for antisense oligonucleotides in which these nanoparticles are used for down-regulation of gene expression by targeting the mRNA resulting in effective gene silencing. The nanoparticle/siRNA dispersions can be stored without loss of biological efficiency.

3.6 Synthesis of carbonated apatite with the model protein ubiquitin by the co-precipitation method

Bone tissue is one of the most frequently used tissues for transplantation, as damage of bone can occur by various reasons such as trauma, tumor resection and others.

Autogeneous, allogeneous and xenogeneous bone graft materials are used in clinical applications. Many complications like infection, pain, loss of sensibility and hematoma were described for these materials[207]. Synthetic calcium phosphate materials are currently under investigation for their potential as a bone-substitution material. Their chemical composition is similar to that of natural bone mineral, and they possess suitable biological properties like biocompatibility, osteoconductivity and biodegradability[159, 208-210].

Besides the scaffold material, another important component in bone regeneration are osteoinductive factors like bone morphogenetic proteins (BMP)[211]. BMPs play a key role in bone development and osteogenesis. 14 different BMPs are known, which belong to the transforming-growth-factor-beta (TGF-β) superfamily[212, 213]. The application of recombinant human bone morphogenetic protein 2 (rhBMP-2) is of great medical interest, because it leads to enhanced bone growth[214].

For our studies we have used the model protein ubiquitin which has been shown earlier to possess very similar adsorption properties like rhBMP-2[215, 216].

Here we studied the way to load a nanocrystalline calcium phosphate with the model protein ubiquitin at pH 10 and room temperature. In the first part, we studied the influence of ubiquitin on the formation and properties of the formed carbonated apatite by comparing ubiquitin-calcium phosphate samples (co-precipitation method) and calcium phosphate samples without ubiquitin (see chapter 4.5.6).

In the second part, we determined how much of the radioactive ubiquitin was incorporated into the calcium phosphate particles by the co-precipitation method

compared to the control ubiquitin-calcium phosphate samples where the formation of calcium phosphate particles occurred first, followed by the addition of ubiquitin.

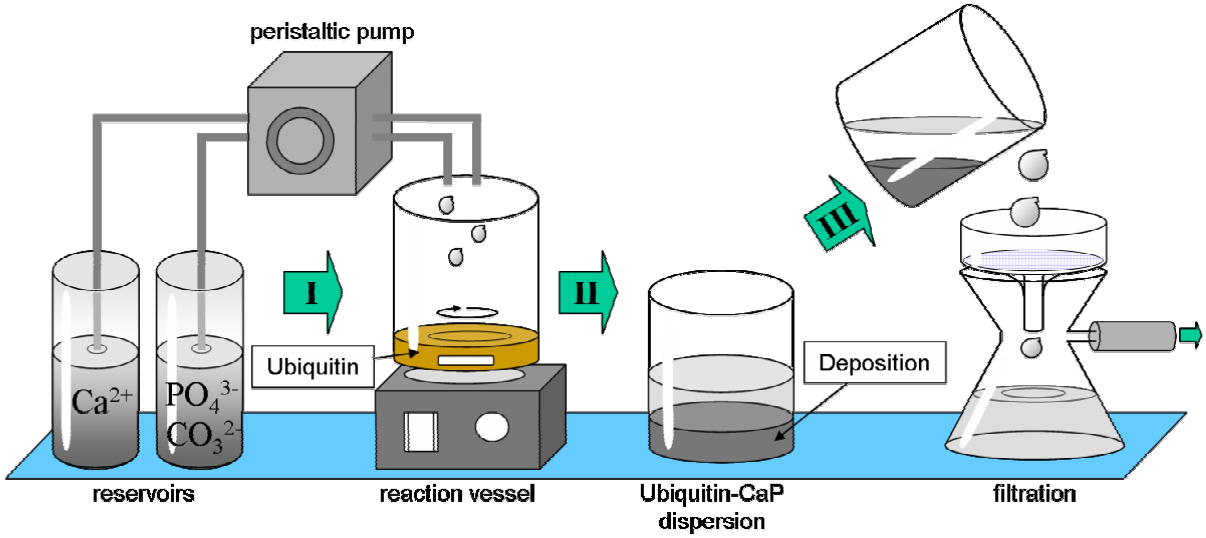

Figure 3.6.1.1: Schematic setup of the apparatus used for the preparation of the ubiquitin-calcium phosphate samples by the co-precipitation method. I: Ca^{2+}-solution and PO_4^{3-}/CO_3^{2-} were mixed in a vessel containing 5 mg of ubiquitin solution to form a precipitate. II: The dispersion stood for 5 hours. III: The dispersion was washed and filtered off. The powder was dried for 12 h at 37 °C.

3.6.1 Characterization of the ubiquitin-calcium phosphate samples

Two types of the samples were used for the characterization: Ubiquitin-calcium phosphate samples prepared by the co-precipitation method and calcium phosphate samples prepared without ubiquitin.

Calcium phosphate particles prepared without ubiquitin are different in shape compared to those obtained in the presence of ubiquitin. Figure 3.6.1.2 (A, B) shows SEM images of the calcium phosphate powder without ubiquitin. The crystals were approximately spherical with a diameter around 50-80 nm.

Ubiquitin molecules presented during precipitation slightly affected the morphology and size of the particles.

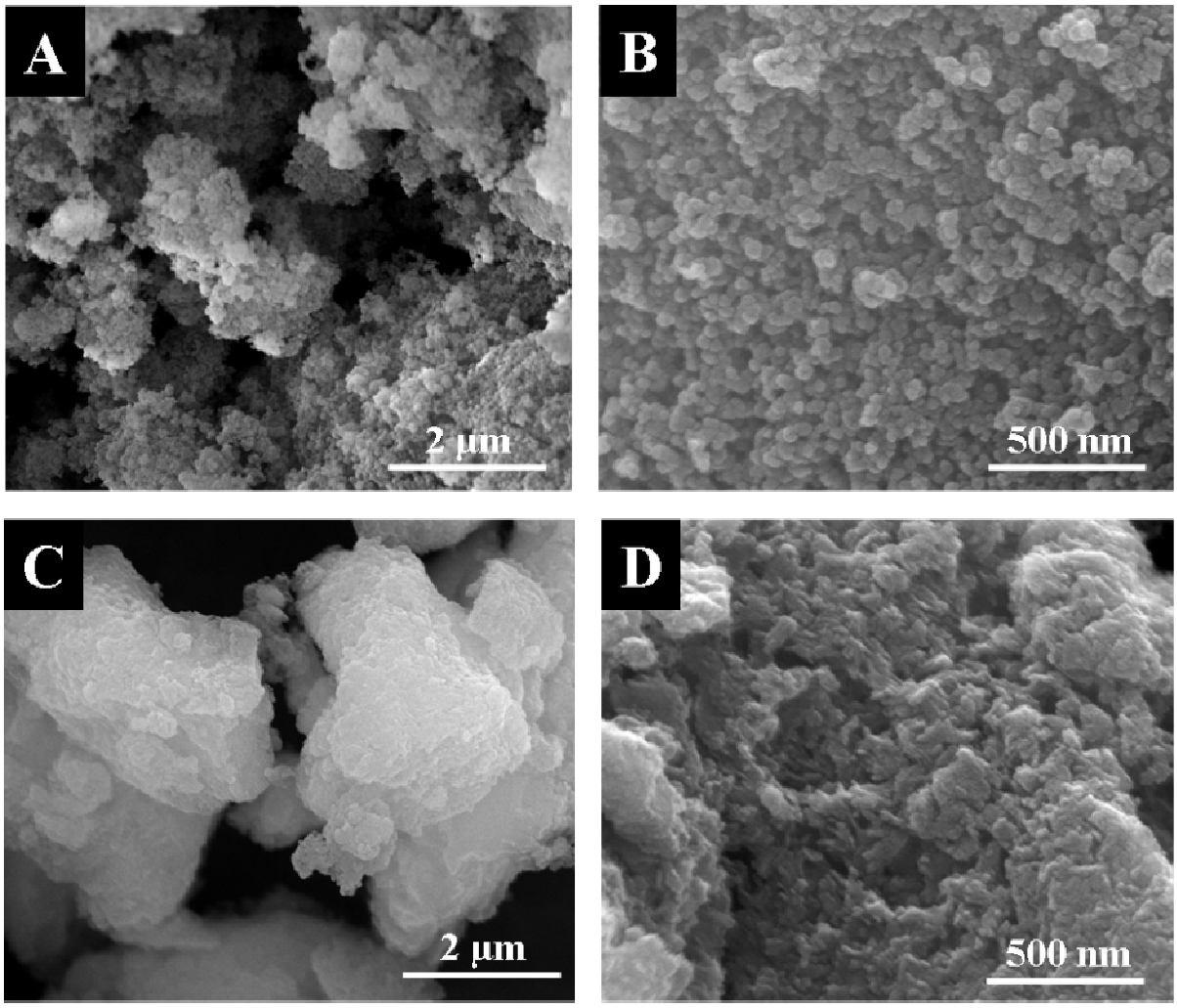

Figure 3.6.1.2: Scanning electron micrograph of calcium phosphate samples without ubiquitin (A, B) and the ubiquitin-calcium phosphate samples prepared by the co-precipitation method (C, D).

As represented in Figure 3.6.1.2 (C, D), the particles prepared by the co-precipitation method with ubiquitin were aggregated and showed no defined form.

It is important to note that ubiquitin led only to a slight change in the structural properties of the nanocrystalline calcium phosphate phase. In Figure 3.6.1.3 the

infrared spectra are shown, recorded for co-precipitated ubiquitin-calcium phosphate samples and for calcium phosphate samples without ubiquitin.

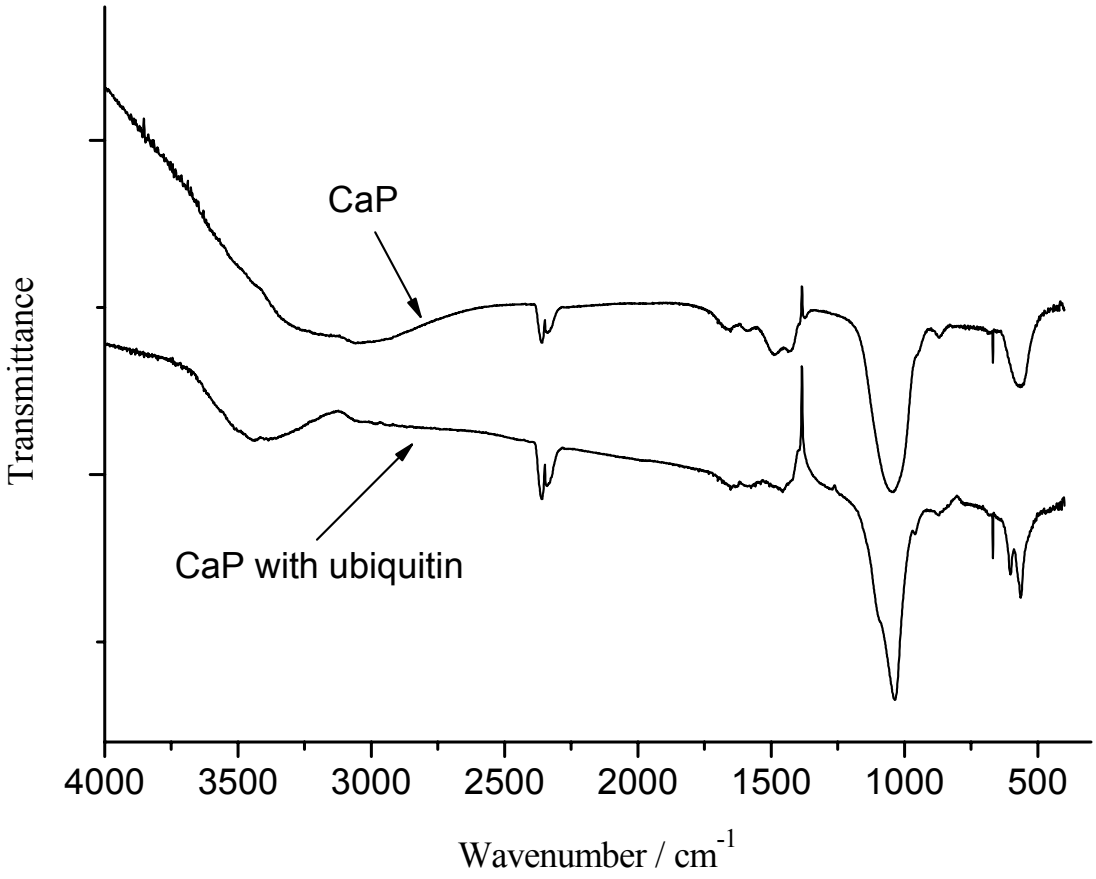

Figure 3.6.1.3: Infrared spectra of calcium phosphate samples without ubiquitin and the ubiquitin-calcium phosphate samples prepared by the co-precipitation method.

Infrared spectroscopy (IR) showed that in both cases infrared absorption bands are typical for calcium phosphate (Figure 3.6.1.3). The presence of calcium, phosphate and oxygen was shown by EDX analysis (Figure 3.6.1.4).

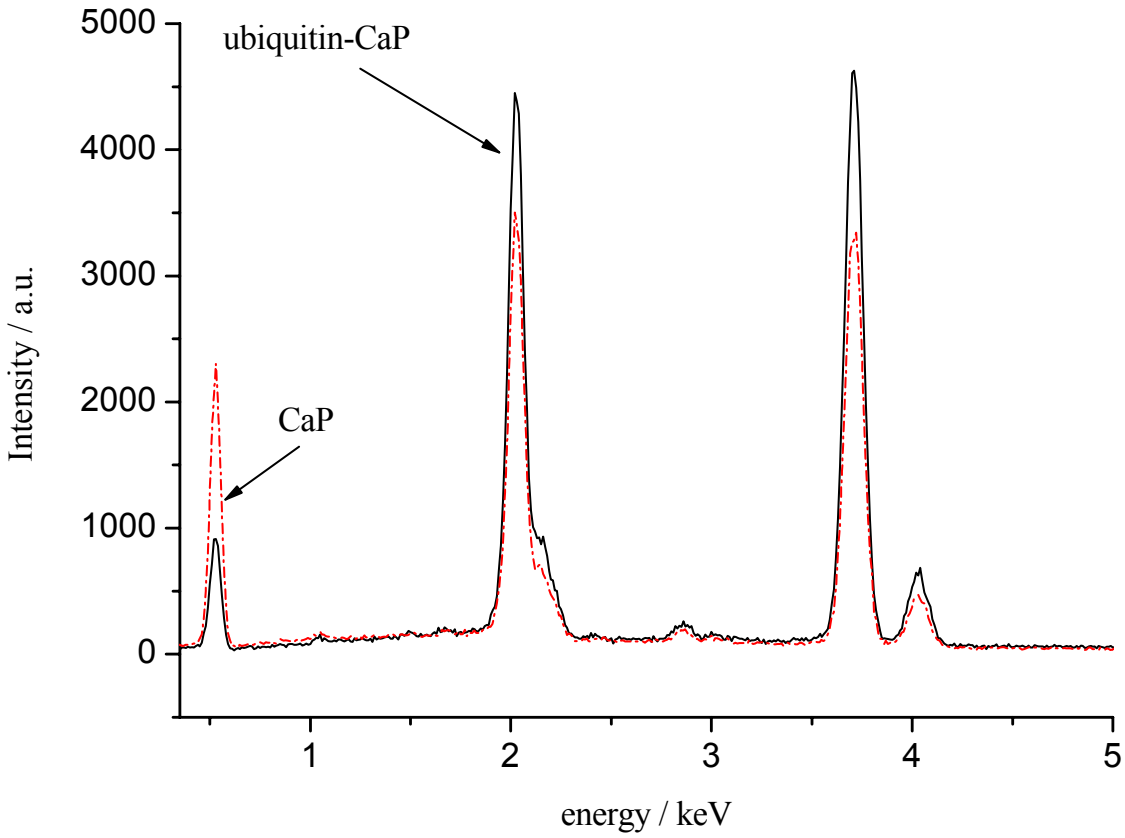

Figure 3.6.1.4: EDX of calcium phosphate samples without ubiquitin (dashed line) and the ubiquitin-calcium phosphate samples prepared by the co-precipitation method (solid line).

Powder X-ray diffraction (XRD) was applied to identify the nanocrystalline structure of calcium phosphate. Figure 3.6.1.5 displays the XRD pattern for the powder corresponding to Figure 3.6.1.2. A difference was observed between calcium phosphate and ubiquitin-calcium phosphate materials. The samples co-precipitated with ubiquitin showed a higher crystallinity than the control samples prepared without ubiquitin, as indicated by narrower diffraction peaks.

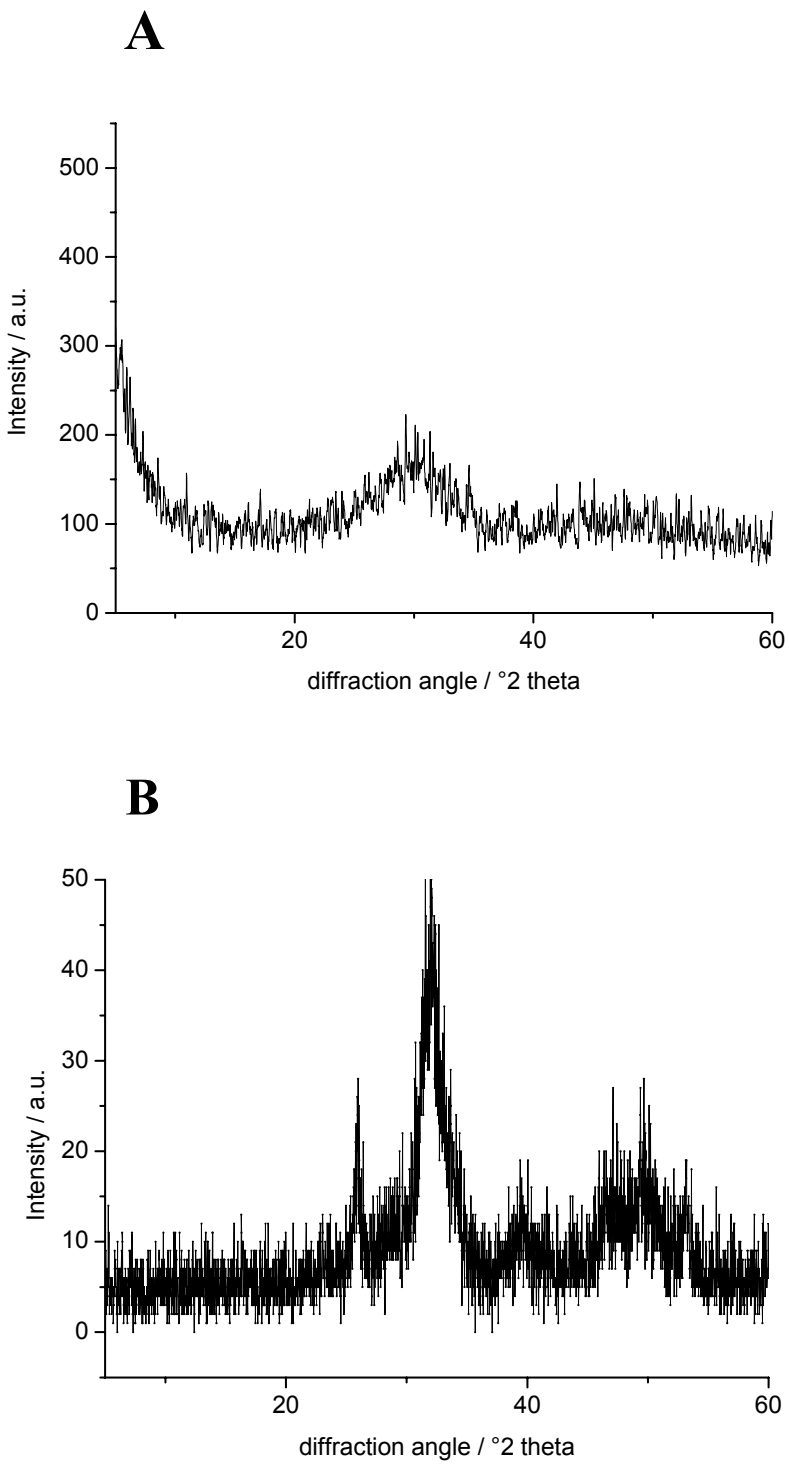

Figure 3.6.1.5: X-ray powder diffractogram of calcium phosphate samples without ubiquitin (A) and the ubiquitin-calcium phosphate samples prepared by the co-precipitation method (B).

The properties of calcium phosphate in the presence of biologically active molecules (osteogenic agents, growth factors, drugs, etc.) were extensively studied earlier[217-220]. The adsorption of proteins onto HA is of interest because the understanding of the interaction between proteins and HA is fundamental for an understanding of biomineralization. Miles *et al.* reported organic materials which affected the formation of biological apatite[221]. Termine *et al.* closer investigated the influence of various macromolecules on HA in solution and showed that biomolecules restrained the crystal growth of HA, and in some cases completely inhibited the transformation of ACP to HA[222].

Bernardi *et al.* showed that at a given pH some proteins bind to the calcium sites on the surface of HA crystals by negatively charged acidic groups and that more basic proteins attach to surface phosphate groups[223].

Numerous reports have shown that proteins and peptides which have a high negative charge inhibited the nucleation and crystal growth of HA[224-226].

In our case we showed that ubiquitin had a only a small influence on the formation of the calcium phosphate.

3.6.2 Measurement of the incorporation of radioactive ubiquitin into the particles

The percentage of incorporated radioactive ubiquitin into the nanoparticles was measured with a γ-counter in ubiquitin-calcium phosphate samples prepared by the co-precipitation method and in control samples.

By the co-precipitation method (Figure 3.6.1.1), 2.081 g of dry ubiquitin-calcium phosphate powder were obtained from 3 L of solution. The concentration of ubiquitin after mixing was 5 μg mL^{-1} which corresponded to 15000 μg ubiquitin in 3 L of the calcium phosphate dispersion. For a calibration curve, 6 samples (1 mL each) were taken from the ubiquitin-calcium phosphate dispersion and measured on the γ-counter (Table 3.6.2.1).

Table 3.6.2.1: Results of the calibration samples for ubiquitin-calcium phosphate prepared by the co-precipitation method.

Sample	counts per minute (cpm)
1	44577.2
2	46175.5
3	46219.9
4	46278.8
5	45563.3
6	46152.0

The average was 45828 cpm corresponding to 5 µg ubiquitin. Therefore, 1 µg of ubiquitin corresponded to 9166 cpm.

Then 3 samples of ubiquitin-calcium phosphate powder with the mass of 0.141 g, 0.066 g and 0.112 g were taken and measured. It was found that these samples contained 63.7 µg, 33.2 µg and 53.3 µg of ubiquitin, respectively. Finally, the mass of ubiquitin in 1 g of ubiquitin-calcium phosphate powder was calculated (Table 3.6.2.2, samples 1A-3A)

The total mass of ubiquitin-calcium phosphate (2.081 g) contained 993 µg of ubiquitin. Therefore, the percentage of incorporated ubiquitin was: 993 / 15000 · 100 % = 6.6 %.

Table 3.6.2.2: Results of γ-Counter for the calculation of ubiquitin contents in the calcium phosphate powder. Samples A series show the results of co-precipitation and B series show the control experiment.

Sample	CaP / g	cmp	Ubiquitin / µg	µg Ubiquitin / g Ubiquitin-CaP	Average µg Ubiquitin / g Ubiquitin-CaP
1A	0.141	584404.1	63.7	452.2	477
2A	0.066	304324.3	33.2	503.0	
3A	0.112	488639.7	53.3	476.0	
1B	0.078	131658.5	13.07	167.6	176
2B	0.049	92010.5	9.14	186.5	
3B	0.054	94267.2	9.36	173.3	

In the same way the bound ubiquitin was determined in the control samples. As control was prepared and dried without ubiquitin and then dispersed in a solution of radioactive ubiquitin. Thus, only the surface was coated. The final concentration of ubiquitin was the same as in the co-precipitation method (5 µg mL^{-1}). 6 samples (1 mL each) were taken from the ubiquitin-calcium phosphate dispersion and measured on the γ-counter (Table 3.6.2.3).

Table 3.6.2.3: Results of the calibration samples for control ubiquitin-calcium phosphate samples.

Sample	counts per minute (cpm)
1	51498.3
2	51855.9
3	50877.7
4	49869.1
5	49057.8
6	48839.5

The average is 50333 cpm corresponding to 5 µg ubiquitin. Therefore, 1 µg of ubiquitin corresponded to 10067 cpm.
Then 3 samples with the following masses 0.078 g, 0.049 g, 0.0540 g were taken from control ubiquitin-calcium phosphate powder and measured. Finally the following masses of ubiquitin were determined (13.07 µg, 9.14 µg and 9.36 µg) and calculated for 1 g of ubiquitin-calcium phosphate powder (Table 3.6.2.2, samples 1B-3B). The total mass of ubiquitin-calcium phosphate (2.006 g) contains 353 µg of ubiquitin. The percentage of bound ubiquitin was: 353 / 15000 · 100 % = 2.35 %.

We found that the total percentage of bound ubiquitin after co-precipitation was 6.6 % which included the protein adsorbed on the surface as well as that incorporated into the crystals. In the control experiments 2.35 % of ubiquitin was found on the surface of the crystals. In this case ubiquitin could only be adsorbed on the surface of calcium phosphate particles, because formation of calcium phosphate particles took place without the presence of ubiquitin. The difference between the total amount of ubiquitin (adsorbed and incorporated) and that adsorbed on the surface (from control samples) was 4.25 %. That means that about 4.25 % of ubiquitin were incorporated into the crystals.
The amount of incorporated ^{125}I-ubiquitin strongly depended on the way of precipitation and ubiquitin incorporated into the calcium phosphate particles three times better when the formation of crystals occurred in the presence of ubiquitin, i.e. by co-precipitation.

3.6.3 Conclusion

We performed the preparation of calcium phosphate samples with ubiquitin by the co-precipitation method. In these experiments ubiquitin served as a model protein, which has similar immobilization properties as rhBMP-2. We showed that the presence of ubiquitin had almost no influence on the crystallinity and crystal morphology.

It was demonstrated that up to 6.6 % of ^{125}I-ubiquitin can be adsorbed/incorporated into the particles and 4.25 % of the protein was incorporated.

The presented co-precipitation method allows the preparation of calcium phosphate particles loaded with proteins similar to ubiquitin. It means that proteins of the BMP family are able to adsorb on the calcium phosphate particles. An implantation of such biofunctionalized calcium phosphate ceramics (e.g. cold-isostatically pressed into an appropriate shape) in bone defects can stimulate the development of new bone at the implantation site.

4 Materials and Methods

4.1 Applied materials for cell culture experiments

4.1.1 Cell culture solutions/antibiotics

Accutase	PAA
BM Cyclin 1 + 2	Roche
DMEM	PAA
FCS	PAA, Biochrom
Glutamine	Gibco BRL/Invitrogen
HEPES	Biomol
PBS	Biochrom
Penicillin/Streptomycin	Gibco BRL/Invitrogen, PAA
Quantum®	PAA
RPMI1640	PAA, Biochrom
Trypsine	Gibco BRL/Invitrogen

4.1.2 Chemicals

Ampicillin	Biomol
EDTA	Merck
Ethanol	JT Baker
Ethidium bromide	Serva
Glycerol	Riedel de Haen
Yeast-extract	Roth
Pepton-hydrolysate	Gibco BRL
SDS	Biomol

4.1.3 Devices

Incubator	Heraeus
Microscopes	Olympus CK2
	Olympus IX51
	Zeiss Axioplan
	Zeiss Axiovert 35
Laminar flow hood	Heraeus
Thermomixer	Eppendorf
Centrifuges	Eppendorf 5415C (Minifuge)
	Heraeus Megafuge 1.0R

4.1.4 Applied consumables und kits

Nucleobond® PC 10000 plasmid DNA purification kit (endotoxin-free)	Macherey-Nagel
multi plate wells (24-, 6-wells)	Nunc, TPP, Sarstedt
Polyfect®	Qiagen, Hilden
Flasks 75 cm^3	Nunc, TPP

4.2 Molecular-biological methods

4.2.1 Preparation of plasmid-DNA from bacterial culture

All works with intact bacteria were carried out under semi-sterile conditions with autoclaved instruments and solutions[227].

4.2.1.2 Transformation of bacteria

250 µl of competent bacteria were thawed from -80 °C and placed on ice. 5 µl of ligation sequences was added and the mixture was incubated on ice for about 30 min. A heat shock was carried out in the thermoblock for 90 s at 42 °C, afterwards 1 mL LB (Luria Bertani) medium was added and incubated for 30 min at 37 °C.

Then the bacteria were centrifuged (Minifuge, 3000 rpm, room temperature, 2 min), smoothed out on LB-ampicillin-plates and then incubated at 37 °C up to 12 h until visible colonies of bacteria appeared[228].

Permanent cultures of transformed bacteria were taken from overnight cultures, placed with 50 % of glycerol and stored at -80 °C.

LB medium:
10 g L^{-1} Pepton-hydrolysate
10 g L^{-1} NaCl
5 g L^{-1} yeast-extract
pH 7.4 with NaOH
+ 100 µg ml^{-1} ampicillin

4.2.1.3 Preparation of plasmid-DNA for transfection of eukaryotic cells

The preparation of plasmid-DNA for transfection of eukaryotic cells was accomplished with a NucleoBond® PC 10000 EF kit (Macherey-Nagel, Düren). Sterile plasticware and autoclaved glassware were used. 100 mL LB-ampicillin-medium was mixed with a bacterial culture and incubated over night under shaking at 37 °C. The bacteria were centrifuged in 50-ml-tubes (Megafuge, 4000 rpm / 3200 g, 15 min, 4 °C). The purification of plasmid-DNA was carried out according to the manufacturer's recommendation (Nucleobond PC 1000 plasmid DNA, Macherey-Nagel). After the precipitation of DNA and washing the DNA precipitates, plasmid-DNA was placed in sterile endotoxin-free water. The concentration was determined by UV-photometry and the DNA was stored at -20 °C.

4.2.2 Synthesis of oligonucleotides

All oligonucleotides were assembled in A. N. Belozersky Institute of Physico-Chemical Biology, M. V. Lomonosov Moscow State University, on an ABI 394A DNA Synthesizer by the cyanoethyl phosphoramidite method according to the manufacturer's recommendations and purified by reversed-phase HPLC. The conditions of reversed-phase HPLC were as follows: Reversed-phase HPLC (Tracor) on a DIAKS-130-CETYL column (4·250 mm); buffer A: 0.1 M ammonium acetate (pH 7); buffer B: 0.1 M ammonium acetate, 40 % MeCN (pH 7); gradient of B from 0 to 100 % in 60 min; flow rate 1 mL min^{-1}; temperature 45 °C.

4.2.3 Fluorescence microscopy

The fluorescence microscopy of EGFP-expressing cells was accomplished by inverse microscope on unfixed cells in cell culture vessels with a suitable fluorescence filter.

4.3. Cell culture methods

All cell culture work was carried out with sterile solutions and devices in a laminar-flow workbench. For the experiments with and without serum the same protocol was used.

4.3.1 Cultivation of secondary cell lines

T-HUVEC were cultivated in bicarbonate-buffered RPMI 1640 with 10 % FCS, 2 mM glutamine, 100 U mL^{-1} penicillin and 100 U mL^{-1} streptomycin (culture medium) at 37 °C and in water-saturated atmosphere with 5 % CO_2.
Cells with confluence of 70-100 % were washed twice with PBS, then diluted with 0.25 % trypsine and with the medium consisting FCS (for trypsine inhibition). After centrifugation of the cells (Biofuge, 900 rpm / 160 g, 5 min, room temperature) the supernatant with trypsine was removed, the cells were resuspended in fresh medium and placed an adequate dilution into new 75 cm^3-flask. The cell density of the suspension was determined by counting in a Neubauer's counting chamber.

T-HUVEC culture medium:
RPMI 1640
10 % FCS
2 mM glutamine
100 U mL^{-1} penicillin
100 U mL^{-1} streptomycin

4.3.2 Cryoconservation and defrosting of cells

For cryoconservation the cells were washed with PBS, trypsinised and centrifuged. Then they were resuspended in 1 mL FCS with 7.5 % DMSO (Dimethyl sulfoxide) and replaced into a cryotube. After they were slowly cooled down during more than 24 h to 80 °C and kept in liquid nitrogen.
The cells were defrosted in a short period of time to 37 °C. To avoid an osmotic shock during the first 5 min, 5 mL FCS was added, the cells were centrifuged (Biofuge, 900rpm / 160 g, 5 min, room temperature), and dissolved in fresh cell culture medium. After 24 h, the medium was changed to eliminate the rests of DMSO.

4.3.3 Cell transfection

The cells were cultured in RPMI 1640 medium (T-HUVEC) or in DMEM (HeLa and LTK), supplemented with 10 % fetal calf serum (FCS) at 37 °C and 5 % CO_2 (T-HUVEC) or 10 % CO_2 (Hela, LTK) and subcultivated according to standard cell culture protocols. One day before the transfection, the cells were trypsinised and seeded in cell culture dishes with $2 \cdot 10^4$ cells per 24-well dish resulting in a cell density of 10^4 cells cm^{-2}. For transfection, Quantum® medium without FCS was also used. Quantum® medium is based on modified RPMI and supplemented with selected fractions of serum components and protein extracts from yeast.
A plasmid DNA, pcDNA3-EGFP, coding for the fluorophor protein EGFP (*enhanced green fluorescent protein*) was purified from *E. coli* using Nucleobond® endotoxin-free plasmid DNA (Macherey-Nagel, Düren, Germany).

4.3.3.1 Transfection with Polyfect®

Transfection with the dendrimer-based commercial agent Polyfect® (Qiagen, Hilden, Germany) was carried out according to the manufacturer's recommendation: 2 µg DNA were dissolved in 100 µL medium without FCS to which 22 µL Polyfect®-solution was added. After mixing, the dispersion stood for 5 min, and then 600 µL cell culture medium were added. From the cell culture, the culture medium was replaced by 1.5 mL fresh medium and the transfection mixture was added. The transfection mixture remained on the cells for 7 h. 2 µg DNA were used per transfection.

4.3.3.2 Standard calcium phosphate transfection

The standard transfection with calcium phosphate was carried out as follows: 4 µL aqueous solution containing 4 µg of DNA were mixed with 10 µL of 2.5 M $CaCl_2$ solution. The dispersion was left to stand for 5 min. The volume of the dispersion was adjusted to 100 µL with water and 100 µL HEPES buffered saline solution (2 · HBS: 280 mM NaCl, 10 mM KCl, 1.5 mM Na_2HPO_4, 12 mM dextrose, 50 mM HEPES, pH=7.05 ± 0.01) were added. Cell culture medium (RPMI 1640 with and without FCS, or Quantum®) was added up to 1 mL. From the cell culture, the culture medium was removed with a syringe and the transfection mixture was added. The duration of the transfection was 7 h. 4 µg DNA were used per transfection.

4.3.3.3 Transfection with custom-made calcium phosphate nanoparticles

The custom-made calcium phosphate nanoparticles were used for transfection as follows: 20 µL of calcium phosphate/DNA nanoparticles dispersion (prepared as shown in Figure 3.1.2.1.) were thoroughly mixed with 1 mL medium (RPMI

1640 with/without FCS for T-HUVEC, DMEM with/without FCS for HeLa and LTK, or Quantum® for T-HUVEC, HeLa, and LTK). From the cell culture, the cell culture medium was removed and 1.0 mL of the transfection mixture was added. The duration of transfection was 7 h.

4.3.3.4 Calculation of transfection efficiency

The efficiency of the transfection was studied by transmission light microscopy and by fluorescence microscopy using an IX51 microscope (Olympus, Hamburg, Germany). A successful transfection was detected by fluorescence microscopy at a magnification of 200x where the encoded fluorophor protein EGFP (enhanced green fluorescent protein) was excited, and counting the cells. Only when pcDNA3-EGFP was successfully incorporated into the nuclear DNA, the synthesis of the fluorophor protein EGFP occurred and these cells showed the green fluorescence of this protein. The transfection efficiency was computed by the ratio of cells in which EGFP was expressed to the total examined number of cells.

4.3.4 Transport of nanoparticles into the cells

T-HUVEC (transformed human umbilical vein endothelial cells) were cultured in RPMI 1640 medium, supplemented with 10 % fetal calf serum (FCS) at 37 °C and 5 % CO_2 (T-HUVEC) and subcultivated according to standard cell culture protocols. 12 hours prior to transfection, the cells were trypsinised and seeded in cell culture dishes with $2 \cdot 10^4$ cells per 24-well dish (density 10^4 cells cm^{-2}).
Plasmid DNA (pcDNA3-EGFP) coding for the fluorophor protein EGFP (*enhanced green fluorescent protein*) was purified from *E. coli* using Nucleobond® endotoxin-free plasmid DNA (Macherey-Nagel, Düren, Germany).

The transfection with the three types of nanoparticles was carried out as follows[163]: 20 µL of the particle dispersion was thoroughly mixed with 1 mL RPMI 1640 with FCS. From the cell culture, the cell culture medium was removed and 1.0 mL of the transfection mixture was added. The cells were transfected for 1 h, 2 h, and 4 h, followed by removal of the medium with the colloids. In the following set of experiments, the duration of transfection was 7 h, then the colloidal dispersion with the medium was removed and replaced by 1 mL of fresh medium. Therefore, only nanoparticles which were either taken up by the cells or strongly adsorbed on the cellular surface remained. Additional samples were taken after 1h (total: 8 h), 17 h (total: 24 h), and 41 h (total: 48 h). Immediately after the indicated time the cells were washed three times with PBS (phosphate buffered saline) to remove all dispersed nanoparticles (i.e. those neither taken up by cells nor adsorbed on cell membranes) and studied by microscopy. Fluorescence microscopy was carried out with an IX51 microscope (Olympus, Hamburg, Germany) and a Leica TCF SP2 laser confocal microscope. A successful incorporation of DNA into the nucleus was indirectly proven by fluorescence microscopy at a magnification of 200x where EGFP was excited. Only when pcDNA3-EGFP was successfully incorporated into the nuclear DNA, the synthesis of the fluorophor protein EGFP occurred and these cells showed the green fluorescence of this protein.

4.3.5 Gene silencing experiments

HeLa-EGFP (genetically modified human transformed cervix epithelial cells expressing enhanced green fluorescent protein; EGFP) were cultured in Dulbecco's modified Eagle's medium (DMEM) supplemented with 10 % fetal calf serum (FCS) and antibiotic G418-sulfate, with the final concentration in medium of 50 µg mL^{-1} at 37 °C under 10 % CO_2 atmosphere. Cells were seeded in 24-well plates one day prior to transfection with $2 \cdot 10^4$ cells per plate resulting

in a cell density of 10^4 cells cm^{-2}. Quantum® medium without FCS was also used. A desalted double-stranded RNA oligonucleotide (EGFP 22-nt[204]) was obtained from Invitrogen (Paisley, UK):

Sense, 5'-GCAAGCUGACCCUGAAGUUCAU-3';

antisense, 5'-AUGAACUUCAGGGUCAGCUUGC-3'.

The calcium phosphate nanoparticles were used for antisense as follows. 20 µL of calcium phosphate/oligonucleotide nanoparticle dispersion were thoroughly mixed with 1.0 mL medium (DMEM with FCS and Quantum®). From the cell culture, the cell culture medium was removed and replaced by 1.0 mL of the antisense mixture. The duration of transfection was 7 h. The experiments with freshly prepared nanoparticles were repeated three times each (N=3). The colloidal dispersions were also stored for 14 days at 4 °C and then used for transfection.

The efficiency of the transfection was determined by fluorescence microscopy using an IX51 microscope (Olympus, Hamburg, Germany; magnification 200x). The numbers of green fluorescing cells and of non-fluorescing cells were manually counted. The transfection efficiency was computed as the ratio of cells in which EGFP was inhibited to the total number of cells. As control, HeLa-EGFP cells cultured in DMEM with FCS medium was used.

4.4 Physicochemical methods

4.4.1 Analytical ultracentrifugation

The ultracentrifuge is a centrifuge optimized for spinning a rotor at very high speeds, capable of generating acceleration as high as 1000000 G (9800 km s^{-2}) The sedimentation coefficient is measured in the unit Svedberg (S) where 1 S = 10^{-13} s. S-distribution can be converted to the particle size distribution using the equation:

$$d_{\mathrm{H}} = \sqrt{\frac{18\eta s}{\rho_{\mathrm{p}} - \rho_{\mathrm{s}}}}$$

where d_H is the particle diameter, s is the sedimentation coefficient, η is the solvent viscosity, ρ_p is the particle density and ρ_s is the solvent density.

This modified Svedberg equation applies a hard sphere approach and is only valid for solid particles.

Ultracentrifugation was performed at 25 °C with an Optima XL-I (Beckman-Coulter) with UV/Vis absorption and on-line Rayleigh Interference optics using the program SEDFIT for evaluation of the sedimentation coefficient distributions without diffusion correction and correction to infinite dilution at Max-Planck-Institute of Colloids and Interfaces in Golm.

4.4.2 Dynamic light scattering (DLS)

Dynamic light scattering is one of the methods used to determine the size of particles. The experiment's theory is based essentially on two assumptions. The first assumption is that the particles are in Brownian motion. And the second one is that the particles observed in the experiment are spherical with a diameter small compared to the molecular dimensions.

Shining a monochromatic light beam onto a solution with spherical particles in Brownian motion causes a Doppler shift when the light hits the moving particle, changing the wavelength of the incoming light. This change is related to the size of the particle. It is possible to compute the sphere size distribution and give a description of the particle's motion in the medium, measuring the diffusion coefficient of the particle:

$$D_T = k_B\, T / 6\, \pi\, \eta R_h$$

where D_T is the translation diffusion coefficient, k_B is the Boltzmann's constant, T is the temperature in Kelvin degrees, η is the viscosity of the solvent and R_h is the hydrodynamic radius.

Since from the light scattering is possible to obtain information about the position of the particles, from the formulas above the radius of the particles is easy to get.

Dynamic light scattering determinations were performed with a Zetasizer (NanoZS from Malvern instruments).

4.4.3 Zeta potential measurements (ZP)

The zeta potential is the electrical potential that exists at the Stern plane of a particle, which is at some small distance from its surface. The zeta potential is derived from measuring the mobility distribution of a dispersion of charged particles as they are subjected to an electric field. The mobility is defined as the velocity of a particle per electric field unit and is measured by applying an electric field to the dispersion of particles and measuring their average velocity.

There are two approximations (by Hückel and by Smoluchowski) to obtain the zeta potential from the measured mobilities. The approximation by Hückel

applies to particles smaller than 10 nm. Because our particles were larger the model of Smoluchowski was used.

$$Be = (\varepsilon \zeta f_b / \eta) (\omega r^2_T \rho / \eta)$$

Be: electrophoretic mobility
ε: dielectric constant
ζ: zeta potential
η: viscosity
ω: frequency of the electrical field
r: radius of the particle
ρ: density of the dispersion
f_b: correction factor

The measurements for the computation of the zeta potential were carried out with a Malvern Zetasizer NanoZS.

4.4.4 Infrared spectroscopy (IR)

Infrared spectroscopy (IR Spectroscopy) is a type of absorption spectroscopy that uses the infrared part of the electromagnetic spectrum (wavelength 760 nm up to 500 µm). Infrared radiation does not trigger electronic excitation in substances but vibrational and/or rotational excitation. To be infrared active, a molecule must posses a dipole moment or must generate a dipole moment by vibration. The main modes of vibration are valence bond vibration, which is the atom vibration along a bond axis, and deformation vibration, which occur in molecules.

The energy in infrared spectra is usually given in wave numbers. The use of wave numbers offers the advantage of being directly proportional to the frequency of the absorbed radiation and thus the energy absorbed.

Infrared spectroscopy deals with the interaction of infrared light with matter. The energy of an infrared photon can be calculated using the Planck energy relation

$$\Delta E = \mathrm{h\ c}\ \upsilon$$

with E the absorbed energy in J, $h=6.626\cdot10^{-34}$ J s Planck's constant, $c=3\cdot10^{10}$ cm s^{-1} the speed of light and υ the wave number in cm^{-1}.

The rate of absorption of infrared energy depends mainly on the mass of the vibrating atoms. Detailed information about the infrared absorptions observed for various functional groups can be found in the literature.

In this work examined samples were mixed with an about 200 fold excess of potassium bromide and pressed into pellets at 10 tons for 15 minutes. Measurements were carried out with a Perkin-Elmer 1720X instrument in transmission mode (resolution 2 cm^{-1}, averaging of 10 scans).

4.4.5 X-ray powder diffractometry (XRD)

X-ray powder diffractometry allows the identification and quantification of crystalline phases. Each atom in crystal under the influence of X-rays scatters radiation and serves as the origin of a new wavefront. Wavefronts will interfere with one another either constructively or destructively, depending on the position of rays (in or out of phase). The occurrence of peaks depends on the constructive interference of the diffracted X-rays and is given by Bragg's law:

$$2 \cdot d \sin\Theta = n \cdot \lambda$$

d: distance between scattering centers

λ wavelength of the X-rays in Å

Θ the diffraction angle (angle between incident beam and scattering plane)

n an integer value (n = 1, 2, 3 etc.)

A STOE IP-PSD diffractometer with primary Ge(111) monochromator and half circle PSD was employed. All diffractograms shown in this work were measured with Cu $K\alpha_1$-radiation (λ=1.54056 Å), with 50 kV and 30 mA.

4.4.6 Scanning electron microscopy (SEM)

Classical microscopes are limited in resolution to the wavelength of visible light (400-750 nm). The scanning electron microscope (SEM) is a type of electron microscope capable of producing high-resolution images of a sample surface. With scanning electron microscopes, much smaller objects can be observed because high energy electrons are used for image creation.

The accelerated electrons are focused by magnetic field lenses into a tight and narrow beam which scans an area of the sample. The diameter of the beam defines the maximum resolution of the instrument. The actual image observed is created by the secondary electron emissions of the scanned sample area. As electron emission from the surface is easier and more intense than from the inside of a sample, a contrast-rich 3 D-image is created.

For SEM observation LEO S420 and ESEM Quanta 400 microscopes with palladium-sputtered samples were used. Additionally, an X-ray detector for energy dispersive X-ray analysis (EDX) permitted the detection of the elements present in the sample.

4.4.7 Transmission electron microscopy (TEM)

The transmession electron microscope is an optical analogue to the conventional light microscope. It is based on the fact that electrons possess a wavelength but at the same time interact with magnetic fields as a point charge. A beam of electrons is applied instead of light, and the glass lenses are replaced by magnetic lenses. The lateral resolution can go down to a few Angstroms.
A very thin slice of the tested material is exposed to a beam of electrons. By the interaction of electrons with consistent material structure, a constant fraction of electrons is transmitted through the sample to a detector. Once a structural imperfection is encountered, the fraction of transmitted electron changes.

Transmission electron microscopy (TEM) was performed with a Philips CM 200 FEG instrument on air-dried nanoparticles prepared on carbon-coated copper grids.

4.5 Experimental procedures

4.5.1 The preparation of calcium phosphate/DNA colloids

The preparation was performed as follows: An aqueous solution of calcium nitrate (6.25 mM or 18 mM) was mixed with an aqueous solution of diammonium or dipotassium hydrogen phosphate (3.74 mM or 10.8 mM). The pH of both solutions was adjusted beforehand to 9 with NaOH (0.1 M). Mixing was achieved by rapidly pumping both solutions into a glass vessel. After about 30 s, 1 mL of the dispersion was taken with a syringe and rapidly mixed with 0.2 or 1 mL of an aqueous solution of DNA (1 mg mL^{-1}) in a polyethylene vessel (Figure 3.1.2.1).

The substitution of calcium by magnesium or aluminum was accomplished by adding either magnesium nitrate or aluminum chloride to the calcium nitrate solution.

The inorganic salts were all of p.a. quality. Ultrapure water (Purelab ultra instrument from ELGA) was used for all preparations. We used DNA (sodium salt) from salmon testes (16.2 A250 units mg^{-1} solid; 6.13 % Na) from Sigma for all experiments.

4.5.2 Preparation of multi-shell nanoparticles

Multi-shell nanoparticles were prepared as follows: First, DNA-coated calcium phosphate nanoparticles (so called single-shell) were prepared by mixing an aqueous solution of calcium nitrate (6.25 or 18 mM) with an aqueous solution of diammonium hydrogen phosphate (3.74 mM or 10.8 mM) at a pH 9. The calcium phosphate dispersion (1 mL) was taken with a syringe and rapidly mixed with 0.2 mL of an aqueous solution of DNA (1 mg mL^{-1}) in a sterile Eppendorf tube (Figure 3.1.2.1). This dispersion had a final concentration of 167 µg DNA mL^{-1} [163]. To form the outter calcium phosphate layer (double-shell

nanoparticles), we added 0.5 mL of calcium nitrate (6.25 or 18 mM) and then 0.5 mL of diammonium hydrogen phosphate (3.74 mM or 10.8 mM). This resulted in a crystallization of calcium phosphate on the surface of the particles. A colloidal stabilization (to prevent aggregation of the calcium phosphate-decorated surfaces) was then accomplished by adding 0.2 mL of DNA solution (1 mg mL^{-1}) to form triple-shell nanoparticles. These dispersions had concentrations of 91 µg DNA mL^{-1} (double-shell) and 167 µg DNA mL^{-1} (triple-shell).

Welzel *et al.* showed by an MTT test that such calcium phosphate/DNA nanoparticles are not cytotoxic[154]. The amounts of DNA per transfection were 3.3 µg (single-shell), 1.8 µg (double-shell), and 3.3 µg (triple-shell).

4.5.3 Preparation of calcium phosphate/DNA/protamine nanoparticles

DNA-coated calcium phosphate nanoparticles were prepared as follows: An aqueous solution of calcium nitrate (18 mM) was mixed with an aqueous solution of diammonium hydrogen phosphate (10.8 mM) (Figure 3.1.2.1). The pH of both solutions was adjusted beforehand to 9 with NaOH (0.1 M). Mixing was accomplished by rapidly pumping both solutions into a glass vessel. In parallel, DNA (1 mg mL^{-1}) was pre-incubated with protamine at 1:1 volume-ratio (0.2 mL DNA and 0.2 mL protamine). After about 30 s, 1 mL of the dispersion was taken with a syringe and rapidly mixed with 0.4 mL of an aqueous solution of DNA/protamine in a sterile Eppendorf tube. Different concentrations of protamine were used: 0.5, 1, 5, 10, 20 mg mL^{-1} so that the final concentrations of protamine in the calcium phosphate/DNA dispersion were 71 µg mL^{-1}, 140 µg mL^{-1}, 710 µg mL^{-1}, 1430 µg mL^{-1} and 2860 µg mL^{-1}. This dispersion had a final concentration of 140 µg DNA mL^{-1}.

Multi-shell nanoparticles were prepared as follows: First, DNA/protamine-coated calcium phosphate nanoparticles were prepared as described above. To

this dispersion, we added 0.5 mL of calcium nitrate (18 mM) and then 0.5 mL of diammonium hydrogen phosphate (10.8 mM). This resulted in a crystallization of calcium phosphate on the surface of the particles. A colloidal stabilization was then accomplished by adding 0.4 mL of DNA/protamine solution. The concentration of DNA was always 1 mg mL^{-1}. The final concentrations of protamine in the dispersion with double-shell nanoparticles were 40 μg mL^{-1}, 80 μg mL^{-1}, 420 μg mL^{-1}, 840 μg mL^{-1} and 1680 μg mL^{-1} and in the dispersion with triple-shell nanoparticles were 71 μg mL^{-1}, 140 μg mL^{-1}, 710 μg mL^{-1}, 1430 μg mL^{-1} and 2860 μg mL^{-1}. These dispersions had concentrations of 80 μg DNA mL^{-1} (double-shell) and 140 μg DNA mL^{-1} (triple-shell). The amounts of protamine per transfection were 1.4 μg, 2.8 μg, 14.2 μg, 28.6 μg, 57.2 μg (single- and triple-shell) and 0.8 μg, 1.6 μg, 8.4 μg, 16.8 μg, 33.6 μg (double-shell). The amounts of DNA per transfection were 2.8 μg (single-shell), 1.6 μg (double-shell), and 2.8 μg (triple-shell).

4.5.4 Preparation of nanoparticles with TRITC-BSA

DNA-coated calcium phosphate nanoparticles were prepared as follows: An aqueous solution of calcium nitrate (18 mM) was mixed with an aqueous solution of diammonium hydrogen phosphate (10.8 mM). The pH of both solutions was adjusted beforehand to 9 with NaOH (0.1 M). Mixing was accomplished by rapidly pumping both solutions into a glass vessel.

Three types of the nanoparticles were prepared. For calcium phosphate nanoparticles functionalized with red-fluorescing TRITC-BSA ("CaP/BSA"), 1 mL of the calcium phosphate dispersion was taken with a syringe and rapidly mixed with 1 mL TRITC-BSA (1 mg mL^{-1}). For calcium phosphate nanoparticles functionalized with both DNA and TRITC-BSA ("CaP/DNA/BSA"), 1 mL of the calcium phosphate dispersion was taken with a syringe and rapidly mixed with 0.2 ml of pcDNA3-EGFP (1 mg mL^{-1}) followed

by 1 mL TRITC-BSA (1 mg mL^{-1}). The transfection ability of these particles was tested. DNA/BSA particles without a calcium phosphate core ("DNA/BSA") were prepared as control: 1 mL of pcDNA3-EGFP solution (1 mg mL^{-1}) was mixed with 1 mL TRITC-BSA (1 mg mL^{-1}). All samples were filtered with a sterile syringe filter with a 0.2 µm cellulose acetate membrane (VWR International) to remove larger aggregates.

4.5.5 Preparation of calcium phosphate/oligonucleotide nanoparticles

The calcium phosphate nanoparticles can be prepared reproducibly by mixing an aqueous solution of calcium nitrate (6.25 mM) with an aqueous solution of diammonium hydrogen phosphate (3.74 mM). The pH of both solutions was adjusted beforehand to 9 with NaOH (0.1 M). Mixing was achieved by rapidly pumping both solutions into a glass vessel. Immediately after mixing, 1.5 mL of the calcium phosphate dispersion was taken with a syringe and rapidly added to the 0.25 mL of an aqueous solution of oligonucleotides in a polyethylene vessel. Three different concentrations of the oligonucleotides were used: 35 µM, 63 µM and 320 µM so that the final concentration of oligonucleotides in the calcium phosphate dispersion was 5 µM, 9 µM and 45 µM, respectively (dilution 1:7). The samples were filtered through a sterile syringe with a 0.45 µm cellulose acetate membrane (Scheicher and Schuell) to remove larger aggregates. The inorganic salts were all of p.a. quality. Ultrapure water (Purelab ultra instrument from ELGA) was used for all preparations. Double-stranded oligonucleotides (25-5/25-comp and 25-G/25-C) were generated by mixing complimentary sequences of oligonucleotides in water, heating to 95 °C, and slowly cooling down to 4 °C.

For gene silencing experiments with double-stranded small interfering RNA (siRNA), all calcium phosphate/siRNA dispersions were prepared in the same

way. The final concentration of dsRNA in the calcium phosphate dispersion was 45 μM in all cases. This sample was not filtered to avoid adsorption on the filter.

4.5.6 Preparation of the ubiquitin-calcium phosphate samples

Carbonated apatite, which is comparable in chemical composition and crystallinity to bone mineral, was obtained by continuous fast precipitation in a crystallization setup. The preparation of three types of samples:

I. Ubiquitin-calcium phosphate samples prepared by the co-precipitation method: Two solutions (18 mM $[CH_3CH(OH)COO]_2Ca$; 10.8 mM Na_2CO_3 + 10.8 mM Na_2HPO_4) were continuously mixed in a glass vessel already containing 1 mL of the ubiquitin solution with a concentration 5 mg mL^{-1} to the final volume of 1 L (Figure 3.6.1.1, I). 2.081 g of dry ubiquitin-calcium phosphate powder were obtained from 3 L of solution. The concentration of ubiquitin after mixing was 5 μg mL^{-1} which corresponded to 15000 μg ubiquitin in 3 L of the calcium phosphate dispersion. Radioactive ubiquitin was used only for γ-counter measurements, for all other analyses non-radioactive ubiquitin was used. The dispersion stood for 5 hours without stirring and then it was washed 5 times with distilled water to remove adsorbed ubiquitin and filtered off (Figure 3.6.1.1, II - III). The powder was dried under air at 37 °C for 12 hours.

II. Calcium phosphate samples without ubiquitin: Two solutions (18 mM $[CH_3CH(OH)COO]_2Ca$; 10.8 mM Na_2CO_3 + 10.8 mM Na_2HPO_4) were continuously mixed in a glass vessel to the final volume of 1 L. Right after mixing, the dispersion was filtered off and dried under air at 37 °C for 12 hours. These samples were used for physicochemical analyses as a control.

III. Control ubiquitin-calcium phosphate samples: Two solutions (18 mM $[CH_3CH(OH)COO]_2Ca$; 10.8 mM Na_2CO_3 + 10.8 mM Na_2HPO_4) were continuously mixed in a glass vessel to the final volume of 3 L. Right after mixing, the dispersion was filtered off and dried under air at 37 °C for 12 hours.

Then 2.006 g of nanocrystalline calcium phosphate powder, which corresponded to the mass of powder synthesized from 3 L dispersion, was redispersed in 3 L water, containing 15 mg of radioactive ubiquitin (final concentration 5 μg mL^{-1}). The dispersion stood for 5 hours without stirring and then it was washed 5 times with distilled water to remove adsorbed ubiquitin and then filtered. The powder was dried under air at 37 °C for 12 hours. These samples were used as a control to determine the amount of ubiquitin incorporated into the particles.

Ubiquitin-calcium phosphate prepared by the co-precipitation method (I) and calcium phosphate without ubiquitin (II) were analyzed by X-ray diffraction (XRD), infrared spectroscopy (IR), energy-dispersive X-ray analysis (EDX) and scanning electron microscopy (SEM).

The percentage of radioactive ubiquitin incorporated into the calcium phosphate materials in co-precipitated samples (I) and control samples (III) was measured with a γ-counter (65 Gamma Counter 1480 Wizard^{TM} 3 ", Wallac).

5 Summary

In this work chemical, biological and biochemical investigations were carried out in the cooperation with the Chair of Molecular Neurobiochemistry at the University of Bochum and with the Institute of Physico-Chemical Biology, Moscow State University. In this cooperation the main purpose was to find optimal conditions for the preparation of stable monodisperse calcium phosphate colloids and their applications in biological investigations on living cells. This interdisciplinary cooperation was necessary to understand major barriers in the gene delivery system and to develop a new system which can overcome these barriers or at least improve the trafficking of nucleic acids into the cells.

We have demonstrated how by a comparatively easy and well reproducible process nanodisperse calcium phosphate/DNA nanoparticles with a size below 100 nm can be prepared, especially if calcium is partially substituted by magnesium or aluminum. These ions obviously have an inhibitory effect on the particle growth of calcium phosphate.

Multi-shell calcium phosphate/DNA-nanoparticles with a calcium phosphate core and DNA/calcium phosphate shells help to protect DNA from the degradation by enzymes (nucleases) inside the cytoplasm of cultured endothelial cells, reaching the efficiency of Polyfect®.

Calcium phosphates should be advantageous due to their high biocompatibility and good biodegradability compared to other types of nanoparticles used for cell transfection such as iron oxide (magnetite), gold or silica. In contrast to the classical calcium phosphate method, the particle/DNA dispersions can be stored for weeks without loss of their transfection efficiency.

We have developed a delivery system for gene silencing in which these nanoparticles are used for down-regulation of gene expression by targeting the mRNA resulting in effective gene silencing. The preparation of stable calcium

phosphate/oligonucleotide dispersions and their successful biological application in vitro to HeLa-EGFP cells was shown.

The most challenging work in non-viral gene therapy is a successful delivery of DNA into the nuclei overcoming all the extracellular and intracellular physico-chemical barriers.

To get information about the targeting of calcium phosphate nanoparticles into T-HUVEC, fluorescence microscopy was used. The routing of nanoparticles inside the cells was studied. It was shown that the transfection efficiency correlates with the distribution of the nanoparticles in the cells. DNA/BSA aggregates alone were not able to penetrate the cell membrane, i.e. the inorganic nanoparticles (calcium phosphate) were necessary as carriers to enter the cell.

We also performed the preparation of calcium phosphate samples with ubiquitin by the co-precipitation method. It was shown that ubiquitin can be adsorbed as well as incorporated into the calcium phosphate particles. This method shows opportunities in the preparation of calcium phosphate ceramics with proteins similar to ubiquitin, i.e. proteins of the BMP family. An implantation of such biofunctionalized calcium phosphate ceramics (e.g. cold-isostatically pressed into an appropriate shape) in bone defects can stimulate the development of new bone at the implantation site.

6 Literatur

[1] R. Vogel, K. Pohl, H. Weller, *Chem. Phys. Lett.* **1990**, *174*, 241.
[2] R. Vogel, P. Hoyer, H. Weller, *J. Phys. Chem.* **1994**, *98*, 3183.
[3] C. T. Chen, Y. C. Chen, *Anal. Chem.* **2005**, *77*, 5912.
[4] S. A. Corr, Y. K. Gun'ko, A. P. Douvalis, M. Venkatesan, R. D. Gunning, *J. Mater. Chem.* **2004**, *14*, 944.
[5] H. Ma, S. Diamond, *Curr. Pharm. Biotech.* **2001**, *2*, 1.
[6] A. Sugunan, J. Dutta, *J. Phys. Sci. Idea* **2004**, *4*, 50.
[7] R. E. Knutti, R. A. Warrick, J. B. Goetsch, *J. Exper. Med.* **1950**, 77.
[8] D. H. Everett, *Basic Principles of Colloid Science*, Royal society of chemistry, London, **1988**.
[9] B. V. Derjaguin, L. D. Landau, *Acta physicochimica URSS* **1941**, *14*, 633.
[10] E. J. W. Verwey, J. T. G. Overbeek, *Theory of the Stability of Lyophobic Colloids*, Elsevier, Amsterdam, **1948**.
[11] Z. Adamczyk, P. Weronski, *Adv. Colloid Interface Sci.* **1999**, *83*, 137.
[12] S. V. Dorozhkin, M. Epple, *Angew. Chem. Int. Ed. Engl.* **2002**, *41*, 3130.
[13] J. D. Termine, E. D. Eanes, *Calcif. Tissue Res.* **1972**, *10*, 171.
[14] E. D. Eanes, J. D. Termine, M. U. Nylen, *Calcif. Tissue Res.* **1973**, *12*, 143.
[15] J. L. Meyer, E. D. Eanes, *Calcif. Tissue Res.* **1978**, *28*, 59.
[16] J. L. Meyer, E. D. Eanes, *Calcif. Tissue Res.* **1978**, *28*, 209.
[17] R. E. Wuthier, G. S. Rice, J. E. Wallace, R. L. Weaver, R. Z. LeGeros, E. D. Eanes, *Calcif. Tissue Int.* **1985**, *37*, 401.
[18] K. Kurashina, H. Kurita, M. Hirano, A. Kotani, C. P. Klein, K. de Groot, *Biomaterials* **1997**, *18*, 539.
[19] F. C. M. Driessens, J. A. Planell, M. G. Boltong, I. Khairoun, M. P. Ginebra, *Proc. Inst. Mech. Eng. [H]* **1998**, *212*, 427.
[20] S. Takagi, L. C. Chow, K. Ishikawa, *Biomaterials* **1998**, *19*, 1593.
[21] M. Otsuka, Y. Matsuda, Y. Suwa, J. L. Fox, W. I. Higuchi, *Chem. Pharm. Bull. (Tokyo)* **1993**, *41*, 2055.
[22] M. Fountoulakis, M. F. Takacs, P. Berndt, H. Langen, B. Takacs, *Electrophoresis* **1999**, *20*, 2181.
[23] M. Mirshahi, L. Camoin, C. Nicolas, I. Ghedira, J. Cozette, J. P. Faure, *Curr. Eye Res.* **1999**, *18*, 327.
[24] R. Freitag, S. Vogt, M. Modler, *Biotechnol. Prog.* **1999**, *15*, 573.
[25] J. Wissing, S. Heim, L. Flohe, U. Bilitewski, R. Frank, *Electrophoresis* **2000**, *21*, 2589.
[26] S. R. Shepard, C. Brickman-Stone, J. L. Schrimsher, G. Koch, *J. Chromatogr. A* **2000**, *891*, 93.
[27] T. Dingermann, *Gentechnik Biotechnik*, Wissenschaftliche Verlagsgesellschaft, Stuttgart, **1999**.
[28] L. Stryer, *Biochemie*, Spektrum der Wissenschaft Verlag, Heidelberg, **1996**.
[29] M. L. Stephenson, P. C. Zamecnik, *Proc. Natl. Acad. Sci. U.S.A.* **1978**, *75*, 285.
[30] P. C. Zamecnik, M. L. Stephenson, *Proc. Natl. Acad. Sci. U.S.A.* **1978**, *75*, 280.
[31] P. Couvreur, C. Malvy, *Pharmaceutical Aspects of Oligonuceotides*, Taylor & Francis, London, **2000**.
[32] A. Arellano, M. Canales, C. Jullian, J. E. Brunet, *Biochem. Biophys. Res. Commun.* **1988**, *150*, 633.
[33] T. C. Rodman, F. H. Pruslin, V. G. Allfrey, *Exp. Cell. Res.* **1984**, *150*, 269.
[34] R. Knippers, B. Otto, R. Bohme, *Nucleic Acids Res.* **1978**, *5*, 2113.

[35] A. Noguchi, N. Hirashima, M. Nakanishi, *Pharm. Res.* **2002**, *19*, 933.
[36] J. Weyermann, D. Lochmann, A. Zimmer, *J. Controlled Release* **2004**, *100*, 411.
[37] J. Weyermann, D. Lochmann, C. Georgens, A. Zimmer, *Eur. J. Pharm. Biopharm.* **2005**, *59*, 431.
[38] D. Lechardeur, K. J. Sohn, M. Haardt, P. B. Joshi, M. Monck, R. W. Graham, B. Beatty, J. Squire, H. O'Brodovich, G. L. Lukacs, *Gene Ther.* **1999**, *6*, 482.
[39] D. Lechardeur, A. S. Verkman, G. L. Lukacs, *Adv. Drug. Deliv. Rev.* **2005**, *57*, 755.
[40] J. Steinhardt, J. Krijn, J. G. Leidy, *Biochemistry* **1971**, *10*, 4005.
[41] D. Fischer, T. Bieber, S. Brusselbach, H. Elsasser, T. Kissel, *Int. J. Pharm.* **2001**, *225*, 97.
[42] J. Bloom, V. Amador, F. Bartolini, G. DeMartino, M. Pagano, *Cell* **2003**, *115*, 71–82.
[43] K. Breitschopf, E. Bengal, T. Ziv, A. Admon, A. Ciechanover, *EMBO J.* **1998**, *17*, 5964–5973.
[44] S. Vijay-Kumar, C. E. Bugg, K. D. Wilkinson, W. J. Cook, *Proc. Natl. Acad. Sci. U.S.A.* **1985**, *82*, 3582.
[45] M. D. Ehlers, *Science* **2003**, *302*, 800.
[46] M. Glotzer, W. Murray, M. W. Kirschner, *Pathway. Nature* **1991**, *349*, 132.
[47] H. Bastians, L. M. Topper, G. L. Gorbsky, J. V. Ruderman, *Mol. Cell. Biol.* **1999**, *10*, 3927.
[48] V. Sudakin, D. Ganoth, A. Dahan, H. Heller, J. Hershko, F. C. Luca, J. V. Ruderman, A. Hershko, *Mol. Biol. Cell.* **1995**, *6*, 185.
[49] G. Freiberg, A. D. Mesecar, H. Huang, J. Y. Hong, S. W. Liebman, *Curr.Genet.* **2000**, *37*, 221.
[50] P. Sung, S. Prakash, L. Prakash, *Proc. Natl. Acad. Sci. U.S.A.* **1990**, *87*, 2695.
[51] T. Harada, C. Harada, Y. L. Wang, H. Osaka, K. Amanai, K. Tanaka, S. Takizawa, R. Setsuie, M. Sakurai, Y. Sato, M. Noda, K. Wada, *Am. J. Pathol.* **2004**, *164*, 59.
[52] I. M. Verma, N. Somia, *Nature* **1997**, *389*, 239.
[53] N. D. Zinder, J. Lederberg, *J. Bacteriol.* **1952**, *64*, 679.
[54] S. Yang, R. Delgado, S. R. King, C. Woffendin, C. S. Barker, Z. Y. Yang, L. Xu, G. P. Nolan, G. J. Nabel, *Hum. Gene Ther.* **1999**, *10*.
[55] A. A. Bukovsky, J. P. Song, L. Naldini, *J. Virol.* **1999**, *73*, 7087.
[56] S. K. Tripathy, H. B. Black, E. Goldwasser, J. M. Leiden, *Nat. Med.* **1996**, *2*, 545.
[57] P. C. Hendrie, D. W. Russel, *Mol. Ther.* **2005**, *12*, 9.
[58] J. C. Glorioso, N. A. DeLuca, D. J. Fink, *Annual Rev. Microbiol.* **1995**, *49*, 675.
[59] J. P. Burand, M. D. Summers, G. E. Smith, *J. Virol.* **1980**, *101*, 286.
[60] R. G. Crystal, *Science* **1995**, *270*, 404.
[61] A. G. Schatzlein, *Anticancer Drugs* **2001**, *12*, 275.
[62] G. L. Andreason, G. A. Evans, *Anal. Biochem.* **1989**, *180*, 269.
[63] J. A. Nicoloff, R. J. Reynolds, *Anal. Biochem.* **1992**, *205*, 237.
[64] M. R. Capecchi, *Cell* **1980**, *22*, 479.
[65] N. S. Yang, J. Burkholder, B. Roberts, B. Martinell, D. Mccabe, *Proc. Natl. Acad. Sci. U.S.A.* **1990**, *87*, 9568.
[66] E. Neumann, M. Schaefer-Ridder, Y. Wang, P. H. Hofschneider, *EMBO J.* **1982**, *1*, 841.
[67] L. M. Mir, H. Banoun, C. Paoletti, *Exp. Cell Res.* **1988**, *175*, 15.
[68] H. Aihara, J. Miyazaki, *J. Nat. Biotechnol.* **1998**, *16*, 867.
[69] M. P. Rols, C. Delteil, M. Golzio, P. Dumond, S. Cros, J. Teissie, *J. Nat. Biotechnol.* **1998**, *16*, 168.
[70] R. Heller, M. Jaroszeski, A. Atakin, D. Moradpour, R. Gilbert, J. Wands, C. Nicolau, *FEBS Lett.* **1996**, *389*, 225.

[71] L. M. Mir, M. F. Bureau, J. Gehl, R. Rangara, D. Rouy, J.-M. Caillaud, P. Delaere, D. Branellec, B. Schwartz, D. Scherman, *Proc. Natl. Acad. Sci. U.S.A.* **1999**, *96*, 4262.
[72] D. Luo, W. M. Saltzman, *Natur. Biotechnol.* **2000**, *18*, 33
[73] A. J. Wolff, V. Budker, *Adv. Genetics* **2005**, *54*, 1.
[74] J. A. Wolff, R. W. Malone, P. Williams, W. Chong, G. AcsadiI, A. Jani, P. L. Felgner, *Science* **1990**, *247*, 1465.
[75] M. A. Hickman, R. W. Malone, K. Lehmann-Buinsma, T. R. Sih, D. Knoell, F. C. Szoka, R. Walzem, D. M. Carlson, J. S. Powell, *Hum. Gene Ther.* **1994**, *5*, 1477.
[76] M. L. Sikes, B. W. O'malley, M. J. Finegold, F. D. Ledley, *Hum. Gene Ther.* **1994**, *5*, 837.
[77] A. Ardehali, A. Fyfe, H. Laks, D. C. Drinkwater, J. H. Qiao, A. J. Lusis, *J. Thorac. Cardiovasc. Surg.* **1995**, *109*, 716.
[78] B. Schwartz, C. Benoist, B. Abdallah, R. Rangara, A. Hassan, D. Scherman, B. A. Demeneix, *Gene Ther.* **1996**, *3*, 405.
[79] J. J. Yoo, S. Soker, L. F. Lin, K. Mehegan, P. D. Guthrie, A. Atala, *J. Urol.* **1999**, *162*, 1115.
[80] R. I. Mahato, K. Kawabata, Y. Takakura, M. Hashida, *J. Drug Target.* **1995**, *3*, 149.
[81] K. Kawabata, Y. Takakura, M. Hashida, *Pharm. Res.* **1995**, *12*, 825.
[82] J.-P. Behr, *Pure and Appl. Chem.* **1994**, *66*, 827.
[83] A. V. Zelenin, V. A. Kolesnikov, O. A. Tarasenko, R. A. Shafei, I. A. Zelenina, V. V. Mikhailov, M. L. Semenova, D. V. Kovalenko, O. V. Artemyeva, T. E. Ivaschenko, O. V. Evgrafov, G. Dickson, V. S. Baranovand, *FEBS Lett.* **1997**, *414*, 319.
[84] R. S. Williams, S. A. Johnston, M. Riedy, M. J. Devit, S. G. Mcelligott, J. C. Sanford, *Proc. Natl. Acad. Sci. U.S.A.* **1991**, *88*, 2726.
[85] K. Moelling, *Cytokines Cell Mol.* **1997**, *3*, 127.
[86] P. L. Felgner, T. R. Gadek, M. Holm, R. Roman, H. W. Chan, M. Wenz, J. P. Northrop, G. M. Ringold, M. Danielsen, *Proc. Natl. Acad. Sci. U.S.A.* **1987**, *84*, 7413.
[87] N. Ishii, J. Fukushima, T. Kaneko, E. Okada, K. Tani, S. I. Takana, *AIDS Res. Hum. Retroviruses* **1997**, *13*, 1421.
[88] D. D. Lasic, N. S. Templeton, *Adv. Drug. Deliv. Rev.* **1996**, *20*, 221.
[89] A. R. Thierry, P. Rabinovich, L. C. Mahan, J. L. Bryant, R. C. Gallo, *Gene Ther.* **1997**, *4*, 226.
[90] E. Salje, U. Bismayer, M. Jansen, *J. Phys. C* **1987**, *20*, 3613.
[91] H. Farhood, N. Serbina, L. Huang, *Biochim. Biophys. Acta* **1995**, *1235*, 289.
[92] G. J. Nabel, E. G. Nabel, Z. Y. Yang, B. A. Fox, G. E. Plautz, X. Gao, L. Huang, S. Shu, D. Gordon, A. E. Chang, *Proc. Natl. Acad. Sci. U.S.A.* **1993**, *90*, 11307.
[93] N. J. Caplen, E. W. Alton, P. G. Middleton, J. R. Dorin, B. J. Stevenson, X. Gao, S. R. Durham, P. K. Jeffery, M. E. Hodson, C. Coutelle, L. Huang, D. J. Porteous, R. Williamson, D. M. Geddes, *J. Nat. Med.* **1995**, *1*, 39.
[94] K. L. Brigham, B. Meyrick, B. Christmann, M. Magnuson, G. King, L. C. Berry, *Am. J. Med. Sci.* **1989**, *298*, 278.
[95] T. Ono, Y. Fujino, T. Tsuchiya, M. Tsuda, *Neurosci. Lett.* **1990**, *117*, 259.
[96] G. E. Plautz, Z. Y. Yang, B. Y. Wu, Z. Gao, L. Huang, G. J. Nabel, *Proc. Natl. Acad. Sci. U.S.A.* **1993**, *90*, 4645.
[97] K. Son, L. Huang, *Gene Ther.* **1996**, *10*, 343.
[98] E. Raz, D. A. Carson, S. E. Parker, T. B. Parr, A. M. Abai, G. Aichinger, S. H. Gromkowski, M. Singh, D. Lew, M. A. Yankauckas, S. M. Baird, G. H. Rhodes, *Proc. Natl. Acad. Sci. USA* **1994**, *91*, 9519.
[99] E. Wagner, C. Plank, K. Zatloukal, M. Cotton, M. L. Birnstiel, *Proc, Natl. Acad. Sci. U.S.A.* **1992**, *89*, 7934.

[100] M. A. Wolfert, P. R. Dash, O. Nazarova, D. Oupicky, *Bioconjug. Chem.* **1999**, *10*, 993.
[101] C. W. Pouton, P. Lukas, B. J. Thomas, A. N. Uduehi, D. A. Milroy, S. H. Moss, *J. Controll. Rel.* **1998**, *53*, 289.
[102] R. Kircheis, L. Wightman, E. Wagner, *Adv. Drug. Deliv. Rev.* **2001**, *53*, 341.
[103] D. G. Anderson, D. M. Lynn, R. Langer, *Angew. Chem.* **2003**, *115*, 3261.
[104] S. Kazuyoshi, S. W. Kim, *J. Controll. Rel.* **2002**, *79*, 271.
[105] C. Rudolph, U. Schillinger, C. Plank, *Biochim. Biophys. Acta* **2002**, *1573*, 75.
[106] R. A. Jain, *Biomaterials* **2000**, *21*, 2475.
[107] R. Gref, Y. Minamitake, M. T. Peracchia, V. Trubetskoy, V. Torchilin, R. Langer, *Science* **1994**, *263*, 1600.
[108] G. Y. Wu, C. H. Wu, *J. Biol. Chem.* **1988**, *263*, 14621.
[109] F. L. Sorgy, Bhattacharya, L. Huang, *Gene Ther* **1997**, *4*, 961.
[110] B. Quintanilla-Vega, D. Hoover, W. Bal, E. K. Silbergeld, M. P. Waalkes, L. D. Anderson, *Am. J. Ind. Med.* **2000**, *38*, 324.
[111] F. L. Graham, A. J. van der Eb, *Virology* **1973**, *52*, 456.
[112] K. Balasubramanian, M. Burghard, *Small* **2005**, *1*, 180.
[113] C. Kneuer, M. Sameti, E. G. Haltner, T. Schiestel, H. Schirra, H. K. Schmidt, C. M. Lehr, *Int. J. Pharm.* **2000**, *196*, 257.
[114] E. F. Fynan, R. G. Webster, D. H. Fuller, J. C. Santoro, H. L. Robinson, *Proc. Natl. Acad. Sci. U.S.A.* **1993**, *90*, 11478.
[115] N. L. Rosi, D. A. Giljohann, C. S. Thaxton, A. K. R. Lytton-Jean, M. S. Han, C. A. Mirkin, *Science* **2006**, *312*, 1027.
[116] Y. Zhang, N. Kohler, M. Zhang, *Biomaterials* **2002**, *23*, 1553.
[117] D. E. Brash, R. R. Reddel, M. Quanrud, K. Yang, M. P. Farrel, C. C. Harris, *Mol. Cell. Biol* **1987**, *7*, 2031.
[118] G. Bhakta, S. Mitra, A. Maitra, *Biomaterials* **2005**, *26*, 2157.
[119] J. H. Choy, S. Y. Kwak, Y. J. Jeong, J. S. Park, *Angew. Chem. Int. Ed.* . **2000**, *39*, 4042.
[120] F. Cavani, A. Trifiro, A. Vaccari, *Catal. Today* **1991**, *11*, 173.
[121] A. K. Salem, P. C. Searson, K. W. Leong, *Nature Materials* **2003**, *2*, 668.
[122] P. Gould, *Materialstoday* **2004**, 37.
[123] A. Fire, S. Xu, M. K. Montgomery, S. A. Kostas, S. E. Driver, C. C. Mello, *Nature* **1998**, *391*, 806.
[124] C. Napoli, C. Lemieux, R. Jorgensen, *Plant Cell* **1990**, *2*, 279.
[125] L. B. Misquitta, M. Paterson, *Proc, Natl. Acad. Sci. U.S.A.* **1999**, *96*, 1451.
[126] S. M. Elbashir, J. Harborth, W. Lendeckel, A. Yalcin, K. Weber, T. Tuschl, *Nature* **2001**, *411*, 494.
[127] M. Scherr, M. A. Morgan, M. Eder, *Curr. Med. Chem.* **2003**, *10*, 245.
[128] O. A. Kent, A. M. MacMillan, *Org. Biomol. Chem.* **2004**, *2*, 1957.
[129] S. Balachandran, P. C. Roberts, L. E. Brown, H. Truong, A. K. Pattnaik, D. R. Archer, G. N. Barber, *Immunity* **2000**, *13*, 129.
[130] J. C. Clemens, C. A. Worley, N. S. Leff, M. Merda, T. Maehama, B. A. Hemmings, J. E. Dixon, *Proc. Natl. Acad. Sci. U.S.A.* **2000**, *97*, 6499.
[131] L. Zou, D. Cortez, S. J. Elledge, *Genes Dev.*, *16*, 198.
[132] S. Moskalenko, D. O. Henry, C. Rosse, G. Mirey, J. H. Camonis, M. A. White, *Nat. Cell Biol.* **2002**, *4*, 66.
[133] H. A. Lowenstam, S. Weiner, *On biomineralization*, Oxford University Press, New York, **1989**.
[134] S. Mann, *J. Mater. Chem.* **1995**, *5*, 935.
[135] S. Mann, *Biomineralization*, Oxford University Press, Oxford, **2001**.

[136] I. Roy, S. Mitra, A. Maitra, S. Mozumdar, *Int. J. Pharm.* **2003**, *250*, 25.
[137] M. Jordan, F. Wurm, *Methods* **2004**, *33*, 136.
[138] A. J. Strain, A. H. Wyllie, *Biochem. J.* **1984**, *218*, 475.
[139] M. Jordan, A. Schallhorn, F. M. Wurm, *Nucleic Acids Res.* **1996**, *24*, 596.
[140] Y. W. Yang, J. C. Yang, *Biomaterials* **1997**, *18*, 213.
[141] M. Köhrmann, W. Haubensack, I. Hemraj, C. Kaehter, V. J. Lessman, M. A. Kiebler, *J. Neurosci. Res.* **1999**, *58*, 831.
[142] M. Urabe, A. Kume, K. Tobita, K. Ozawa, *Anal. Biochem.* **2000**, *278*, 91.
[143] S. Prabha, W. Z. Zhou, V. Labhasetwar, *Int. J. Pharm.* **2002**, *244*, 105.
[144] P. Washbourne, A. K. McAllister, *Curr. Opinion Neurobiol.* **2002**, *12*, 566.
[145] Y. Kakizawa, K. Miyata, S. Furukawa, K. Kataoka, *Adv. Mater.* **2004**, *16*, 699.
[146] M. X. Tang, C. T. Redemann, F. C. Szoka jr., *Bioconjugate Chem.* **1996**, *7*, 703.
[147] C. Chen, H. Okayama, *Mol. Cell. Biol.* **1987**, *7*, 2745.
[148] C. Seelos, *Anal. Biochem.* **1997**, *245*, 109.
[149] E. H. Chowdhury, M. Kunou, M. Nagaoka, A. K. Kundu, T. Hoshiba, T. Akaike, *Gene* **2004**, *341*, 77.
[150] Y. Kakizawa, K. Kataoka, *Langmuir* **2002**, *18*, 4539.
[151] X. Zhu, L. Lu, B. L. Currier, A. J. Windebank, M. J. Yaszemski, *Biomaterials* **2002**, *23*, 2683.
[152] S. Nsereko, M. Amiji, *Biomaterials* **2002**, *23*, 2723.
[153] A. Loyter, G. Scangos, D. Juricek, D. Keene, F. H. Ruddle, *Exp. Cell. Res.* **1982**, *139*, 223.
[154] T. Welzel, I. Radtke, W. Meyer-Zaika, R. Heumann, M. Epple, *J. Mater. Chem.* **2004**, 2213.
[155] E. Orrantia, P. L. Chang, *Exp. Cell. Res.* **1990**, *190*, 170.
[156] T. Welzel, W. Meyer-Zaika, M. Epple, *Chem. Commun.* **2004**, 1204.
[157] J. S. Blum, J. S. Temenoff, H. Park, J. A. Jansen, A. G. Mikos, M. A. Barry, *Biomaterials* **2004**, *25*, 5809.
[158] R. H. Miller, C. T. Tran, W. S. Robinson, *Virology* **1984**, *139*, 53.
[159] J. C. Elliot, *Structure and chemistry of the apatites and other calcium orthophosphates*, Elsevier, Amsterdam, **1994**.
[160] K. Takahashi, Y. Sawasaki, J. Hata, K. Mukai, T. Goto, *In Vitro Cell. Dev. Biol.* **1990**, *26*, 265.
[161] I. Seruga, M. A. Gonzalez, A. Serrano, J. L. Abad, A. Bernad, H. H. Riese, *Anal. Biochem.* **2001**, *296*, 143.
[162] S. P. Wilson, F. Liu, R. E. Wilson, P. R. Housley, *Anal. Biochem.* **1995**, *226*, 212.
[163] V. V. Sokolova, I. Radtke, R. Heumann, M. Epple, *Biomaterials* **2006**, *27*, 3147.
[164] H. T. Schmidt, A. E. Ostafin, *Adv. Mater.* **2002**, *14*, 532.
[165] S. Sengupta, D. Eavarone, I. Capila, G. Zhao, N. Watson, T. Kiziltepe, R. Sasisekharan, *Nature* **2005**, *436*, 568.
[166] F. Y. Cheng, C. H. Su, Y. S. Yang, C. S. Yeh, C. Y. Tsai, C. L. Wu, D. B. Shieh, *Biomaterials* **2005**, *26*, 729.
[167] H. Cölfen, *Macromol. Chem. Rapid Commun.* **2001**, 22.
[168] R. Balhorn, L. Brewer, M. Corzett, *Molecular reproduktion and development* **2000**, *56*, 230.
[169] V. Torchilin, *Adv. Drug. Deliv. Rev.* **2005**, *57*, 95.
[170] N. Pante, M. Kann, *Mol. Biol. Cell.* **2002**, *13*, 425.
[171] L. Josephson, C. H. Tung, A. Moore, R. Weissleder, *Bioconjug. Chem.* **1999**, *10*, 186.
[172] M. Lewin, N. Carlesso, C. H. Tung, X. W. Tang, D. Cory, D. T. Scadden, R. Weissleder, *Nat. Biotechnol.* **2000**, *18*, 410.

[173] M. Zhao, M. F. Kircher, L. Josephson, R. Weissleder, *Bioconjug. Chem.* **2002**, *13*, 840.
[174] V. Torchilin, R. Rammohan, V. Weissig, T. S. Levchenko, *Proc. Natl. Acad. Sci. U.S.A.* **2001**, *98*, 8786.
[175] F. L. Sorgi, S. Bhattacharya, L. Huang, *Gene Ther.* **1997**, *4*, 961.
[176] F. F. Becker, *J. Gen. Physiology* **1961**, *44*, 433.
[177] M. Junghans, J. Kreuter, A. Zimmer, *Nucleic Acids Res.* **2000**, *28*, 10 E45.
[178] R. Zhou, R. C. Geiger, D. A. Dean, *Expert Opin. Drug Deliv.* **2004**, *1*, 127.
[179] T. Masuda, H. Akita, H. Harashima, *FEBS Letters* **2005**, *579*, 2143.
[180] S. C. de Smedt, K. Remaut, B. Lucas, K. Braeckmans, N. N. Sanders, J. Demeester, *Adv. Drug. Deliv. Rev.* **2005**, *57(1)*, 191.
[181] J. Zabner, A. J. Fasbender, T. Moninger, *J. Biol. Chem.* **1995**, *270*, 18997.
[182] G. L. Lukacs, P. Haggie, O. Seksek, D. Lechardeur, N. Freedman, A. S. Verkman, *J. Biol. Chem.* **2000**, *275*, 1625.
[183] A. Coonrod, F. Q. Li, M. Horwitz, *Gene Ther.* **1997**, *4*, 1313.
[184] M. Graessman, J. Menne, M. Liebler, I. Graeber, A. Graessman, *Nucleic Acids Res.* **1989**, *17*, 6603.
[185] A. Fasbender, J. Zabner, B. G. Zeiher, M. J. Welsh, *Gene Ther.* **1997**, *4*, 1173.
[186] S. L. Schmid, R. Fuchs, P. Male, I. Mellman, *Cell* **1988**, *52*, 73.
[187] A. El Ouahabi, M. Thiry, V. Pector, R. Fuks, J. M. Ruysschaert, M. Vandenbranden, *FEBS Lett.* **1997**, *414*, 187.
[188] M. Brisson, W. C. Tseng, C. Almonte, S. Watkins, L. Huang, *Hum. Gene Ther.* **1999**, *10*, 2601.
[189] W. C. Tseng, F. R. Haselton, T. D. Giorgio, *Biochim. Biophys. Acta* **1999**, *1445*, 53.
[190] W. T. Godbey, K. K. Wu, A. G. Mikos, *Proc. Natl. Acad. Sci. USA* **1999**, *96*, 5177.
[191] H. Schreier, *Pharm. Acta Helv.* **194**, *68*, 145.
[192] B. Mitterauer, *Med. Hypoth.* **2004**, *62*, 907.
[193] P. Y. Lu, F. Xie, M. C. Woodle, *Adv. Genetics* **2005**, *54*, 115.
[194] R. K. Leung, P. A. Whittaker, *Pharmacol. Therapeut.* **2005**, *107(2)*, 222.
[195] A. Muramatsu, M. Iwai, T. Morikawa, S. Tanaka, T. Mori, Y. Harada, T. Okanoue, *Carcinogenesis* **2002**, *23*, 351.
[196] T. V. Chirila, P. E. rakoczy, K. L. garrett, X. Lou, I. J. Constable, *Biomaterials* **2002**, *23*, 321.
[197] J. S. Gill, X. Zhu, M. J. Moore, L. Lu, M. J. Yaszemski, A. J. Windebank, *Biomaterials* **2002**, *23*, 2773.
[198] J. R. Kovacs, Y. Zheng, H. Shen, W. S. Meng, *Biomaterials* **2005**, *26*, 6754.
[199] M. Junghans, S. M. Loitsch, S. C. Steiniger, J. Kreuter, A. Zimmer, *Eur. J. Pharm. Biopharm.* **2005**, *60(2)*, 287.
[200] I. J. Bruce, J. Taylor, M. Todd, M. J. Davies, E. Borioni, C. Sangregorio, T. Sen, *J. Magn. Magn. Mater.* **2004**, *284*.
[201] A. Campo, T. Sen, J.-P. Lellouche, I. J. Bruce, *J. Magn. Magn. Mater.* **2005**, *293*, 33.
[202] A. Gourishankar, S. Shiukla, R. Pasricha, M. Sastry, K. N. Ganesh, *Curr. Appl. Physics* **2005**, *5*, 102.
[203] M. Okazaki, Y. Yoshika, S. Yamaguchi, M. Kaneno, J. C. Elliott, *Biomaterials* **2001**, *22*, 2459.
[204] O. Donze, D. Picard, *Nucleic Acids Res.* **2002**, *30*, e46.
[205] P. Sazani, A. Astriab-Fischer, R. Kole, *Antisense and nucleic acid drug development* **2003**, *13*, 119.
[206] C. D. Kaufman, Z. Izsvak, A. Katzer, Z. Ivics, *Journal of RNAi and Gene Silencing* **2005**, *1*, 97.
[207] E. H. Hartman, P. H. M. Spauwen, J. A. Jansen, *J. Invest. Surg.* **2002**, *15*, 185.

[208] R. Z. LeGeros, *Calcium phosphates in oral biology and medicine*, Karger, Basel, **1991**.
[209] C. Combes, C. Rey, *Biomaterials* **2002**, *23*, 2817.
[210] R. Z. LeGeros, in *Hydroxyapatite and related materials* (Eds.: P. W. Brown, B. Constantz), CRC Press, Boca Raton, **1994**, pp. 3.
[211] A. Linde, E. Hedner, *Calcif. Tissue Int.* **1995**, *56*, 549.
[212] E. H. J. Groeneveld, E. H. Burger, *Eur. J. Endocrinol.* **2000**, *142*, 9.
[213] M. Laub, T. Seul, E. Schmachtenberg, H. P. Jennissen, *Mater. Wiss. Werkstofftechn.* **2001**, *32*, 926.
[214] M. Wiemann, H. Rumpf, D. Bingmann, H. P. Jennissen, *Mater. Wiss. Werkstofftechn.* **2001**, *32*, 931.
[215] H. P. Jennissen, T. Zumbrink, M. Chatzinikolaidou, J. Steppuhn, *Mater. Wiss. Werkstofftechn.* **1999**, 838.
[216] M. Chatzinikolaidou, M. Laub, H. Rumpf, H. P. Jennissen, *Mater. Wiss. Werkstofftechn.* **2002**, *33*, 720.
[217] M. J. Glimcher, *Philos. Trans. R. Soc. London Ser.304* **1984**, *13*, 479.
[218] L. Addadi, S. Weiner, *Angew. Chem. Int. Ed. Engl.* **1992**, *31*, 153.
[219] Y. Liu, P. Layrolle, J. de Bruijn, C. van Blitterswijk, K. de Groot, *J. Biomed. Mater. Res.* **2001**, *57*, 327.
[220] G. Decher, *Science* **1997**, *277*, 1232.
[221] A. E. W. Miles, *Structural and chemical organisation of teeth*, Academic Press, New York:, **1967**.
[222] J. D. Termine, R. A. Peckauskas, A. S. Posner, *Arch. Biochem. Biophys.* **1970**, *140*, 318.
[223] G. Bernardi, *Enzyme structure. Methods in enzymology*, Academic Press, New York:, **1973**.
[224] C. Chen, A. L. Boskey, *Calcif. Tiss. Int.* **1985**, *37*, 395.
[225] R. W. Romberg, P. G. Werness, B. L. Riggs, K. G. Mann, *Biochemistry* **1986**, *25*, 1176.
[226] P. A. Raj, M. Johnsson, M. J. Levine, G. H. Nancollas, *J. Biol. Chem.* **1992**, *267*, 5968.
[227] J. Sambrook, E. F. Fritsch, T. l. Maniatis, *CSH Laboratory Press* **1989**.
[228] D. Hanahan, *J. Mol Biol.* **1983**, *166*, 557.

7 Appendix

7.1 List of abbreviations

A	adenine
ACP	amorphous calcium phosphate
Amp	ampicillin
ATCC	american type cell culture collection
Bp	base pair
BSA	bovine serum albumin
C	cytosine
CMV	cytomegalovirus
DCPD	dicalcium phosphate dihydrate
DEAE	diethylaminoethyldextran
DESY	Deutsches Elektronen Synchrotron
DLS	dynamic light scattering
DMEM	Dulbeccos modified Eagles medium
DNA	deoxyribonucleic acid
ds	double stranded
E. coli	Escherichia coli
EDTA	ethylenediaminetetraacetate
EDX	energy dispersive X-ray analysis
EGFP	enhanced green fluorescent protein
FCS	fetal calf serum
G	guanine
HA	hydroxyapatite
HASYLAB	Hamburger Synchrotronstrahlungslabor
HBS	Hanks buffered saline
HEPES	4-2-hydroxyethyl-1-piperazineethanesulfonic acid
HIV	human immune deficiency virus
ICDD	International Centre for Diffraction Data
kDa	kilodalton
LB	Luria Bertani

mRNA	messenger RNA
MTT	methyl thiazole tetrazolium bromide
NLS	nuclear localisation sequence
nm	nanometre
OD	optic density
PBS	phosphate buffered saline
PCR	polymerase chain reaction
RISC RNA	induced silencing complex
RNA	ribonucleic acid
RNAi	RNA interference
rRNA	ribosomal RNA
SDS	sodium dodecyl sulfate
SV40	Simian virus 40
SEM	scanning electron microscopy
siRNA	small interfering RNA
TEB	tris-EDTA boric acid
T-HUVEC	transformed human umbilical vein endothelial cells
TRITC	trimethylrhodaminisothiocyanate
TEM	transmission electron microscopy
TCP	tricalcium phosphate
tRNA	transfer RNA
UV	ultraviolet
XRD	x-ray (powder) diffractometry

7.2 Safety and disposal of chemicals

All chemical compounds used in experiments for this work are listed below. The column "symbol" lists the international hazard symbols appropriate for the specific compounds. R-Phrase and S-Phrase are listings of dangers and safety precautions required by German law.

compound	**symbol**	**R-Phrase**	**S-Phrase**	**disposal**
$AlCl_3$	X_i	34	26-36/37/39-45	2
$[CH_3CH(OH)COO]_2Ca$	--	--	--	2
$Ca(NO_3)_2 \cdot 4\ H_2O$	O, X_i	8-36	-	2
$CaCl_2 \cdot 2\ H_2O$	X_i	36	22-24	2
Ethanol	F	11	7-16	1
HCl (37 % in H_2O)	C	34-37	26-36/37/39-45	4
HNO_3 (65 % in H_2O)	C, O	35	23-26-36/37/39-45	4
KCl	--	--	--	2
$Mg(NO_3)_2 \cdot 4\ H_2O$	X_i	8-36/37/38	17-26-36	2
NaCl	--	--	--	2
Na_2CO_3	--	--	--	2
Na_2HPO_4	--	--	--	2
$NaH_2PO_4 \cdot 2\ H_2O$	--	--	--	2
NaOH	C	35	26-37/39-45	5
$(NH_4)_2HPO_4$	--	--	--	2

Disposal:

1: organic solvents were disposed in the organic solvents disposal container for non-halogenated solvents

2: solid were disposed in the container for solid waste

3: inorganic compounds were made acidic, dissolved in water, and transferred to the container for acidic heavy metal solutions

4: acids were transferred in to the container for heavy metal solutions

5: bases were neutralised and transferred into waste water

7.3 Publications

1. O. Prymak, V. Sokolova, T. Peitsch, M. Epple, "The crystallization of fluoroapatite dumbbells from oversaturated aqueous solution", Crystal Growth & Design 6 (2006) 498-506.
2. V. Sokolova, I. Radtke, R. Heumann, M. Epple, "Effective transfection of cells with multi-shell calcium phosphate-DNA nanoparticles", Biomaterials 27 (2006) 3147–3153
3. V. Sokolova, O. Prymak, W. Meyer-Zaika, H. Cölfen, H. Rehage, A. Shukla, M. Epple, "Synthesis and characterization of DNA-functionalized calcium phosphate nanoparticles with multiple shells", Mater. Wiss. Werkstofftechn. 37 (2006) 441-445
4. V. Sokolova, O. Prymak, W. Meyer-Zaika, E. Kubareva, T. S. Oretskaya, M. Epple, "Functionalization of calcium phosphate nanoparticles by oligonucleotides and their application for gene silencing" (submitted).
5. V.Sokolova, A. Kovtun, R. Heumann, M. Epple, "Tracking the pathway of calcium phosphate/DNA nanoparticles during cell transfection by incorporation of red-fluorescing TRITC-BSA into these nanoparticles" (submitted)

7.4 Presentations and posters

1. 7th Symposium Biomaterials and Biomechanics: Fundamentals and Clinical Applications, Essen, 06.-08.10.2004, V. Sokolova, T. Welzel, W. Meyer-Zaika, I. Radtke, R. Heumann, M. Epple, "Transfection of cells with custom-made calcium phosphate nanoparticles" (poster)
2. XVIIIth Aachen Colloquium on Biomaterials, Aachen, 15.-16.03.2005, V. Sokolova, W. Meyer-Zaika, I. Radtke, R. Heumann, M. Epple, "Transfection of cells with multi-shell calcium phosphate-DNA nanoparticles" (poster)
3. 8th International Symposium Biomaterials and Biomechanics: Fundamentals and Clinical Applications, Essen, 21.-23.09.2005, V. Sokolova, W. Meyer-Zaika, I. Radtke, R. Heumann, and M. Epple, "Transfection of cells with multi-shell calcium phosphate-DNA nanoparticles" (poster)
4. Jahrestagung der Deutschen Gesellschaft für Biomaterialien, Würzburg, 07.-08.10.2005, V. Sokolova, W. Meyer-Zaika, I. Radtke, R. Heumann, and M. Epple, "Transfektion von Zellen mit mehrschaligen Calciumphosphat-DNA-Nanopartikeln" (oral presentation)
5. 2006 MRS Spring Meeting, San Francisco, 17.-21.04.2006, V. Sokolova, W. Meyer-Zaika, I. Radtke, R. Heumann, M. Epple, "Effective transfection of cells with multi-shell calcium phosphate-DNA nanoparticles" (oral presentation).
6. 9th Essen Symposium Biomaterials and Biomechanics: Fundamentals and Clinical Applications, Essen, 05.-08.09.2006, V. Sokolova, G. Kovtun, O. Prymak, W. Meyer-Zaika, E.A. Kubareva, E.A. Romanova, T.S. Oretskaya, R. Heumann, M. Epple, "Functionalization of calcium phosphate nanoparticles by oligonucleotides and their application for gene silencing " (oral presentation).
7. 9th Essen Symposium Biomaterials and Biomechanics: Fundamentals and Clinical Applications, Essen, 05.-08.09.2006, V. Sokolova, G. Kovtun, R. Heumann, M. Epple , "Tracking the pathway of calcium phosphate/DNA nanoparticles during cell transfection by marking with red-fluorescing TRITC-BSA" (poster).
8. 13. Heiligenstaedter Kolloquium: Technische Systeme fuer Biotechnologie und Umwelt, Heilbad Heiligenstadt, 25.-27.2006, V. Sokolova, G. Kovtun, W. Meyer-Zaika, I. Radtke, R. Heumann, M. Epple, "Oligonucleotide-functionalized calcium phosphate nanoparticles for antisense strategy" (oral presentation).

7.5 Curriculum Vitae

Name:	Viktoriya Sokolova
Date of Birth:	29.12.1981
Place of Birth:	Kharkiv, Ukraine
Family status:	married
Nationality:	Ukrainian

EDUCATION:

from 01.10.2003 -	PhD student at the University of Duisburg-Essen, Campus Essen, Department of Chemistry (Prof. Dr. M. Epple). Assistant of practical course in inorganic chemistry: leading of students, examination, correction of protocols
01.09. – 30.09.2003	PhD student at the Ruhr-University Bochum, Department of Chemistry (Prof. Dr. M. Epple)
May 2003:	Student Exchange Program at the Ruhr-University Bochum (Leonard-Euler program)
2002-2003:	W.N. Karasin Kharkiv National University, Ukraine. *Diploma of Magister* with Honors. Full education in speciality Physiology. *Qualification:* Magister of physiology *Title of Diploma thesis:* „Stable and metastable states of red blood cells and their relation to the osmotic and temperature conditions “
1998-2002:	W.N. Karasin Kharkiv National University, Ukraine. *Diploma of Bachelor* Fundamental education in speciality Biology. *Qualification:* Bachelor of biology. *Title of Diploma thesis:* „Stimulation of the cognitive activity during the study of definition in Anatomy and Physiology of human “.
1989-1998:	Lyceum № 149, Kharkiv, Ukraine. Middle school education. Average note is 4.85 by maximum 5.0. Special achievements in medicine and biology.

EXPERIENCE:

Oct.2000 –June 2003:	President of physiology club Win in Kharkiv, Ukraine
Sept. 2002-June 2003:	Representative of ICEP (International Counselors Exchange program) in the Ukraine
June-Sept. 2001, 02, 03:	Counselor in Kennolyn Camp, California, USA

DIPLOMAS:

Diploma for the first, second and third place in the Ukrainian and International diving competitions, Candidate for a Master of Diving

Diploma for the help in the organization und carrying out of Ukrainian biological Olympiad

Diploma of American Red Cross

Acknowledgment

I am grateful to my supervisor Prof. Dr. Matthias Epple for welcoming me into his group and for providing the excellent working facilities that contributed substantially to this thesis.

I thank Prof. Dr. R. Heumann for outstanding cooperation and great ideas. I thank Dr. I. Radtke, H. Breuker, C. Grote-Westrick, S. Karassek for the help with cell experiments and for answers on many questions.

I thank Prof. Dr. T.S. Oretskaya, Dr. E. Kubareva and Dr. E. Romanova for the provided oligonucleotides and for the nice time during our stay in Moscow.

I want to thank Dr. H. Cölfen and A. Völkel for the assistance with analytical ultracentrifugation measurements.

I want to thank Prof. Dr. H.P. Jennissen and Dr. K. Zurlinden for a great cooperation and for the assistance with measurements of radioactive ubiquitin.

I thank Prof. Dr. H. Rehage and Dr. A. Shukla for a fruitful cooperation and for the assistance with the interpretation of the results from dynamic light scattering.

I am grateful to all colleagues in our department for useful advices, for the help in many situations and friendly talks.

And also I want to thank my grandmother, my brother, and all my friends for their great support.

Hiermit erkläre ich, dass ich bisher keine weiteren Promotionsversuche unternommen habe.

Essen 19.07.2006

Hiermit erkläre ich, dass ich die vorliegende Arbeit selbstständig verfasst und keine anderen als die angegebenen Hilfsmittel verwendet habe.